COLLIDER PHYSICS OF EXTRA COMPACT DIMENSIONS

By

CHRISTOPHER DAVID MCMULLEN

Bachelor of Science
California State University
Northridge, California
1994

Master of Science
California State University
Northridge, California
1998

Submitted to the Faculty of the
Graduate College of the
Oklahoma State University
in partial fulfillment of
the requirements for
the Degree of
DOCTOR OF PHILOSOPHY
August, 2002

COLLIDER PHYSICS OF EXTRA

COMPACT DIMENSIONS

Thesis Approved:

Satyanarayan Nandi

Thesis Adviser

Satyanarayan Nandi, for K.S. Babu (out of Country)

J.W. Gibbs

Satyanarayan Nandi for B. Binegar (out of Country)

Timothy J. Gilbertson

Dean of the Graduate College

PREFACE

The theories involving extra dimensions beyond the usual spacetime provide a unique way to understand both the usual SM interactions such as the weak, electromagnetic, and strong as well as the gravitational interaction in a unified way. Six such extra spacelike dimensions are also required in superstring theory, currently the most promising candidate to understand all interactions. The sizes of these extra dimensions can be anywhere between 10^{-32}m to sub-millimeter, depending on the specific scenario. One unique prediction of these theories is the existence of the Kaluza-Klein (KK) excitations of any particle that propagates into these extra compact dimensions. The phenomenological implications of these models have been at the forefront of current research since the proposal of Arkani-Hamed, Dimopoulos, and Dvali (ADD) regarding the viability of the existence of such large extra compact dimensions.

This research was conducted to explore the potential for discovering Kaluza-Klein (KK) excitations of Standard Model (SM) fields at high-energy colliders such as the FermiLab Tevatron and the Large Hadron Collider (LHC). Two scenarios investigated include the universal extra dimensions (UED) and fermi-phobic models. Specific objectives of this analysis included (a) characterization of possible final state combinations that arise from collider processes involving exchanges or direct production of KK excitations, (b) calculation of the cross sections for KK processes relative to SM background, (c) determination of the prospects of discovering KK excitations, and (d) placement of constraints on the sizes of extra dimensions propagated by SM fields in the

event that any KK signal remains undetected. The results presented in this thesis will be very useful in looking for the signals of the existence of these extra dimensions, potentially leading to their discovery.

ACKNOWLEDGMENTS

I wish to convey my sincere appreciation to my research adviser, Dr. S. Nandi, for his constructive guidance, encouragement, patience, and example. I also wish to extend my sincere appreciation to the remaining members of my research committee who also provided support and guidance: Dr. K.S. Babu, Dr. X. Xie, and Dr. B. Binegar. My thankfulness also extends to Dr. Duane Dicus and Dr. Cosmin Macesanu who provided willing assistance and shared their expertise.

This research was supported in part by the U.S. Department of Energy Grant Numbers DE-FG03-98ER41076 and DE-FG02-01ER45684.

TABLE OF CONTENTS

LIST OF TABLES

LIST OF FIGURES

NOMENCLATURE

Particles

f	fermion; spin one-half particle; lepton or quark.
l	electrically charged lepton; one of three generations (electron, muon, and tau); interacts with the photon and weak gauge bosons.
ν	electrically neutral lepton; one of three generations (electron, muon, and tau neutrino); interacts with the weak gauge bosons; with corresponding lepton, forms $SU(2)_L$ doublet; extremely light, originally thought to be massless.
q	quark; one of six varieties, also in three generations (up, down; charm, strange; top, bottom) – three left-handed doublets and six right-handed singlets; carries fractional electric charge; bound together in hadrons (baryons and mesons); interacts with gluons, photons, and the weak gauge bosons; with a $\bar{}$ = antiquark.
e	electron; e^+ is the positron (anti-electron).
μ	muon; very much like the electron, but heavier.
τ	tau lepton; very much like the muon, but heavier.
ν_e	electron neutrino.
ν_μ	muon neutrino.
ν_τ	tau neutrino.
u	up quark; electric charge +2/3; lightest quark.
d	down quark; electric charge -1/3; slightly heavier than the u.
c	charm quark; electric charge +2/3; heavier than the s, but lighter than the b.
s	strange quark; electric charge -1/3; heavier than the d, but lighter than the c.
t	top quark; electric charge +2/3; heaviest known quark.
b	bottom quark; electric charge -1/3; lighter than the t.

Gauge Bosons

X,Y	spin one gauge boson; represents one of the following gauge bosons.
g	gluon; mediator of the strong interaction among quarks, gluons and quarks carry (strong) color charge (gluons come in one of eight colors, while quarks come in one of three colors); massless.
γ	photon; mediator of the electromagnetic interaction among electrically charged objects; massless.
W	W boson; electric charge minus or plus one; mediates the weak interaction among quarks or leptons; very massive.
Z	Z boson; electrically neutral; mediates the weak interaction among quarks or leptons; very massive.

Units

c	$c = 1$ speed of light in vacuum is set equal to one in these units; length and time are set on an equal footing.
h-bar	h-bar = 1 Planck's constant is set (in the usual 3+1 dimensions) is set equal to one in these units; length and mass are set on an equal footing.
GeV	Giga electron volt; 10^9 electron volts; typical unit of mass or decay rate.
pb	pico barn; 10^{-12} barns = 10^{-36} cm^2; typical unit of cross section.

Kaluza-Klein Excitations

$\star$	gauge boson Kaluza-Klein excitation (e.g. $Z^\star$).
$\bullet$	fermion Kaluza-Klein excitation for same chirality as the corresponding SM fermion (e.g. $u^\bullet$); applicable only to the universal scenario.
$\circ$	fermion Kaluza-Klein excitation for opposite chirality as the corresponding SM fermion (e.g. e°); applicable only to the universal scenario.
N,n	mode of the Kaluza-Klein excitation (e.g. $g_n^\bullet$).

Abbreviations

ADD	Arkani-Hamed, Dimopoulos, and Dvali (specific model with extra dimensions)
EW	Electroweak (electromagnetic plus weak interactions)

KK Kaluza-Klein (feature of theories with compact extra dimensions)

LEP high-energy e^+e^- collider (finished data, turning into the LHC)

LEP2 Run 2 at LEP (the second data run)

LHC Large Hadron Collider (high-energy collider to be running in a few years)

QCD Quantum Chromodynamics (SU(3) QED analog of the strong ineraction among gluons and quarks)

QED Quantum Electrodyanmics (theory of the interactions the photon has with electrically charged objects)

SM Standard Model (conventionally accepted model of particle interactions)

SUSY Supersymmetry

UED Universal Extra Dimensions (specific model with extra dimensions)

VEV vacuum expectation value (as in the Higgs VEV)

Symbols

α electromagnetic coupling or fine structure.

α_S strong coupling.

a color index.

abcd *a*, *b*, *c*, and *d* are also used to represent parton-level processes ($ab \rightarrow cd$).

A supersymmetric Higgs field.

A^μ electromagnetic gauge field; (Lorentz contracts with A_μ).

$A^{\mu a}$ QCD gauge field; (Lorentz contracts with $A_\mu{}^a$).

b color index.

B^μ gauge field with Lorentz index m.

c color index.

C^μ gauge field with Lorentz index m.

c_n factors in the effective propagator.

cos trigonometric cosine function.

$\delta^{\mu\nu}$ Kronecker delta.

$\delta(y)$ delta function evaluated at y.

D propagator; (with *eff*, effective propagator).

D right-handed (in the SM) down-type quark multiplet.

D effective propagator when modulus-squared of propagator is used.

D dimension (as in usual 4D).

D_3 D_3-brane; the SM wall.

D_{3+N} higher-dimensional brane.

D^{μ} covariant derivative with respect to μ.

$\in$ element of (in set notation).

$\varepsilon^{\mu\nu}$ gauge boson polarization state.

E right-handed (in the SM) charged lepton multiplet.

eff effective (as in D_{eff}).

e.g. for example.

Eq. Equation.

Eqs. Equations.

exp exponential.

ϕ phi; extra dimension polar angle.

ϕ phi; azimuthal angle for experimental cuts.

$\phi_{ij}^{\ a}$ massive spin-0 particles.

$f_{a/A}$ parton distribution.

f^{abc} structure constant.

F form factor.

$F^{\mu\nu}$ electromagnetic field strength tensor; (Lorentz contracts with $F_{\mu\nu}$).

$F^{\mu\nu a}$ gluon field strength tensor; (Lorentz contracts with $F_{\mu\nu}{}^{a}$).

Fig. Figure.

γ_5 anti-commuting matrix formed out of the Dirac gamma matrices; the gamma matrix used in 5D Lorentz contractions involving γ^M.

γ^μ 4D Dirac gamma matrices.

Γ decay rate, or width.

G prefix for 109 (as in GeV).

g strong coupling, coupling.

g_5 5D strong coupling, 5D coupling.

$g^{\mu\nu}$ metric tensor.

G_a KK mode a of the graviton.

G_k KK excitation of graviton corresponding to mode k.

η pseudorapidity.

η^μ arbitrary four-momentum vector.

H the Higgs boson; responsible for particle masses.

i index.

i imaginary number.

i.e. that is.

j index.

j subprocess label.

κ a gravitational parameter.

k^{μ} momentum with Lorentz index μ.

k_y mode of the KK graviton field along the y direction.

λ Higgs couplings.

Λ vertex factor.

ln natural logarithm.

L left.

L left-handed (in the SM) lepton multiplet.

L Lagrangian density.

L parton luminosity.

l mode l for a Kaluza-Klein excitation; (or lepton – see particles).

μ Lorentz index; 0 for time, 1 for x_1, 2 for x_2, 3 for x_3.

m mode m for a Kaluza-Klein excitation.

M amplitude.

M,m compactification scale.

M,m mass (as in m_e or m_n).

max maximum.

m_g mass of the graviton.

min minimum.

mm millimeter; 10^{-3} meters.

m_y contribution of the y dimension to the graviton mass.

M 5D Lorentz index; 4 for extra dimension y.

M_D fundamental Planck scale (in extra dimensions).

M_P usual (3+1)-dimensional Planck scale.

n	Lorentz index; 0 for time, 1 for x_1, 2 for x_2, 3 for x_3.
n	mode n for a Kaluza-Klein excitation.
n_i	mode i for a Kaluza-Klein excitation.
N	5D Lorentz index; 4 for extra dimension y.
N,n	number of extra dimensions.
N	right-handed (in the SM) neutrino multiplet.
$N \rightarrow M$	an $N \rightarrow M$ process has N initial and M final states.
π	pi; ratio of the circumference of a circle to its diameter.
p	prefix for 10^{-12} (as in pb).
p	proton.
p	momentum; (with a / represents contraction with a Dirac gamma matrix).
p_T	transverse momentum.
p^μ	momentum with Lorentz index μ.
$P_{L,R}$	left- and right-handed projection operators.
prod	production.
θ	theta; polar angle for experimental cuts.
Q	scale.
Q	left-handed (in the SM) quark multiplet.
ρ	ρ-parameter; important in electroweak precision measurements.
R	right.
R,r	radius of the extra compact dimension (r in the fermi-phobic case, R in the universal case, also r for gravity in the fat-brane scenario).
R	ratio of cross sections.
Ref.	Reference.

σ cross section.

σ spins (used in the context of polarization summations).

s direct-channel Mandelstam variable; (^ represents subprocess).

S a statistical factor.

S^1 circle; (as in S^1/Z_2).

sin trigonometric sine function.

SU(2) special unitary gauge group; (also describes spinor rotations).

SU(3) special unitary gauge group; describes QCD.

τ relative factor between the process and subprocess energies.

τ^i generators of SU(2).

t Cross-channel Mandelstam variable; (^ represents subprocess).

T prefix for 1012 (as in TeV).

T^a generators of SU(3).

tot total.

u cross-channel Mandelstam variable; (^ represents subprocess).

u_i fermion external line (Feynman rule).

U right-handed (in the SM) up-type quark multiplet.

U(1) elementary unitary gauge group.

v one of the Mandelstam s, t, u variables.

v_i anti-fermion external line (Feynman rule).

$V_{\rho\sigma}{}^u$ tensors.

ω a gravitational parameter.

Ω dimensionless solid angle.

w	one of the Mandelstam s, t, u variables.
Ξ_M	covariant derivative with respect to $_M$ when field propagates in the bulk.
x	a coordinate.
x_a	momentum fraction.
x_a	gravitational coordinate (a refers to all extra dimensions).
x_i	usual Cartesian coordinates.
x_y	argument of the form factor for the fat brane scenario.
x_z	gravitational coordinate exclusive to gravity.
y	extra dimension coordinate.
y	rapidity.
yr	year.
z	cosine of the azimuthal angle.
z	extra dimension coordinate exclusive to gravity.
Z_2	in S^1/Z_2, a compactification orbifold.
Z'	additional Z bosons studied in Z' physics.
∂	partial derivative operator.
∂_μ	partial differentiation with respect to Lorentz index μ.
¯	Anti- as in anti-particle (as in anti-up or anti-fermion); bar appears the symbol for the particle.
‘	represents a distinct quark flavor (when following a quark q).
‘$_n$	represents the subtraction of m_n^2 from a Mandelstam variable.
*	complex conjugation.
^	refers to subprocess (above variable).
!	factorial.

$\sim$	on the order of.
$\sim_n$	represents the subtraction of $4\ m_n^2$ from a Mandelstam variable.
/	missing (as in missing energy).
/	represents the contraction of momentum and the Dirac gamma matrices (when striked through a momentum variable).
{}	set (consists of elements enclosed).
()	multiplet (consists of fields enclosed).
$\|\|^2$	modulus-square (of enclosure).
d_/d_	differentiation of label 1 with respect to label 2.
...	continuing in the same sequence.
2→2	process with 2 initial and 2 final states.

I

INTRODUCTION

Background, Historical Perspective, and Motivations

Background

Usual Dimensions. Everyday experience suggests the presence of three dimensions of space and one dimension of time. That is, observable objects appear to be confined to motion along three Euclidean spatial directions. Any theory that consists of extra spatial dimensions must not permit the motion of matter to contradict these notions. Furthermore, the laws of physics, such as Newton's inverse-square law for the interaction of massive objects and Maxwell's equations governing the electromagnetic interaction of charged particles, must not be changed at measurable scales.

Extra Dimensions. These obvious constraints on model building restrict the nature of any extra spatial dimensions. The free propagation of particles into Euclidean extra dimensions presents immediate problems. First, macroscopic matter composed of the lightest generation of Standard Model (SM) particles[†] would no longer be confined to the three usual Cartesian directions. An apparent consequence would be the ease with which a prisoner could escape from a 3D prison cell. Secondly, gravitons, which mediate the interactions between massive objects, propagating in extra Euclidean dimensions would give rise to a drastically altered form of Newton's law.

[†]The lightest generation fermions include the electron, the electron neutrino, the up quark, and the down quark. Macroscopic matter is comprised mainly of protons, neutrons, and electrons, in which the up and down type quarks are bound together inside the protons and neutrons.

Similarly, photons, which mediate the electromagnetic interactions, would drastically alter Coulomb's law.

There are a few simple ways around these problems. One obvious answer is to forbid particles from propagating in the direction of any extra dimensions, but this is not easily motivated nor is it physically interesting unless some particles – perhaps heavier, quickly-decaying particles – see the extra dimensions, in which case they must comply with the aforementioned constraints. The popular resolution is to choose compact dimensions, such as those naturally described by toroidal or spherical coordinates, with a sufficiently small radius. The restriction on the size of the radii prevents macroscopic motion into perceptible distances in the direction of the extra dimensions. Finally, it is possible to include a binding factor to govern the probability that particles will penetrate into extra dimensions. In this manner, observable objects can move along Cartesian coordinates, but not stray from the usual three-dimensional wall with significant likelihood.

Historical Perspective

Unification. Kaluza implemented the idea of extra dimensions with the hope of unifying two fundamental forces of nature – gravity and electromagnetism. This idea was appealing to Einstein, who also possessed aspirations of demonstrating that quantum physics was merely an effective $(3 + 1)$-dimensional theory that stemmed from a classical theory in higher dimensions. However, the results of their theoretical pursuits led to predictions that were in obvious disagreement with the known universe. Popular present-day models with extra dimensions incorporate quantum mechanics

in the full higher-dimensional theory.

Superstring Theory. Superstring theories predict six extra dimensions. This was one of the initial problems in the development of string theory. It was later realized that if these extra dimensions were compact that their sizes would be immeasurably small because the scale of string theory is naturally on the order of the Planck scale ($\sim 10^{19}$ GeV). However, Arkani-Hamed, Dimopoulos, and Dvali (ADD) have shown, in the past few years, that it may be phenomenologically viable for such extra dimensions to be much larger – perhaps as large as sub-millimeter.

Motivations

Theoretical Aspects. It is possible to construct higher-dimensional theories by straightforward generalization of the usual $(3 + 1)$-dimensional Lagrangian. New physics theories involving extra dimensions may explain theoretical problems. For example, it may be possible to explain why there appear to be three light generations of SM particles or why the masses of SM particles range from very light neutrinos (much lighter than the electron) to the very heavy top quark (174 GeV).

Superstring theory is among the best available candidates for unifying the fundamental forces of nature, including gravity, and offers prospects for other aesthetically pleasing solutions to current theoretical problems. Therefore, any features inherent in superstring theory, such as the prediction of six extra dimensions, are very well motivated for phenomenological studies. A general string-inspired model features six extra dimensions, where gravitons can propagate into all of the extra dimensions. A superstring-inspired model also incorporates supersymmetry.

Supersymmetry is a symmetry between bosons and fermions, and is arguably the most promising extension of the standard theory of particle interactions. One benefit of supersymmetric theories is that it is not necessary to fine-tune parameters at each order in perturbation theory. Supersymmetry also permits the combination of the gravity and particle spectrum, gives rise to quantum field theories that are finite to all orders in perturbation theory, and as a local gauge symmetry becomes supergravity. However, supergravity is not finite, but this can be resolved by extending further to superstring theory.

Large Extra Dimensions ADD proposed, in the last few years, that the extra dimensions predicted by string and superstring theories may be much larger than the traditional Planck scale ($\sim 10^{-33}$ cm). They demonstrated that large extra compact dimensions may solve the hierarchy problem: The fundamental Planck scale may be on the order of the electroweak scale, such that there is in fact only one fundamental scale for interactions, and not on the traditional $(3+1)$-dimensional Planck scale.

Phenomenological Aspects. Models with extra dimensions can provide testable predictions, whereby extra dimensions may be discovered or bounds can be placed on their radii. Furthermore, it is possible that extensions of current theories that include extra dimensions may be able to explain various experimental discrepancies. While the agreement between theory and experiment is overwhelming in most cases in the SM, there are a few discrepancies on the order of one standard deviation or more (this is typical with b-quark asymmetry measurements). An extension of the SM involving extra dimensions that does not significantly affect results that are in agreement, but does improve the agreement of other measurements would be phenomenologically

interesting.

Experimental Aspects. The phenomenology of theories with extra dimensions may be physically accessible to near-future experiments. The original ADD model with two extra compact dimensions of the same radius propagated only by gravity predicts a radius in the sub-millimeter regime, which is just beyond the reach of present experimental tests of Newton's law of gravity. If SM fields propagate in the bulk – the extra dimensions – and the fundamental Planck scale and electroweak scale are each on the order of a TeV, as ADD proposed for solving the hierarchy problem (that the two fundamental scales, the electroweak and Planck scales, which are vastly different in $3 + 1$ dimensions, might both be on the order of a single scale, which is the electroweak scale), then the Kaluza-Klein (KK) excitations of these fields are just beyond the limits of current colliders. Several experimental groups attempting to improve the sensitivity of gravitation tests of Newton's law, and future colliders such as the Large Hadron Collider (LHC) and the next generation linear colliders may be on the verge of discovering extra dimensions. If not, then the constraints on the sizes of extra dimensions will be significantly heightened.

Experimental Searches

Non-Collider Searches

Test's of Newton's Law. Newton's law of gravity has been tested from astronomical scales to the sub-millimeter regime. There is much experimental difficulty in measuring the power of Newton's law at short distance scales. For example, isolating the gravitational interaction between two objects a short distance apart from

electrostatic forces is an inherent problem. The best constraints stem from tabletop rotational experiments, Casimir force measurements, and van der Waals interaction experiments.

Astrophysics and Cosmology. Stringent constraints on the nature of extra dimensions also arise from astrophysical and cosmological observations. Supernovae reactions, in particular data from SN1987A, offer the best astrophysical constraints. For every SM reaction, there are analogous reactions involving the exchanges of KK fields, which enhance the predicted signal. The sizes of extra dimensions must not be too large or this prediction will not agree with experimental observations. Cosmological observations place constraints on new physics based on alterations that would be made in the physics of the early universe. For example, stable KK excitations of various fields may result in an abundance of exotic particles that are not observed in the known universe.

Collider Searches

Indirect Effects. If any of the SM fields are confined to the usual (3+1)-dimensional wall, there will be manifest violation of KK number conservation that will permit copious tree-level exchanges of KK excitations. In the original ADD model, this includes only the exchanges of gravitons. If the SM electroweak (EW) gauge fields also propagate in the bulk there will be larger effects from the exchanges of KK EW gauge bosons and there may also be tree-level corrections to the ρ-parameter. Among the best experimental data for indirect effects are EW precision measurements. These KK exchanges will reduce, or in some instances enhance, the SM production rate for

two SM fields colliding and producing SM final states. The sizes of extra dimensions play an integral role in the size of this reduction or enhancement, enabling bounds to be placed on their sizes.

Direct Production. If the collider energy is high enough compared to the scale of the KK excitations, it may be possible to directly produce KK excitations at near-future colliders. Depending on the model, this may include the direct production of a tower of KK gravitons, or the direct production of the lowest-lying KK excitations of various SM fields. These KK excitations are generally favored by cosmological considerations to decay very rapidly into SM fields. This results in an enhancement of the production rates for any combination of SM fields that is normally produced. It may also be possible to reconstruct the mass of the decaying KK excitation to establish the sizes of the extra dimensions.

Model-Building

Generic Features

Propagation. Conventional phenomenological models are string-inspired and therefore feature up to six extra compact dimensions. Gravity propagates in all of the extra dimensions. All extra dimensions are smaller than a millimeter in radius. Other fields may or may not propagate in one or more extra dimensions. They also employ the motivation of ADD for solving the hierarchy problem, which places the radii of any extra dimensions seen by SM fields on the order of an inverse-TeV, otherwise their KK excitations would have already been detected at high-energy colliders.

Kaluza-Klein Excitations. Fields propagating in compact dimensions naturally

have associated with them a tower of KK excitations arising from the imposed boundary conditions. The masses of the various KK modes differ by multiples of the compactification scale. Thus, the mass of the lowest-lying KK excitation of the graviton is 10 MeV or less, while the mass of the lowest-lying KK excitation of a SM field propagating in the bulk is on the order of a TeV. The zero modes are the usual SM fields and the graviton.

Models

ADD Model. Only the gravitons propagate into the extra compact dimensions in the class of models based on the approach of ADD [1], where the compactification is symmetric – *i.e.*, all of the N extra dimensions have the same compactification radius R. The fundamental Planck scale M_D is much smaller than the four-dimensional Planck scale M_P [2], which are related by

$$M_P^2 = M_D^{N+2} R^N \,. \tag{1}$$

Any SM fields that propagate into the bulk would have KK excitations with masses at the 10 MeV scale or less. The non-observation of such states up to about a TeV implies, in this class of models, that all of the SM fields are confined to the usual SM D_3 brane. Hence, the only source of new contributions to collider processes arises from the KK excitations of the graviton. Although the contributions of individual KK modes, with $(3+1)$D gravitational strength, to collider processes is extremely small, a very large number of such modes contribute in a TeV-scale collider process because the compactification scale μ is so small ($\mu \sim \text{mm}^{-1} \sim 10^{-3}$ eV). The net KK effect can cause a significant deviation from the SM production rates. Bounds on the

fundamental Planck scale from analyses of various collider processes are typically on the order of a TeV [3, 4] for these symmetric compactification models.

Fermi-Phobic Model. One way to permit some or all of the SM fields to propagate into the bulk is to relax the constraint that the extra compact dimensions be symmetric. Let us first consider the case where only the SM gauge bosons propagate into the bulk. As an example, it is possible to devise a model with asymmetrical compactification with five TeV^{-1}-size extra compact dimensions and one mm-size extra dimension, where the SM gauge bosons (and perhaps the Higgs boson) propagate into one of the TeV^{-1}-size dimensions. It was shown in Ref. [5] that this model satisfies all of the current astrophysical and cosmological constraints [6]. These asymmetric scenarios have a more direct effect in high-energy collider processes. Originating with the suggestion by Antoniadis [7], some of the studies that have been done for the collider phenomenology of the scenario in which the SM gauge bosons can propagate into the bulk, but where the SM fermions can not [8], include: the effects on EW precision measurements [9], Drell-Yan processes in hadronic colliders [10], $\mu^+\mu^-$ pair production in electron-positron colliders [10], EW processes in very high-energy electron-positron colliders [11], and multijet production in very high-energy hadronic colliders [12]. The typical bound on the compactification scale is 1–2 TeV.

Universal Model. The universal extra dimensions (UED) model, where all of the SM fields propagate into one or more extra compact dimensions, may intuitively seem more natural than selectively confining SM fields to the usual SM D_3 brane. This scenario may be thought of as a generalization of the usual SM wall to a D_{3+N} brane, where N represents the number of extra compact dimensions into which the SM

fields propagate. In this universal model of Appelquist, Cheng, and Dobrescu [13], KK number conservation governs all of the couplings involving KK excitations. In particular, each such vertex involves at least two KK excitations. At the tree-level, then, KK effects can not manifest themselves indirectly at colliders, and direct production is only possible in pairs of KK states. Although KK number conservation is broken at the one-loop level, the lowest-lying KK excitations of the light fermions and the massless gauge bosons do not decay to the SM zero-modes at any order without a special mechanism to support this decay. Thus, the lowest-lying KK excitations of the light fermions and the massless gauge bosons may be completely stable. Possible decay mechanisms have been proposed in the literature [13, 14, 15]. Collider bounds for this universal scenario are comparatively light: The current mass bound [13, 15, 16] for the first KK excited modes is relatively low ($\sim$ 350-400 GeV).

Additional Models. It is possible to construct a variety of models in the process of selecting which fields to confine to the SM wall. The possibilities include: The leptophobic model, in which only the quarks and gauge bosons propagate in the bulk; the leptophilic model, where only the leptons and gauge bosons propagate in the bulk; the chromophobic model, in which only the quarks and gluons propagate in the bulk; the chromophilic model, where the quarks and gluons are confined to the SM wall; a scenario where the gluons propagate in one extra dimension of a given size, the EW gauge bosons and leptons propagate in another extra dimension of a given size, and the quarks propagate in both extra dimensions; and models where different particles are localized at different points along the extra dimensions. In analogy with Z' physics, if a significant discrepancy between a measurement and a SM prediction

results in a near-future collider experiment, some of these models may be analyzed with attempts to explain such a discrepancy without disturbing the vast realm of data for which experiment and SM predictions are in overwhelming agreement.

Overview

General Remarks

Model Dependence. The low-energy phenomenology of superstring-inspired models with large extra compact dimensions depends on the mechanism of new physics by which the SM fields are constrained, if at all, to motion in the usual D_3 brane of the usual three spatial dimensions. It might naively be speculated that as more SM fields are free to propagate into the bulk, then the collider bounds on the compactification scale would significantly strengthen. A non-universal model where the gauge bosons propagate into the bulk, but the fermions are confined to the usual SM D_3 brane, for example, does produce more stringent collider bounds than a model where all of the SM fields are confined to the D_3 brane. However, scenarios with universal extra dimensions, in which all of the SM fields propagate into the bulk, have much weaker collider bounds.

Kaluza-Klein Number. This is due to tree-level KK number conservation, which dictates that colliding SM initial states cannot produce single KK excitations and also forbids tree-level indirect collider effects. In the non-universal scenarios, the SM fields that are confined to the D_3 brane appear in the Lagrangian with delta functions, thereby permitting couplings that violate KK number conservation.

Specifics

Considerations. Two phenomenological string-inspired models with extra dimensions are analyzed in detail. This includes the fermi-phobic model and the UED model. The SM fields that are not confined to the wall are assumed to all propagate into one and the same extra compact dimension. The effects of the KK excitations of the graviton are neglected because the dominant effects are due to the KK excitations of the SM fields (except in the fat-brane mechanism for the decays of UED fields, in which case the KK gravitons play a crucial role in the decay processes). When any SM fields cannot propagate along a particular extra compact dimension, it is assumed that all of these fields are localized at the same position along that compact dimension. These analyses are performed at the tree-level (leading order). Constraints on the size of the extra dimensions are placed for each scenario based on predictions for the production rates of various final state pairs relative to the relevant SM background.

Fermi-Phobic Scenario. As in the scenario proposed in Ref. [5], only the SM gauge bosons (and perhaps the Higgs boson) propagate into one of the TeV^{-1}-size extra dimensions.[‡] The best discovery prospects for KK excitations arise from the effects that the KK excitations of the gluons have on multijet production at the LHC. At the LHC energy, substantial deviations from the SM predictions are found for dijet final states up to a compactification scale of about 7 TeV; whereas for the Tevatron, the KK contribution only exceeds the SM background for small compactification

[‡]However, these results apply to any compactified string model in which the gluons propagate into one such extra dimension.

scales ($\lesssim$ 2.0 TeV). For the direct production of a $g^\star$ on-shell at the LHC, which subsequently decays into q-$\bar{q}$ pairs, the effect is not as pronounced as the dijet case, but is still significant. The contribution of the production of two on-shell $g^\star$'s is much less significant.

Also investigated are the effects that the KK excitations of the EW gauge bosons have on various e^+e^- collider processes. These effects are the modifications to the SM cross sections which arise from the exchanges of KK excitations of the EW gauge bosons. Included in are dijet production, associated Higgs production, single photon production, muon pair production, and Bhabha scattering. Although the compactification scale must be quite small ($\lesssim$ 2 TeV) for a 6% effect to be observed at the LEP2 energies, substantial deviations are found from the SM cross sections for a future collider with running at a collider energy of 600 GeV (e.g., a compactification scale of 3.5 TeV produces an effect of 20% for muon pair, dijet, and Higgs production), and an even greater effect is predicted at higher energies.

UED Scenario. A detailed study is made of the collider implications of the universal scenario, in which all of the SM fields propagate into one TeV^{-1}-size extra compact dimension. The dominant constraints on the size of the extra dimension stem from QCD effects at proton-proton collisions at the Tevatron and prospective proton-antiproton collisions at the LHC. The effects that these KK excitations have on the cross sections are calculated for the pair production of KK excitations of the gluons, $g_n^\star$, and two distinct KK quark towers, $q_n^\bullet$ and q_n°, in proton-antiproton collisions. The signatures of these KK excitations depend on the stability of the lowest-lying KK excitations of the light quarks and gluons. The Tevatron Run I mass bound for

KK quark and gluon final states is about 350–400 GeV, while Run II can push this limit up to 450–550 GeV, depending on the luminosity. The LHC can probe much further: The LHC will either discover UED KK excitations of the quarks and gluons or extend the mass limit to about 3 TeV.

In addition to QCD effects, there are EW effects from the KK excitations. Because KK excitations must be pair-produced and can not simply contribute to EW processes via virtual exchanges, tree-level effects will be difficult to detect at near-future e^+e^- colliders. Indeed, the recent LEP2 energy was about half the current bound on the mass of the lowest-lying KK excitation. Eventually, LEP-type colliders may be up and running that will have the potential to directly produce UED KK excitations, but until such time EW effects will be predominant at high-energy hadronic colliders such as the LHC. The LHC can probe 2-3 times further for QCD effects than EW effects, but the EW signal is much cleaner, especially when there are no final state jets. These results are therefore significant for potentially offering support if QCD measurements detect hints of universal extra dimensions, and may stand out better against SM backgrounds.

II

FORMALISM

General Remarks

Model Comparisons

Similarities. The procedure for obtaining the effective 4D theory is the same in the fermi-phobic and universal models. The interactions among gauge bosons are also identical in the two scenarios, as are the gauge boson propagators, gauge boson masses, and summation over polarizations. Similarly, the KK towers of the gauge bosons are identical in the two models.

Distinguishing Features. In the UED model, KK number is conserved in all interactions. However, in the fermi-phobic model, the SM wall can absorb unbalanced 5D momentum in interactions involving fermions, permitting a KK vertex with two fermions coupling to a single gauge boson. This provides a natural decay mechanism for the KK excitations that is not available in the UED scenario.

→ Also, in the UED scenario, there are two towers of KK fermions corresponding to each SM fermion, while in either scenario there is just one tower of KK gauge bosons corresponding to each SM gauge boson. This can be attributed to different multiplet structure corresponding to a theory with an odd versus an even number of dimensions. In the usual 4D SM, each 4D fermion state is a two-component Weyl spinor, while the analogous 5D fermion multiplets consist of massless four-component vector-like fermions.

Effective Theory

Procedure. The interest lies in tree-level parton subprocesses involving the exchanges or direct production (or both) of KK excitations of gauge bosons. The starting point is the generalization of the 4D SM Lagrangian density to the 5D Lagrangian density. The 5D fields can be Fourier expanded in terms of the extra dimension. Integration over the fifth dimension then yields the effective 4D Lagrangian density, which includes the usual 4D SM Lagrangian density plus terms involving the KK excitations of the SM gauge fields.

Feynman Rules. These KK terms dictate the possible couplings that the KK excitations can have both with each other and with the SM fields, and provide the Feynman rules for these vertices as well as the KK propagators. Because the form of the KK terms that results in the effective 4D Lagrangian density is identical to the form of the SM terms, the Feynman rules for the allowed KK interactions are proportional to the corresponding SM interactions. Similarly, the Feynman rules for the KK propagators and summation over KK gauge boson polarizations are the same as in the SM apart from the difference in mass.

Fermi-Phobic Model

QCD Interactions

Five Dimensions. In the model under consideration, the SM gauge bosons can propagate into one large extra compact dimension. The terms in the 5D Lagrangian density relevant to the QCD interactions are (1) the terms involving the contraction

of the 5D gluon field strength tensors $F^a_{MN} = \partial_M A^a_N - \partial_N A^a_M - g_5 f^{abc} A^b_M A^c_N$ with 5D indices $M, N \in \{0, 1, ..., 4\}$, where g_5 is the 5D strong coupling and a,b,c are the usual gluon color indices; and (2) the terms involving the quark fields, which contain a delta function to constrain the SM fermions to the D_3 brane:

$$\mathcal{L}_5 = -\frac{1}{4} F^a_{MN} F^{MNa} + i\bar{q}\gamma^\mu D_\mu q \delta(y) \,. \tag{2}$$

Here, D_μ is the usual 4D covariant derivative, μ,ν are the usual 4D spacetime indices, and the compactified extra dimension coordinate y is related to the radius of the extra dimension r by $y = r\phi$.

Compactification. Compactification on a S^1/Z_2 orbifold with the orbifold symmetry $y \to -y$ (a circle with the identification that the point on the other side of $y = 0$ has the same value) is considered such that $A^a_\mu(x, -y) = A^a_\mu(x, y)$, and the gauge choice $A^a_4(x, y) = 0$ is imposed. This is the unitary gauge. The 5D gluon field $A^a_\mu(x, y)$ can then be Fourier expanded in terms of the compactified dimension y as

$$A^a_\mu(x, y) = \frac{1}{\sqrt{\pi r}} \left[A^a_{\mu 0}(x) + \sum_{n=1}^{\infty} A^a_{\mu n}(x) \cos(n\phi) \right] , \tag{3}$$

where the normalization of $A^a_0(x)$ is one-half that of $A^a_n(x)$. When the 5D Lagrangian density is integrated over the extra dimension y, this sum represents a tower of KK excitations $A^a_{\mu n}(x)$ of the gluon field. The $n = 0$ mode gluon is identified with the observed massless gluon of the SM, denoted by g, while the $n > 0$ KK modes, denoted by $g^\star_n$, have masses $m_n = n\,\mu$ where μ is the compactification scale $(1/r)$. It will prove convenient to refer to the $n = 0$ and $n > 0$ modes separately by letting "gluon" or g represent just the $n = 0$ mode, and letting "KK excitation of the gluon" or $g^\star$ or $g^\star_n$ strictly imply $n > 0$.

Vertex Factors. The detailed procedure for integrating over the fifth dimension y to obtain, in the effective 4D theory, the factors for the allowed vertices involving KK excitations of the gluons may be found in the Appendix A, and lead to the coupling strengths displayed in Fig. 1. Notice that a single $g^\star$ can couple to quarks, but not to gluons. Furthermore, quark-less vertices with N $g^\star$'s only have non-vanishing coupling strengths if the modes n_1,n_2,...,n_N of the $g^\star$'s satisfy the relation

$$|n_1 \pm n_2 \pm \cdots \pm n_{N-1}| = n_N \,. \tag{4}$$

Although this relation, Eq. (4), governs the possible vertices, it is not a law expressing 5D momentum conservation for $N \to M$ processes: For example, a $g^\star$ can not decay into gluons at the tree level, although this process is permitted when a quark loop is introduced. Also worth noting are the factors of $\sqrt{2}$, which originate from the different rescaling of the $n = 0$ and $n > 0$ modes, necessary to obtain canonically normalized kinetic energy terms in the effective 4D Lagrangian density [17].

Propagators and Polarization Sums. Another difference between the Feynman rules for the g and the $g^\star$ lies in the propagator. The $g^\star$ propagator is that of a usual massive gauge boson, shown here in the unitary gauge:

$$-i\Delta^{ab}_{\mu\nu n}(p^2) = -i\delta^{ab}\frac{g_{\mu\nu} - \frac{p_\mu p_\nu}{m_n^2}}{p^2 - m_n^2 + i m_n \Gamma_n} \,. \tag{5}$$

At tree-level, the $g^\star_n$ decays into $q\bar{q}$ pairs with (total) width $\Gamma_n = 2\,\alpha_s(Q) m_n$.[§] The decay width can not be neglected because the subprocess energy $\sqrt{\hat{s}}$ runs up to 14 TeV at the LHC, while interest lies in TeV-scale compactification. For diagrams where a virtual g or $g^\star$ exchanges between two quark pairs (*e.g.*, in $q\bar{q} \to q\bar{q}$), there

[§]The top quark mass is negligible relative to the very heavy $g^\star$.

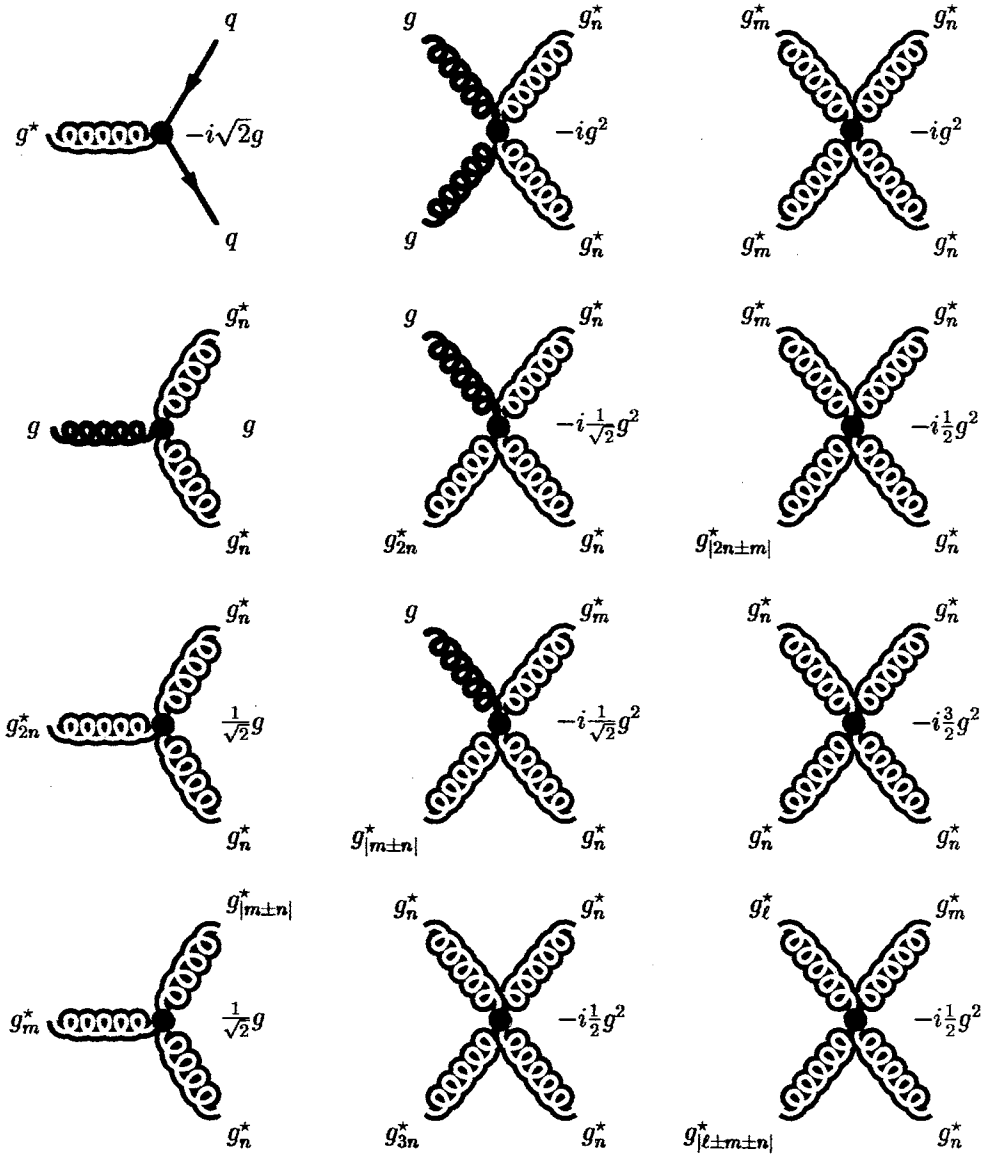

Figure 1: Relative coupling strengths of vertices involving $g^\star$'s. Only the overall factors are shown: The q-$\bar{q}$-$g^\star$ vertex also involves the SU(3) matrix element and the Dirac γ_μ matrix; triple vertices of g's and $g^\star$'s also include the usual SU(3) structure functions and the momenta factors; and quadruple vertices of g's and $g^\star$'s also contain the usual structure function factors as well as the metric tensors $g_{\mu\nu}$. Here, n, m, and ℓ are distinct positive integers ($n \neq m \neq \ell$).

is the usual diagram with the g propagator in addition to a tower of diagrams with $g_n^\star$ propagators, or, equivalently, an effective propagator given by the sum

$$\Delta_{eff}(p^2) = c_0\Delta_0(p^2) + \sum_{n=1}^{\infty} c_n\Delta_n(p^2)\,. \tag{6}$$

Notice that c_n incorporates the different q-$\bar{q}$-g and q-$\bar{q}$-$g_n^\star$ vertex factors (*i.e.*, $c_0 = 1$, $c_{n>0} = 2$). This effective propagator can be generalized to the case of arbitrary vertices with appropriate choices of the c_n factors (including setting c_n equal to zero when either vertex is forbidden).

The mass of the $g^\star$ also enters into the expression for the cross section via summations over polarization states when external $g^\star$'s are present. For the direct production of $g^\star$'s, the summation of polarization states is given by

$$\sum_\sigma \epsilon_{\mu n}^{a*}(k,\sigma)\epsilon_{\nu n}^{b}(k,\sigma) = \left(-g_{\mu\nu} + \frac{k_\mu k_\nu}{m_n^2}\right)\delta^{ab}\,. \tag{7}$$

Compare this to the case of external g's, in which case a projection such as

$$\sum_\sigma \epsilon_{\mu}^{a*}(k,\sigma)\epsilon_{\nu}^{b}(k,\sigma) = \left[-g_{\mu\nu} + \frac{(\eta_\mu k_\nu + \eta_\nu k_\mu)}{(\eta\cdot k)} - \frac{\eta^2 k_\mu k_\nu}{(\eta\cdot k)^2}\right]\delta^{ab} \tag{8}$$

can be made to eliminate unphysical longitudinal polarization states (and thereby satisfy gauge invariance), for arbitrary four-vector η_μ.

EW Interactions

Five Dimensions. As it is unlikely that a significant number of lowest-lying KK excitations will be directly produced in the near future at e^+e^- colliders, the focus here is on tree-level processes involving the exchanges of KK excitations of the EW gauge bosons. This necessarily restricts us to the case where the initial and final state fermions are each confined to the SM D_3 brane since otherwise, as shall be

seen shortly, the couplings for the processes of interest here are either zero or highly suppressed when KK number is not conserved, depending on which fields see the extra dimensions. Thus, for simplicity, considered is the case in which the EW gauge bosons can propagate into a single extra TeV^{-1}-size dimension, but where the SM fermions are restricted to lie on the SM wall (at the same location in the extra dimension). As for the Higgs boson, it is restricted to lie on the SM D_3 brane when associated Higgs production is investigated (else there is either no effect or a suppressed effect).

The terms in the 5D Lagrangian density that involve fermion fields contain a delta function to constrain the SM fields to the usual 4 spacetime dimensions, and similarly for terms involving the Higgs field in the case in which the Higgs does not propagate in the bulk. The relevant parts of the 5D Lagrangian density can be expressed as

$$\mathcal{L}_5 = \Big[\mid \Xi_M H \mid^2 + i g_5 \bar{f} \gamma^\mu D_\mu f \delta(y) \Big], \tag{9}$$

where f is a SM fermion field, H represents the Higgs doublet(s), D_M with 5D spacetime index $M \in 0, 1, \ldots, 4$ is the 5D generalization of the usual covariant derivative D_μ with 4D spacetime index μ, the factor $\mid \Xi_M H \mid^2$ denotes $\mid D_M H \mid^2$ for a Higgs propagating in the bulk and $\mid D_\mu H \mid^2 \delta(y)$ for a Higgs localized to the SM boundary, and the compactified extra dimension coordinate y is related to the radius of the extra dimension r by $y = r\phi$.

Compactification. Again compactification on a S^1/Z_2 orbifold is considered with the identification $\phi \to -\phi$. In terms of the compactified dimension y, an EW gauge field $A_\mu(x, y)$ can then be Fourier expanded as

$$A_\mu(x, y) = \frac{1}{\sqrt{\pi r}} \Big[A_{\mu 0}(x) + \sqrt{2} \sum_{n=1}^{\infty} A_{\mu n}(x) \cos(n\phi) \Big]. \tag{10}$$

The normalization for the $n = 0$ field $A_0(x)$ is one-half that of the $n > 0$ field $A_n(x)$. Integration over y results in a tower of $A_{\mu n}(x)$ KK excitations. The $n = 0$ modes of the 5D photon, $W^{\pm}$, and the Z are identified as the SM photon, $W^{\pm}$, and Z. The $n > 0$ KK modes of these fields are represented with a star ($\star$), as in $\gamma_n^{\star}$.

Vertex Factors. The detailed procedure for integrating over the fifth dimension y to obtain, in the effective 4D theory, the factors for the allowed vertices involving KK excitations of the EW gauge bosons is similar to the procedure for the couplings of quarks and gluons to KK excitations of the gluons. The difference is that any Higgs fields confined to the boundary induce mixing terms [17] between the EW gauge bosons and their KK excitations. This causes a slight reduction in the couplings involving KK excitations compared to the case in which the Higgs fields propagate into the extra dimension; in addition, previously forbidden couplings are allowed with a suppression factor. However, because this mixing is highly suppressed (by a factor of $\sim m_W^2/\mu^2$), only the couplings given by the case in which the Higgs fields propagate into the bulk are used, to a good approximation. The couplings for the vertices involving KK excitations of the A^{μ}, B^{μ}, and C^{μ} fields are then given in terms of the corresponding couplings between SM fields by the factors given in the previous section for purely gluonic couplings (with only a few subtle differences); the corresponding couplings for KK excitations of the photon, $W^{\pm}$, and Z are then related to the former via the usual mixing relations. In particular, there is a factor of $\sqrt{2}$ relative to the analogous SM coupling for a vertex involving a single KK excitation and two SM fermions confined to the SM D_3 brane, which originates from the different rescaling of the $n = 0$ and $n > 0$ modes necessary to obtain canonically normalized kinetic

energy terms in the effective 4D Lagrangian density [17]. Also worth noting is that a single $X_n^\star$ can not couple to two (or three) Y's, where $X, Y \in \{\gamma, W^\pm, Z\}$ and $X_n^\star$ denotes a KK excitation of gauge boson X with mode $n > 0$. In fact, $X^\star$'s can only couple to other $X^\star$'s and $Y^\star$'s if the modes $n_1, n_2, \ldots, n_N$ of these KK excitations satisfy KK number conservation.

Propagators and Polarization Sums. Another difference between the Feynman rules for the EW gauge bosons $\{X\}$ and their KK excitations $\{X_n^\star\}$ is that the KK excitations are considerably heavier. For a compactification scale $\mu = 1/r$, the mass of the nth KK excitation is:

$$m_{X_n^\star} = \sqrt{m_X^2 + n^2\mu^2}\,. \tag{11}$$

The $X_n^\star$ propagator is that of a usual massive gauge boson:

$$-i\Delta_{\mu\nu}(X_n^\star, p^2) = -i\frac{g_{\mu\nu} - \frac{p_\mu p_\nu}{m^2_{X_n^\star}}}{p^2 - m^2_{X_n^\star} + i m_{X_n^\star}\Gamma_{X_n^\star}}\,. \tag{12}$$

At tree-level, the $W_n^\star$ and $Z_n^\star$ have the same decay rates as the W and Z except for a factor of $2\frac{m_{W_n^\star}}{m_W}$ for the $W_n^\star$ and similarly for the $Z_n^\star$; also, the KK excitations are heavy enough to include the top quark in the decay rates. The $\gamma_n^\star$ decays to fermion pairs with total width $\frac{14}{3}\alpha(m_{\gamma_n^\star})m_{\gamma_n^\star}$.[¶] For diagrams where a $X_n^\star$ exchanges between two fermion pairs (*e.g.*, in $e^+e^- \to t\bar{t}$), there is the usual diagram with the X propagator in addition to a tower of diagrams with $X_n^\star$ propagators, or, equivalently, an effective propagator given by the sum

$$\Delta_{eff}(X, p^2) = c_{X_0}\Delta(X_0, p^2) + \sum_{n=1}^{\infty} c_{X_n^\star}\Delta(X_n, p^2)\,. \tag{13}$$

The factors $\{c_{X_n}\}$ incorporate the different f_1-f_2-X and f_1-f_2-$X_n^\star$ vertex factors (*i.e.*,

[¶]The top quark mass is negligible relative to the very heavy KK excitations.

$c_{X_0} = 1$, $c_{X_{n>0}} = 2$). This effective propagator can be generalized to the case of arbitrary vertices via adjustment of the c_{X_n} factors (including setting c_{X_n} equal to zero when either vertex is forbidden).

UED Model

QCD Interactions

Five Dimensions. The 4D SM quark multiplets for one generation are denoted by $Q_L^{\rm SM}(x)$, $U_R^{\rm SM}(x)$, and $D_R^{\rm SM}(x)$. For example, the first generation is:

$$Q_L^{\rm SM}(x) = q_L(x) = \begin{pmatrix} u(x) \\ \\ d(x) \end{pmatrix}_L , \quad U_R^{\rm SM}(x) = u_R(x) , \quad D_R^{\rm SM}(x) = d_R(x) . \tag{14}$$

Each 4D state is a two-component Weyl spinor. The analogous 5D quark multiplets consist of massless four-component vector-like quarks, which are denoted by $Q(x,y)$, $U(x,y)$, and $D(x,y)$. When these 5D fields are decomposed into 4D fields, corresponding to each 4D field are a left-handed and right-handed zero mode. Each mode is a two-component Weyl spinor in 4 dimensions.

Compactification. Half of the zero modes, which are not present in the 4D SM, may be projected out via the simple orbifold compactification choice, S_1/Z_2 (Z_2:$y \to -y$). The gauge fields polarized along the usual SM directions must be even under $y \to -y$ such that the zero modes will correspond to the usual 4D gauge fields, which implies that the gauge fields polarized along the y direction must be odd. For the quark fields, each of the KK ($n > 0$) modes for each multiplet will have a left-chiral and right-chiral part. The $Q_L^n(x)$, $U_R^n(x)$, and $D_R^n(x)$ components must be associated with the part of $Q(x,y)$, $U(x,y)$, and $D(x,y)$ that is even under $y \to -y$ in order to recover the

appropriate SM chiral zero mode states. The remaining components, $Q_R^n(x)$, $U_L^n(x)$, and $D_L^n(x)$, must be associated with the part of $Q(x,y)$, $U(x,y)$, and $D(x,y)$ that is odd under $y \to -y$ such that the zero modes not observed in the SM will be projected out. Each of the 5D multiplets $Q(x,y)$, $U(x,y)$, and $D(x,y)$ can therefore be Fourier expanded in terms of the compactified dimension y as

$$Q(x,y) = \frac{1}{\sqrt{\pi R}}\left\{\begin{pmatrix} u(x) \\ d(x) \end{pmatrix}_L + \sqrt{2}\sum_{n=1}^{\infty}\left[Q_L^n(x)\cos\left(\frac{ny}{R}\right) + Q_R^n(x)\sin\left(\frac{ny}{R}\right)\right]\right\} \quad (15)$$

$$U(x,y) = \frac{1}{\sqrt{\pi R}}\left\{u_R(x) + \sqrt{2}\sum_{n=1}^{\infty}\left[U_R^n(x)\cos\left(\frac{ny}{R}\right) + U_L^n(x)\sin\left(\frac{ny}{R}\right)\right]\right\} \quad (16)$$

$$D(x,y) = \frac{1}{\sqrt{\pi R}}\left\{d_R(x) + \sqrt{2}\sum_{n=1}^{\infty}\left[D_R^n(x)\cos\left(\frac{ny}{R}\right) + D_L^n(x)\sin\left(\frac{ny}{R}\right)\right]\right\}. \quad (17)$$

Fermion Masses. The SM fermion masses arise from the Yukawa couplings through the Higgs vacuum expectation value (VEV), while the KK modes receive mass from the kinetic term in the 5D Lagrangian density as well as from the Yukawa couplings via the Higgs VEV's. First calculated is the mass arising from the kinetic term. The 5D Lagrangian density for the kinetic terms and interactions of the 5D gluon field $A_M^a(x,y)$ with the 5D $Q(x,y)$ fields are:

$$\mathcal{L}_5 = i\bar{Q}(x,y)\left\{\Gamma^M\left[\partial_M + ig_5 T^a A_M^a(x,y)\right]\right\}Q(x,y). \quad (18)$$

Here, g_5 is the 5D strong coupling, M is the 5D analog of the Lorentz index μ, *i.e.*, $M \in \{\mu, 4\}$, and the 5D gluon fields $A_M^a(x,y)$ can be Fourier expanded in terms of the compactified extra dimension y just as in the fermi-phobic case:

$$A_\mu^a(x,y) = \frac{1}{\sqrt{\pi R}}\left[A_{\mu 0}^a(x) + \sqrt{2}\sum_{n=1}^{\infty}A_{\mu,n}^a(x)\cos(\frac{ny}{R})\right] \quad (19)$$

$$A_4^a(x,y) = \frac{\sqrt{2}}{\sqrt{\pi R}}\sum_{n=1}^{\infty}A_{4,n}^a(x)\sin(\frac{ny}{R}). \quad (20)$$

The normalization of $A_0^a(x)$ is one-half that of the $n > 0$ modes, necessary to obtain canonically normalized kinetic energy terms for the gluon fields in the effective 4D Lagrangian density [17]. As previously stated, under the transformation $y \to -y$, the decomposed gluon fields transform as $A_\mu^a(x,-y) = A_\mu^a(x,y)$ and $A_4^a(x,-y) = -A_4^a(x,y)$. The choice here is to work in the unitary gauge, where the gauge choice $A_{4,n}^a(x) = 0$ [18] can be applied.

Integrating the kinetic part of Eq. (18) over the compactified dimension y yields the 4D Lagrangian density, and similarly for $U(x,y)$ and $D(x,y)$. This effective 4D Lagrangian density consists of the usual kinetic terms for the SM fields, kinetic terms for the massive Dirac spinors $Q^n(x)$, $U^n(x)$, and $D^n(x)$, and mass terms for the KK excitations with mass $M_n^{KK} = n/R = n\mu$, where μ is the compactification scale, $1/R$.

Thus, in the absence of the Higgs mechanism, the KK excitations have masses given by $M_n = M_n^{KK} = n/R = n\mu$. Additional mass contributions from the Yukawa couplings of the 5D quark multiplets via the Higgs VEV's are obtained by writing the 5D Lagrangian density for the couplings of the 5D quark multiplets to the 5D Higgs field, Fourier expanding these 5D fields in terms of the compactified dimension y, and integrating over the extra dimension. The eigenvalues of the resulting mass matrix give the net mass M_n of the KK modes in terms of the mass of the corresponding quark field M_q and the mass from the compactification M_n^{KK}:

$$M_n = \sqrt{(M_n^{KK})^2 + M_q^2}. \tag{21}$$

Relative to the compactification scale, the SM quark masses are negligible except for the top mass M_t.

Quark Towers. Each KK $q_n^\bullet$ and q_n° state is identified as a combination of Q, U, and D. In the limit of massless SM quarks, this combination can be expressed as:

$$Q^n_{L,R}(x) \equiv P_{L,R} \begin{pmatrix} u^\bullet_n(x) \\ d^\bullet_n(x) \end{pmatrix}, \quad U^n_{R,L}(x) \equiv P_{R,L} u^\circ_n, \quad D^n_{R,L}(x) \equiv P_{R,L} d^\circ_n, \tag{22}$$

where the projection operators are defined as $P_{L,R} \equiv \frac{1}{2}(1 \mp \gamma_5)$. In general, there is an additional Yukawa contribution to the masses, in which the U_R and U_L fields contribute to the mass of the $q_n^\bullet$ via the Higgs VEV, and similarly for contributions to q_n° from Q_L and Q_R. For example, taking the SM c quark to be massless, the combination of the second-generation up-type quark component of the KK multiplet $Q^n_{2L}(x)$ with the second-generation up-type quark component of $Q^n_{2R}(x)$ is identified as the single KK charm quark $c^\bullet$, which receives KK mass $M_n = n\mu = 1/R$ from the kinetic term. There is a second KK tower corresponding to the SM charm quark, which comes from $U^n_{2R}(x)$ and $U^n_{2L}(x)$, denoted by c°. By $g^\star_n$ is denoted KK mode n of the gluon, and by $q^\bullet_n$ and q°_n are denoted denote KK mode n of two distinct towers of KK excitations of a given SM quark field q. Each KK quark tower contains terms that are even and odd under Z_2 parity. However, in KK quark pair production, the KK final states will be polarized with helicity corresponding to their even states ($Q_L(x)$, $U_R(x)$, and $D_R(x)$)in the cross channels, and the components associated with the odd part of the 5D fields ($Q_R(x)$, $U_L(x)$, and $D_L(x)$) will only show up in direct channel production.[‖] For KK quark-gluon production, the final KK states will

[‖]This relies on the expansion in Eq. 22, which is valid for KK excitations of massless SM quarks. Massive KK quarks receive an additional small mass contribution from the Higgs mechanism. Also, recall that the choice has been made to work in the unitary gauge with gauge choice, $A_4^{q^n}(x) = 0$.

again be polarized with helicity corresponding to the even states. This is because the projection operators ensure the conservation of Z_2 parity. Regarding the notation, n will be strictly nonzero unless explicitly stated otherwise.

Vertex Factors. The QCD interactions involving KK excitations include purely gluonic couplings as well as couplings with quark fields. The purely gluonic case was discussed in previously in the fermi-phobic QCD interaction section of the Formalism, and the resulting couplings are identical to those of this universal scenario. The Feynman rules for the QCD interactions involving the KK excitations of the gluons and the two towers of KK excitations corresponding to each of the quark fields can be obtained by integrating the second part of Eq. (18) over the compactified dimension y via Fourier expansion of the 5D fields in terms of y, and similarly for $U(x,y)$ and $D(x,y)$.

The detailed procedure for integrating over the fifth dimension y to obtain, in the effective 4D theory, the factors for the allowed vertices involving the $q_n^\bullet$ and q_n° fields may be found in the Appendix B, and lead to the coupling strengths displayed in Fig. 2. The states with helicity corresponding to the odd states under Z_2 parity ($Q_R(x)$, $U_L(x)$, and $D_L(x)$) only appear in couplings involving $q_n^\bullet$ $q_n^\bullet$ or $q_n^\circ q_n^\circ$, and do not show up when a SM quark is present. A SM quark can only couple to KK states with helicity corresponding to the even states (($Q_L(x)$, $U_R(x)$, and $D_R(x)$). The triple KK vertices with $q_n^\bullet$ and q_n° fields involve the integration of three cosines for the even parts and one cosine and two sines for the odd parts. This latter integration results in a minus sign relative to the first one whenever the KK gluon is more massive than either KK quark, which results in the presence of a γ_5 in these vertices. Note also

that the two towers $q_n^\bullet$ and q_n° do not couple to one another. The Feynman rules for the purely gluonic vertices are summarized in Ref. [12]. Notice that a single KK mode can not couple to SM fields. This is a consequence of the more general tree-level conservation of KK number, which dictates that N KK modes, n_1,n_2,...,n_N, can only couple to one another if they satisfy KK number conservation. KK number conservation strictly applies at every vertex, as well as for tree-level $N \to M$ processes, but is broken at the loop-level. The higher modes can therefore decay to the lower modes at the loop-level, but the lowest-lying KK modes of the light quarks and massless gluons will be completely stable unless there exists another form of new physics to serve as a decay mechanism. This point will be returned to in Section 5.

Propagators and Polarization Sums. The gluon propagators and summation over external polarizations are identical to those in the fermi-phobic case. The $q_n^\bullet$ and q_n° propagators have the form of a usual massive quark:

$$-i\Delta_n^{a'b'}(p^2) = i\delta^{a'b'}\frac{\not{p} + M_n}{p^2 - M_n^2 + iM_n\Gamma_q^n}. \tag{23}$$

The decay widths of the $g_n^\star$'s, $q_n^\bullet$'s, and q_n°'s depend on stability of the lowest-lying KK excitations of the up quark, down quark, and gluon. However, these decay widths are immaterial for production processes, since KK number conservation forbids any s-channel KK propagators from arising in tree-level subprocesses with initial SM fields.

EW Interactions

Five Dimensions. The multiplet structure of the 5D quark fields is identical to that presented for the QCD interactions of the UED model. The 5D lepton fields, $L(x,y)$, $E(x,y)$, and $N(x,y)$, also have the same structure. This is a reflection of

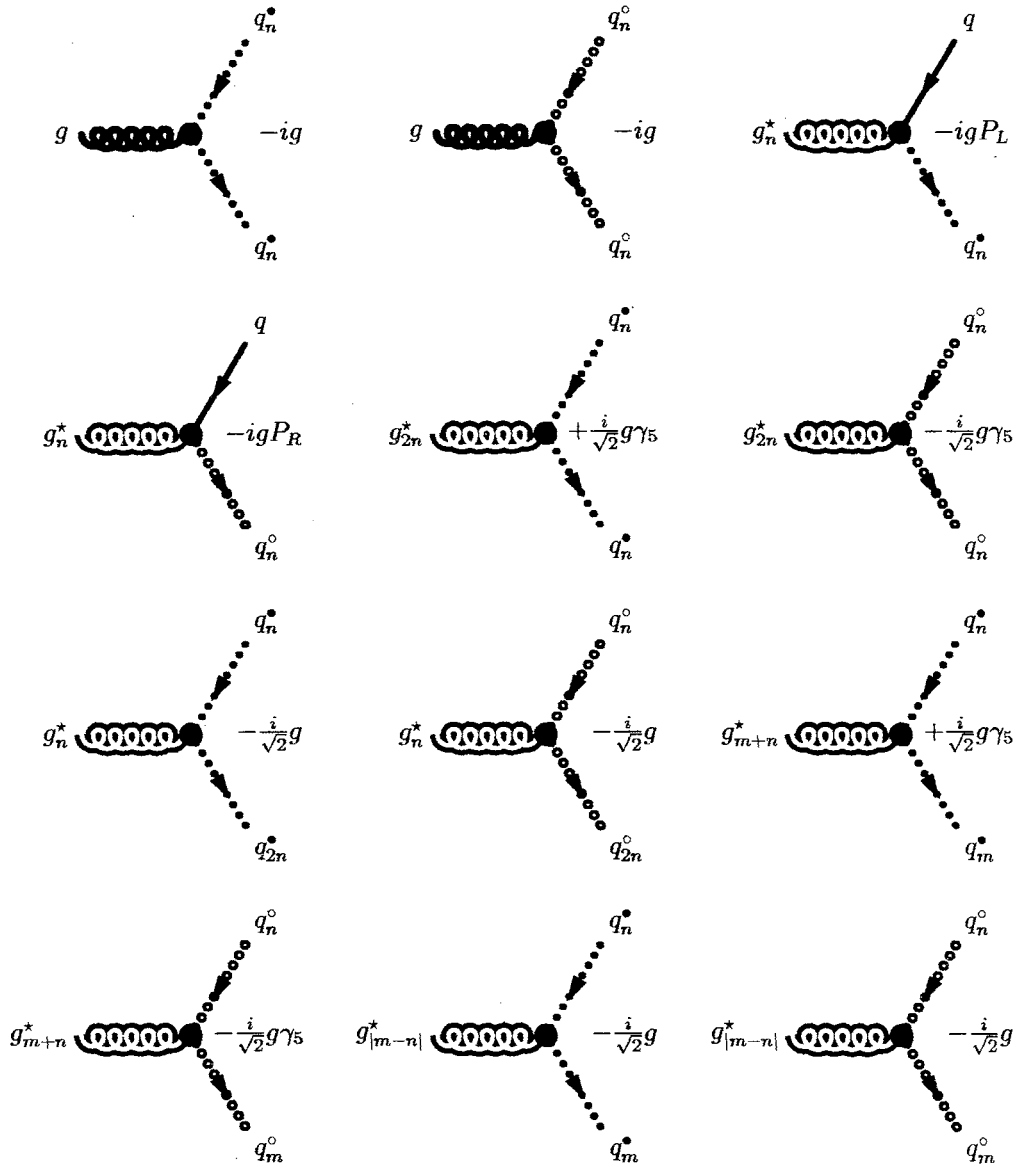

Figure 2: Relative coupling strengths of vertices involving $q_n^\bullet$'s and q_n°'s. Only the overall factors are shown: These vertices also involve the usual SU(3) matrix element and the Dirac γ_μ matrix. Here, n and m are distinct positive integers ($n \neq m$) and the projection operators are defined as $P_{L,R} \equiv (1 \mp \gamma_5)/2$.

the fact that the lepton and quark multiplets have the same structure in the 4D SM, and the procedure employed here based on a straightforward generalization to five dimensions. The 5D Lagrangian is simply the 5D EW fermi-phobic Lagrangian without the delta functions, just as in the QCD case.

Compactification. The same compactification scheme is employed as in the previous cases. The Fourier expansions of the EW gauge fields are identical to those of the fermi-phobic model, just as in the QCD case. The Fourier expansions of the quarks are the same as in the QCD interactions of the UED model. Also, the leptons have Fourier expansions in complete analogy with the quarks. Thus, two distinct KK towers correspond to each SM charged lepton and neutrino.

Mass Matrix. The mass matrix for the leptons is again completely analogous to that of the quarks. Therefore the masses of the KK leptons come in multiples of the compactification scale (neglecting the SM lepton masses). The masses of KK photons are also multiples of the compactification scale, while the KK excitations of the W and Z bosons add in quadrature.

Feynman Rules. The vertex factors for purely EW gauge interactions are identical to those of the fermi-phobic model. However, there are some novelties present in the vertex factors for the couplings of the fermions to EW gauge fields. KK excitations of the W boson only couple to one tower of SM fermions because of the left-handed projection operator normally associated with the W boson in the SM, and similarly for couplings of the SM W boson to KK fermions. KK excitations of the Z boson couple to a SM and KK fermion with the usual projections of the corresponding QCD interactions, while the SM Z boson couples to pairs of KK fermions just as in the

SM. The photon couples to fermions analogously to the gluon for the case of QCD interactions in the UED model. Nothing is new, compared to the KK Feynman rules for the prior cases, in the way of propagators and polarizations sums.

III

ANALYTICAL RESULTS

Fermi-Phobic Model

QCD Interactions

Dijet Production. For dijet production, all tree-level diagrams are included which do not contain any $g^\star$'s in the final state, since the $g^\star$'s would quickly decay into $q\bar{q}$ pairs, thereby producing additional jets.** Thus, the KK excitations only appear in two-jet diagrams via virtual $g^\star$ propagators. The net tree-level effect of the $g^\star$'s on dijet production is the replacement of the SM gluon propagator by an effective KK propagator, wherever five-momentum is conserved. Employing gauge invariance, the second term in Eq. (12) is dropped in this analysis of dijet production. It is then convenient to define $D_n(p^2)$ and $D_{\mathit{eff}}(p^2)$ as

$$\begin{aligned} D_n(p^2) &= \frac{c_n}{p^2 - m_n^2 + i m_n \Gamma_n} \\ D_{\mathit{eff}}(p^2) &= \frac{c_0}{p^2} + \sum_{n=1}^{\infty} c_n D_n(p^2) \,. \end{aligned} \tag{24}$$

Here, c_n represents the fact that the q-$\bar{q}$-g and the q-$\bar{q}$-$g_n^\star$ vertex factors differ by a $\sqrt{2}$ (*i.e.*, $c_0 = 1$, $c_{n>0} = 2$). In the amplitude-squared, it is therefore necessary to evaluate terms of the form

$$\frac{1}{2}\Big[D^\star_{\mathit{eff}}(\hat{v}) D_{\mathit{eff}}(\hat{w}) + D_{\mathit{eff}}(\hat{v}) D^\star_{\mathit{eff}}(\hat{w})\Big] = \sum_{m,n=0}^{\infty} c_m c_n \frac{\hat{v}_m \hat{w}_n + m_m \Gamma_m m_n \Gamma_n}{(\hat{v}_m^2 + m_m^2 \Gamma_m^2)(\hat{w}_n^2 + m_n^2 \Gamma_n^2)}, \tag{25}$$

**Neglected are the contributions from cases where multiple jets are produced, but only two of them pass the various cuts.

where $\hat{v}$ and $\hat{w}$ are any of the three usual (subprocess) Mandelstam variables (*i.e.*, $\hat{v}, \hat{w} \in \{\hat{s}, \hat{t}, \hat{u}\}$), and $\hat{v}'_n$ represents the subtraction of m_n^2 from $\hat{v}$ (*i.e.*, $\hat{v}'_n \equiv \hat{v}_n - m_n^2$). (In Eq. (25) an exception is made to include the $n = 0$ and $n > 0$ modes together for conciseness.) This sum converges somewhat rapidly:[††] Since $\sqrt{\hat{s}}$ runs up to 14 TeV for the LHC, the sum can be truncated after a couple dozen terms (*i.e.*, when n becomes at least a couple of times greater than 14 TeV $/\mu$, where μ is the compactification scale). The choice made here is $n_{max} = 50$. From five-momentum conservation, there are no internal $g^\star$'s for any tree-level dijet diagrams involving external gluons (*e.g.*, the KK excitations do not affect the process $q\bar{q} \to gg$). The diagrams to which the KK excitations do contribute are illustrated in Fig. 3.

The total dijet cross section $\sigma(pp \to 2\,\text{jets})$ is obtained from the individual subprocess cross sections $\hat{\sigma}(ab \to cd)$ and the parton distributions $f_{a/A}(x_A, Q)$ and $f_{b/B}(x_B, Q)$ by integrating over the momentum fractions x_A and x_B and summing over all possible subprocesses $ab \to cd$:

$$\sigma(pp \to 2\,\text{jets}) = \sum_{ab \to cd} \int_{4p_T^2/s}^{1} d\tau \frac{d\mathcal{L}}{d\tau} \hat{\sigma}(ab \to cd)\,. \tag{26}$$

Here, p_T is the transverse momentum and $d\mathcal{L}/d\tau$ is the parton luminosity:

$$\frac{d\mathcal{L}}{d\tau} = \int_{\tau}^{1} \frac{dx_A}{x_A} f_{a/A}(x_A, Q) f_{b/B}(x_B, Q)\,. \tag{27}$$

Single On-Shell $g^\star$ Production. Three-jet KK final states predominantly** arise

[††] When generalizing to the case where the gluons may propagate into more than one large extra dimension, the sum in the effective propagator is formally divergent. However, this problem has been widely addressed in the literature [19], where various solutions have been proposed.

**The contributions of virtual $g^\star$ exchanges for which no external on-shell $g^\star$'s are produced to the three-jet KK cross section contain an extra factor of $\alpha_S(Q)$ relative to the contribution of single on-

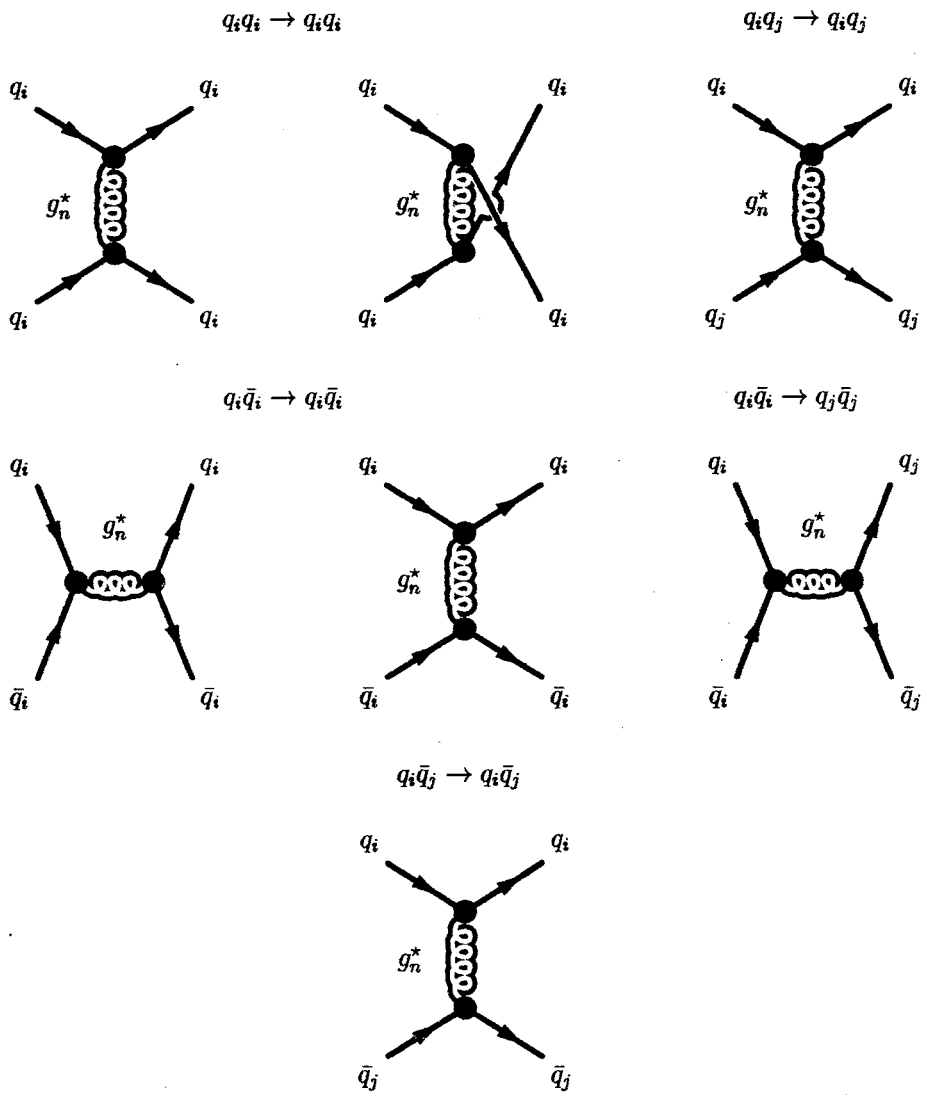

Figure 3: Dijet diagrams involving KK excitations of the gluons. The indices i and j represent distinct ($i \neq j$) quark flavors.

from subprocesses where a $g^\star$ is produced on-shell and subsequently decays into $q\bar{q}$, *e.g.*, via $q\bar{q} \to g_n^\star \to g_n^\star g \to q\bar{q}g$. The concentration is on the production of the $g^\star$, postponing the consideration of its subsequent decay for the meantime. The subprocesses satisfying five-momentum conservation for which a $g^\star$ is produced on shell are:

$$\begin{aligned} q\bar{q} &\to g_n^\star g \\ qg &\to qg_n^\star \\ \bar{q}g &\to \bar{q}g_n^\star , \end{aligned} \tag{28}$$

where the mode n of the external $g^\star$ is necessarily identical to that of any virtual $g^\star$'s. Therefore, there is no summation over modes in these propagators; instead, the three-jet cross section involves a summation over the possible modes ($n \geq 1$) of the external $g^\star$'s. The Feynman diagrams for these three KK subprocesses are illustrated in Fig. 4. The amplitude for $q\bar{q} \to g_n^\star g$ is

$$\begin{aligned} \mathcal{M}(q\bar{q} \to g_n^\star g) = &- i4\pi\alpha_s(Q)\bar{v}_j(p_1)\Big[T^e_{ki}T^f_{jk}\Big(\frac{V^t_{\rho\sigma}}{\hat{t}} + \frac{V^s_{\rho\sigma}}{\hat{s}'_n}\Big) \\ &+ T^f_{ki}T^e_{jk}\Big(\frac{V^u_{\rho\sigma}}{\hat{u}} - \frac{V^s_{\rho\sigma}}{\hat{s}'_n}\Big)\Big]u_i(p_2)\epsilon^{*\rho}_e(k_1)\epsilon^{*\sigma}_f(k_2)\,, \end{aligned} \tag{29}$$

where the scale Q is identified with the mass of the $g^\star$, $\hat{v}'_n$ represents (as before) subtraction of m_n^2 from the Mandelstam variable $\hat{v} \in \{\hat{s}, \hat{t}, \hat{u}\}$ (*i.e.*, $\hat{v}'_n = \hat{v} - m_n^2$), and the $V^v_{\rho\sigma}$ tensors are given by

shell $g^\star$ production. However, since virtual $g^\star$ exchange is significant for dijet production, the many virtual $g^\star$ exchange diagrams leading to three jets in the final state — for which no external $g^\star$'s are produced on shell — may also have a significant effect. Although these purely virtual exchange contributions are not calculated here, it is noted that they would likely enhance these results.

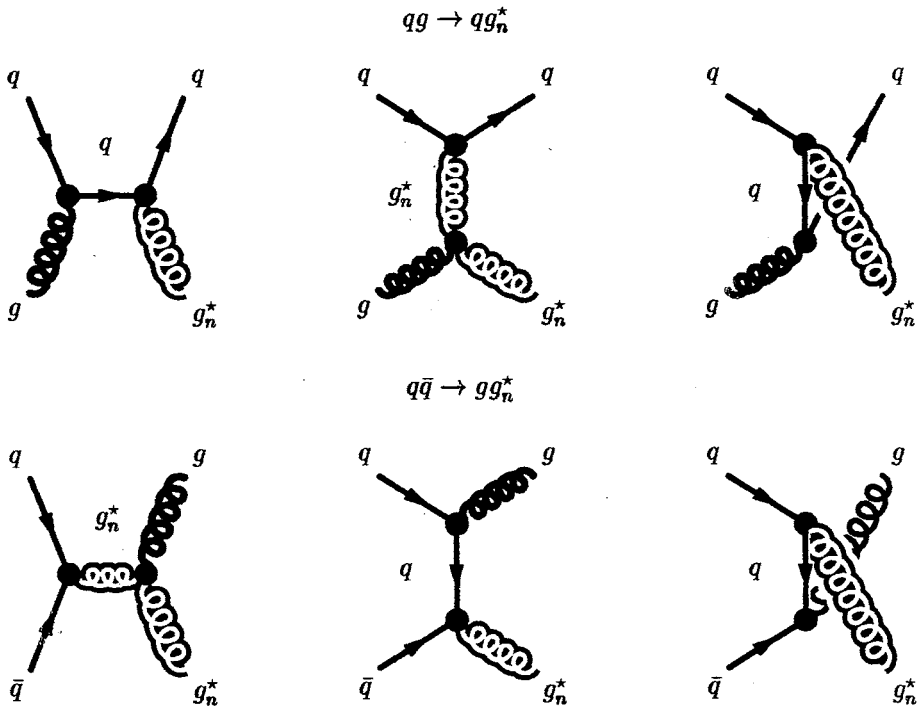

Figure 4: Diagrams involving the production of a single on-shell $g^\star$. The diagrams for $\bar{q}g \to \bar{q}g_n^\star$ are obtained by replacing q with $\bar{q}$ in the diagrams for $qg \to qg_n^\star$.

$$V^s_{\rho\sigma} = \sqrt{2}\gamma^\mu\Big[(k_2+2k_1)_\sigma g_{\mu\rho} + (-k_1+k_2)_\mu g_{\rho\sigma} - (2k_2+k_1)_\rho g_{\sigma\mu}\Big] \tag{30}$$

$$V^t_{\rho\sigma} = \sqrt{2}\gamma_\rho(\not{p}_1 - \not{k}_1)\gamma_\sigma \tag{31}$$

$$V^u_{\rho\sigma} = \sqrt{2}\gamma_\sigma(\not{k}_1 - \not{p}_2)\gamma_\rho\,. \tag{32}$$

After summing over final states and averaging over initial states, the resulting amplitude-squared is[††]

$$\bar{\sum}|\mathcal{M}(q\bar{q} \to g_n^\star g)|^2 = \frac{8}{27}\pi^2\alpha_S^2(Q)\Big[\Big(\frac{m_n^4}{\hat{s}'^2_n} + \frac{m_n^2}{\hat{s}'_n}\Big)\Big(8\frac{\hat{s}'^2_n}{\hat{t}\hat{u}} - 18\Big) - 17 + 4\frac{\hat{s}'^2_n}{\hat{t}\hat{u}} + 18\frac{\hat{t}\hat{u}}{\hat{s}'^2_n}\Big], \tag{33}$$

which is related to the amplitude-squared for $qg \to qg_n^\star$ via crossing symmetry:

[††] *FORM* [20], a symbolic manipulation program, is employed in the evaluation of the amplitudes-squared for single and double on-shell $g^\star$ production.

$$\bar{\sum}|\mathcal{M}(qg\to qg_n^\star)|^2 = \frac{1}{9}\pi^2\alpha_S^2(Q)\Big[\Big(\frac{m_n^4}{\hat{u}_n'^2}+\frac{m_n^2}{\hat{u}_n'}\Big)\Big(18-8\frac{\hat{u}_n'^2}{\hat{s}\hat{t}}\Big) + 17 - 4\frac{\hat{u}_n'^2}{\hat{s}\hat{t}} + 18\frac{\hat{s}\hat{t}}{\hat{u}_n'^2}\Big]. \tag{34}$$

The amplitude-squared for $\bar{q}g \to \bar{q}g_n^\star$ is in turn identical to that of $qg \to qg_n^\star$ by time-reversal invariance. Upon integration over $\hat{t}$, the single $g^\star$ on-shell production cross sections assume the form

$$\sigma_{KK}(pp\to g^\star+\text{jet}) = \frac{1}{2\pi}\sum_j\sum_{g_n^\star}\int\limits_{m_n^2/s}^1 dx_A \int\limits_{m_n^2/sx_A}^1 dx_B f_{a/A}(x_A,Q) f_{b/B}(x_B,Q)\int\limits_{-1}^1 dz\,\bar{\sum}|M_{jn}|^2\,\frac{\hat{s}_n'}{\hat{s}^2}, \tag{35}$$

where the first summation runs over all possible subprocesses j producing a single $g^\star$ on-shell, and the second summation is over all $g_n^\star$'s that can be produced for subprocess j in light of the given pp collider energy $\sqrt{s}$.[‡‡] Observe that $M_{jn}(m_n) = M_{j1}(nm_1)$ so that $\sum_{n=1}^{n_{max}} M_{jn}(m_n) = \sum_{n=1}^{n_{max}} M_{j1}(nm_1)$. Preparation has now been made to account for the decay of the $g_n^\star$ into $q\bar{q}$ pairs. Working in the narrow width approximation, the dimensionless solid angle $d\Omega_4/4\pi$ is integrated over to obtain the total single on-shell $g^\star$ cross section (prior to cuts):

$$\sigma_{KK}(pp\to\text{jet}+g^\star\to 3\,\text{jets}) = \int\frac{d\Omega_4}{4\pi}\sigma_{KK}(pp\to g^\star+\text{jet}). \tag{36}$$

[‡‡]Note that the scale $Q = m_n$ for the $n > 1$ modes exceeds the compactification scale μ. When $Q > \mu$, the running of $\alpha_s(Q)$ transforms from a logarithmic to a power law behavior [21]. This has the effect of reducing the contributions of the higher order modes to the total multijet cross sections [22], but only slightly at LHC energies since only a few KK modes can be produced on-shell.

Double On-Shell $g^\star$ Production. Double on-shell $g^\star$ production is analogous to single on-shell $g^\star$ production, except that in this case the predominant KK subprocesses involve the production of two on-shell $g^\star$'s which subsequently decay into $q\bar{q}$ pairs, *e.g.*, $q\bar{q} \to g \to g_n^\star g_n^\star \to q\bar{q}q\bar{q}$. Also, the single on-shell $g^\star$ case did not involve the $g_n^\star$-$g_m^\star$-$g_\ell^\star$ nor the g-g-$g_n^\star$-$g_n^\star$ vertices, which are now part of the picture. Focusing on the production of the $g^\star$'s for the present and applying five-momentum conservation, the subprocesses for which two $g^\star$'s are produced on shell are:

$$\begin{aligned} q\bar{q} &\to g_n^\star g_n^\star \\ q\bar{q} &\to g_n^\star g_m^\star \\ gg &\to g_n^\star g_n^\star , \end{aligned} \tag{37}$$

where the two external $g^\star$'s are necessarily in the same mode n for initial gluons, but not for initial quarks. The Feynman diagrams for these three KK subprocesses are illustrated in Fig. 5. The diagrams for $q\bar{q} \to g_n^\star g_n^\star$ are the same as for $q\bar{q} \to g_n^\star g$ except that the $\hat{s}$-channel diagram can have either a virtual g or a virtual $g_{2n}^\star$ propagator. Thus, the amplitude for this process is the same as that given by Eq. (29) with the $g_n^\star$ propagator replaced by g and $g_{2n}^\star$ propagators, where the coefficient of the $\hat{s}$-channel amplitude is reduced by $1/\sqrt{2}$ for the g case. Likewise, the subprocess $q\bar{q} \to g_n^\star g_m^\star$ is simply $q\bar{q} \to g_n^\star g_n^\star$ with the s-channel altered for the possible propagators and the mass of either external line altered by a factor of m/n. The amplitude for $gg \to g_n^\star g_n^\star$ is

$$\mathcal{M}(gg \to g_n^\star g_n^\star) = -\, i4\pi\alpha_s(Q)\Big(f^{abc} f^{cef} \frac{V^s_{\alpha\beta\rho\sigma}}{\hat{s}} + f^{bec} f^{acf} \frac{V^t_{\alpha\beta\rho\sigma}}{\hat{t}'_n} + f^{bfc} f^{ace} \frac{V^u_{\alpha\beta\rho\sigma}}{\hat{u}'_n} + V^{4abef}_{\alpha\beta\rho\sigma} \Big) \epsilon^\alpha_a(p_1) \epsilon^\beta_b(p_2) \epsilon^{*\rho}_e(k_1) \epsilon^{*\sigma}_f(k_2)\,, \tag{38}$$

where

$$V^s_{\alpha\beta\rho\sigma} = \Big[(-p_1+p_2)_\mu g_{\alpha\beta} + (2p_1+p_2)_\alpha g_{\beta\mu} - (p_1+2p_2)_\beta g_{\mu\alpha}\Big] \cdot \Big[(2k_1+k_2)_\sigma g_{\nu\rho} + (-k_1+k_2)_\nu g_{\rho\sigma} - (k_1+2k_2)_\rho g_{\sigma\nu}\Big] g^{\mu\nu} \tag{39}$$

$$V^t_{\alpha\beta\rho\sigma} = \Big[(p_1+k_1)_\mu g_{\beta\rho} + (p_1-2k_1)_\beta g_{\rho\mu} + (-2p_1+k_1)_\rho g_{\mu\beta}\Big] \cdot \Big[(2p_2-k_2)_\sigma g_{\alpha\nu} + (-p_2+2k_2)_\alpha g_{\nu\sigma} - (p_2+k_2)_\nu g_{\alpha\sigma}\Big] g^{\mu\nu} \tag{40}$$

$$V^u_{\alpha\beta\rho\sigma} = \Big[(p_1+k_2)_\mu g_{\beta\sigma} + (p_1-2k_2)_\beta g_{\sigma\mu} + (-2p_1+k_2)_\sigma g_{\mu\beta}\Big] \cdot \Big[(2p_2-k_1)_\rho g_{\alpha\nu} + (-p_2+2k_1)_\alpha g_{\nu\rho} - (p_2+k_1)_\nu g_{\alpha\rho}\Big] g^{\mu\nu} \tag{41}$$

$$V^{4abef}_{\alpha\beta\rho\sigma} = f_{abc}f_{efc}(g_{\alpha\rho}g_{\beta\sigma} - g_{\alpha\sigma}g_{\beta\rho}) + f_{aec}f_{fbc}(g_{\alpha\sigma}g_{\beta\rho} - g_{\alpha\beta}g_{\sigma\rho}) + f_{afc}f_{bec}(g_{\alpha\beta}g_{\sigma\rho} - g_{\alpha\rho}g_{\beta\sigma})\,. \tag{42}$$

The amplitudes-squared for these subprocesses, summed over final states and averaged over initial states, are obtained to be

$$\bar{\sum}|\mathcal{M}(q\bar{q} \to g_n^\star g_n^\star)|^2 = \frac{8}{27}\pi^2\alpha_S^2(Q)\Big[648m_n^6\frac{1}{\tilde{s}_n\hat{t}\hat{u}} - 738m_n^4\Big(\frac{1}{\tilde{s}_n\hat{s}} - 27\frac{1}{\hat{s}^2} + 164\frac{1}{\hat{t}\hat{u}} - 16\frac{1}{\hat{t}^2} - 16\frac{1}{\hat{u}^2} - 27\frac{1}{\tilde{s}_n^2}\Big) + 9m_n^2\Big(32\frac{\hat{s}}{\hat{t}\hat{u}} - 144\frac{1}{\hat{s}}\Big) - 68 + 16\frac{\hat{s}^2}{\hat{t}\hat{u}} + 18\frac{\hat{t}\hat{u}}{\hat{s}\tilde{s}_n} + 27\frac{\hat{t}\hat{u}}{\hat{s}^2} + 27\frac{\hat{t}\hat{u}}{\tilde{s}_n^2}\Big] \tag{43}$$

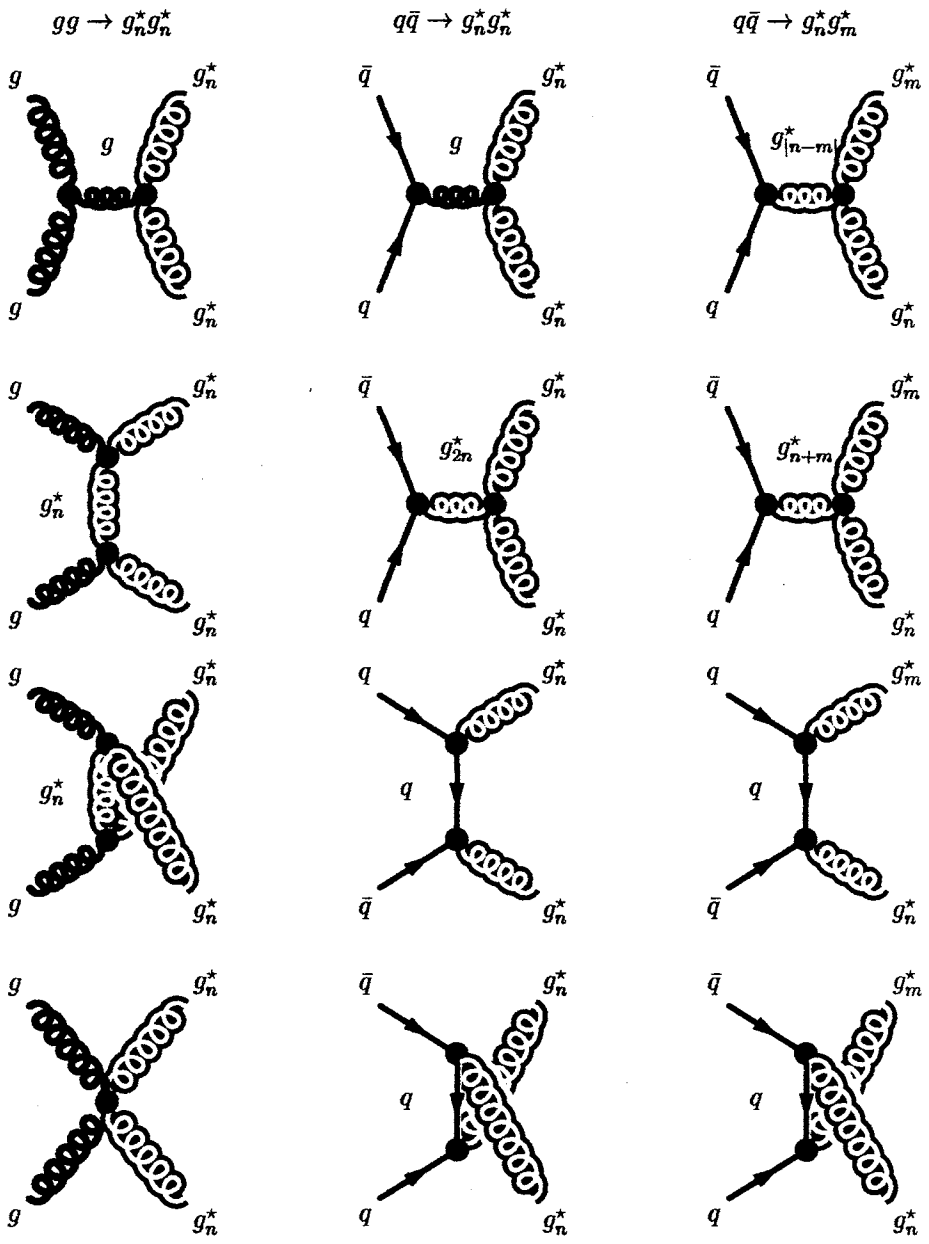

Figure 5: Diagrams involving the production of two on-shell $g^\star$'s. The modes n and m are distinct ($n \neq m$).

$$\bar{\sum}|\mathcal{M}(q\bar{q}\to g_n^\star g_m^\star)|^2 = \frac{8}{27}\pi^2\alpha_S^2(Q)\Big[-14\frac{\hat{s}\hat{t}^2}{\hat{u}}+2\frac{\hat{t}^3}{\hat{u}}-20\hat{t}\hat{u}$$
$$+\Big(-8\frac{\hat{t}^2}{\hat{u}^2}m_m^2m_n^2+30\hat{t}m_m^2+14\frac{\hat{t}}{\hat{u}}m_m^4-25\frac{\hat{t}}{\hat{u}}m_m^2m_n^2$$
$$-44m_m^4-24m_m^2m_n^2-16\frac{m_m^4m_n^2}{\hat{u}} \qquad (44)$$
$$+32\frac{m_m^4m_n^4}{\hat{u}^2}+8\frac{m_m^6m_n^2}{\hat{t}\hat{u}}+8\frac{m_m^4m_n^4}{\hat{t}\hat{u}}$$
$$+m\leftrightarrow n\Big)+t\leftrightarrow u\Big]\frac{1}{\hat{s}-(m_m+m_n)^2}\frac{1}{\hat{s}-(m_m-m_n)^2}$$
$$\bar{\sum}|\mathcal{M}(gg\to g_n^\star g_n^\star)|^2 = \frac{9}{4}\pi^2\alpha_S^2(Q)\Big(\frac{s^2}{\hat{t}_n'\hat{u}_n'}-1\Big)$$
$$\cdot\Big(6\frac{m_n^4}{\hat{t}_n'\hat{u}_n'}-6\frac{m_n^2}{\hat{s}}+2\frac{\hat{s}^2}{\hat{t}_n'\hat{u}_n'}+\frac{\hat{t}_n'\hat{u}_n'}{\hat{s}^2}-4\Big), \qquad (45)$$

where $\tilde{s}_n \equiv \hat{s}-4m_n^2$. (In this notation, the replacements indicated by $t\leftrightarrow u$ do not affect the two terms that involve neither t nor u.)

In the results for the matrix element squares, as given in Eqs. $(29-31)$, there are no terms that grow with energy, and the matrix elements for these subprocesses are tree-unitary. This is not true for the individual diagrams for the subprocesses: There are delicate cancellations between the diagrams for each subprocess. These cancellations occur only because of the relations among the couplings as dictated by the compactification of the five-dimensional KK theory to four dimensions, and also due to the special relations for the masses of the various KK states. For example, in the process $q\bar{q}\to g_n^\star g_n^\star$, the presence of the $g_{2n}^\star$ exchange is crucial with its mass $2n\mu$ and its coupling as dictated by the KK Yang-Mills theory. This is a new example of tree-unitarity for a class of massive vector boson theories other than the known spontaneously broken gauge theories [23].

These subprocess j amplitudes-squared combine to give the total KK cross section

for $g_n^\star$'s produced on-shell as

$$\sigma_{KK}(pp \to g^\star g^\star) = \frac{1}{4\pi} \sum_j \sum_{g^\star \text{pairs}} \int_{\rho_{mn}}^1 dx_A \int_{\rho_{mn}/x_A}^1 dx_B f_{a/A}(x_A, Q) f_{b/B}(x_B, Q) \int_{-1}^1 dz \, \bar{\sum} |M_j|^2 \, \frac{1}{\hat{s}} \sqrt{1 - \frac{(m_m + m_n)^2}{\hat{s}}}, \tag{46}$$

where $\rho_{mn} = (m_m + m_n)^2/s$ and the second summation runs over all $g_n^\star, g_m^\star$ pairs that can be produced for energy $\sqrt{s}$. Again, the narrow width approximation is applied to account for the decay of the $g^\star$'s into $q\bar{q}$ pairs:

$$\sigma_{KK}(pp \to g^\star g^\star \to 4\,\text{jets}) = \int \frac{d\Omega_5}{4\pi} \int \frac{d\Omega_7}{4\pi} \sigma_{KK}(pp \to g^\star g^\star). \tag{47}$$

EW Interactions

Direct Channel Production. For fermion-antifermion pair production, the KK excitations of the EW gauge bosons manifest themselves through a tower of diagrams with $\gamma_n^\star$ and $Z_n^\star$ propagators. The net tree-level effect of the $\gamma_n^\star$'s and $Z_n^\star$'s on charged lepton pair production is the replacement of the SM propagator by an effective KK propagator. Gauge invariance is employed to drop the second term in Eq. (12) in this analysis of fermion pair production. The effective moduli-squared of the propagators for direct-channel $\gamma_n^\star$ and $Z_n^\star$ exchange and the corresponding direct-channel $\gamma_n^\star$-$Z_n^\star$ interference are thus[††]

[††]When generalizing to the case where the EW gauge bosons may propagate into more than one large extra dimension, the sum in the effective propagator is formally divergent. However, various solutions to this problem have been proposed in the literature [19].

$$|D_{\mathit{eff}}(\gamma,s)|^2 = \frac{1}{2}\sum_{m,n=0}^{\infty} c_{\gamma_m}c_{\gamma_n}\frac{s'_{\gamma_m}s'_{\gamma_n}+m_{\gamma_m}\Gamma_{\gamma_m}m_{\gamma_n}\Gamma_{\gamma_n}}{(s^2_{\gamma_m}+m^2_{\gamma_m}\Gamma^2_{\gamma_m})(s^2_{\gamma_n}+m^2_{\gamma_n}\Gamma^2_{\gamma_n})}$$

$$|D_{\mathit{eff}}(Z,s)|^2 = \frac{1}{2}\sum_{m,n=0}^{\infty} c_{Z_m}c_{Z_n}\frac{s'_{Z_m}s'_{Z_n}+m_{Z_m}\Gamma_{Z_m}m_{Z_n}\Gamma_{Z_n}}{(s^2_{Z_m}+m^2_{Z_m}\Gamma^2_{Z_m})(s^2_{Z_n}+m^2_{Z_n}\Gamma^2_{Z_n})} \qquad (48)$$

$$\Big[D^*_{\mathit{eff}}(Z,s)D_{\mathit{eff}}(\gamma,s) + D_{\mathit{eff}}(\gamma,s)D^*_{\mathit{eff}}(Z,s)\Big] = \sum_{m,n=0}^{\infty} c_{\gamma_m}c_{\gamma_n}\frac{s'_{\gamma_m}s'_{Z_n}+m_{\gamma_m}\Gamma_{\gamma_m}m_{Z_n}\Gamma_{Z_n}}{(s^2_{\gamma_m}+m^2_{\gamma_m}\Gamma^2_{\gamma_m})(s^2_{Z_n}+m^2_{Z_n}\Gamma^2_{Z_n})}.$$

Here s'_{X_n} is shorthand for the subtraction of $m^2_{X_n}$ from s (*i.e.*, $s'_{X_n} \equiv s - m^2_{X_n}$) and c_{X_n} represents the fact that the f-$\bar{f}$-X and the f-$\bar{f}$-$X^\star_n$ vertex factors differ by a $\sqrt{2}$ (*i.e.*, $c_{X_0} = 1$, $c_{X_{n>0}} = 2$). (An exception is made in the effective propagator equations by including the $n = 0$ and $n > 0$ modes together for more compact notation.)

Cross-Channel Production. The effective propagator formulae for cross-channel exchanges and interference are the same as in Eq. 48 with the replacement of the direct-channel Mandelstam variable s by the cross-channel variable t (or u). The interference between direct-channel exchanges of $\gamma^\star_n$'s and cross-channel exchanges of $Z^\star_n$'s is described by

$$\Big[D^*_{\mathit{eff}}(Z,t)D_{\mathit{eff}}(\gamma,s) + D_{\mathit{eff}}(\gamma,s)D^*_{\mathit{eff}}(Z,t)\Big] = \sum_{m,n=0}^{\infty} c_{\gamma_m}c_{\gamma_n}\frac{s'_{\gamma_m}t'_{Z_n}+m_{\gamma_m}\Gamma_{\gamma_m}m_{Z_n}\Gamma_{Z_n}}{(s^2_{\gamma_m}+m^2_{\gamma_m}\Gamma^2_{\gamma_m})(t^2_{Z_n}+m^2_{Z_n}\Gamma^2_{Z_n})}. \qquad (49)$$

Finally, the effective propagator formulae for direct-channel exchanges of $Z^\star_n$'s and cross-channel exchanges of $\gamma^\star_n$'s are identical to Eq. 49 with the replacement $\gamma \leftrightarrow Z$. For collider energies in the range 100 GeV $\leq \sqrt{s} \leq$ 1 TeV and compactification scales $\mu > 1$ TeV, the sums in the effective propagators converge quite rapidly. Thus, they can be truncated after only a few terms with negligible error. The KK cross

sections for the production of two SM fermion final states in high-energy collisions are simply obtained by replacement of the usual SM moduli-squared propagators by these effective moduli-squared propagators.

UED Model

QCD Interactions

Subprocesses. In mind is the production of pairs of KK excitations of the gluons, $g_n^\star$, and quarks, $q_n^\bullet$ and q_n°, in proton-antiproton collisions at the Tevatron Run I or II energy or proton-proton collisions at the LHC energy. The focus is on the parton subprocesses in this section and postpone numerical results to the following sections where the stability of the lowest-lying KK excitations is addressed. The various subprocesses are enumerated in Table 1. The calculations are performed at the tree-level (Fig.'s 6–9, and restrict ourselves to two final states. Due to KK number conservation, not only must the KK excitations be produced in pairs, but they necessarily have the same mode n, which is the same mode that any KK propagators will have. Neglected are the quark masses except for the top mass M_t, but neglect the content of top flavor in the colliding protons and antiprotons. Thus, the top quark only enters into the calculation of the cross sections for $gg \to q_n^\bullet \bar{q}_n^\bullet$ and $q\bar{q} \to q'^\bullet_n \bar{q}'^\bullet_n$, and the analogous subprocesses for the q_n°'s. Also neglected are the decay widths of all SM and KK particles in this section since massive propagators will not appear in the s-channel due to tree-level KK number conservation and the neglect of initial top quarks. The decay widths will be incorporated in the subsequent decay of the final states, where possible mechanisms for the decay of the lowest-lying KK states will be

Double KK gluon production		KK quark-gluon production	
$gg \to g_n^\star g_n^\star$	$q\bar{q} \to g_n^\star g_n^\star$	$qg \to q_n^\bullet g_n^\star$	$qg \to q_n^\circ g_n^\star$
Double KK quark production			
$gg \to q_n^\bullet \bar{q}_n^\bullet$	$gg \to q_n^\circ \bar{q}_n^\circ$	$q\bar{q} \to q_n^\bullet \bar{q}_n^\bullet$	$q\bar{q} \to q_n^\circ \bar{q}_n^\circ$
$qq \to q_n^\bullet q_n^\bullet$	$qq \to q_n^\circ q_n^\circ$	$q\bar{q} \to q'^\bullet_n \bar{q}'^\bullet_n$	$q\bar{q} \to q'^\circ_n \bar{q}'^\circ_n$
$qq' \to q_n^\bullet q'^\bullet_n$	$qq' \to q_n^\circ q'^\circ_n$	$q\bar{q}' \to q_n^\bullet \bar{q}'^\bullet_n$	$q\bar{q}' \to q_n^\circ \bar{q}'^\circ_n$
$q\bar{q} \to q_n^\bullet \bar{q}_n^\circ$	$q\bar{q} \to q_n^\circ \bar{q}_n^\bullet$	$qq' \to q_n^\bullet q'^\circ_n$	$qq' \to q_n^\circ q'^\bullet_n$
$q\bar{q}' \to q_n^\bullet \bar{q}'^\circ_n$	$q\bar{q}' \to q_n^\circ \bar{q}'^\bullet_n$	$qq \to q_n^\bullet q_n^\circ$	

Table 1: Subprocesses leading to double KK production at hadronic colliders. Not shown are subprocesses that are simply related by the exchange of a particle and antiparticle, as in $\bar{q}g \to \bar{q}_n^\bullet g_n^\star$.

discussed.

Double KK Gluon Production. Double KK gluon production subprocesses consist of $gg \to g_n^\star g_n^\star$ and $q\bar{q} \to g_n^\star g_n^\star$. The former subprocess involves direct-channel SM gluon exchange, cross-channel KK gluon exchanges, and the four-point interaction. The latter subprocess is unique in that there are five tree-level Feynman diagrams, which include direct-channel SM gluon exchange and cross-channel $q_n^\bullet$ and q_n° exchanges. For the purely gluonic subprocess, the amplitude-squared,** summed over final states and averaged over initial states, is:

$$\overline{\sum} |\mathcal{M}(gg \to g_n^\star g_n^\star)|^2 = \frac{9}{4}\pi^2 \alpha_S^2(Q) \left(\frac{\hat{s}^2}{\hat{t}'_n \hat{u}'_n} - 1 \right) \cdot \left(6\frac{M_n^4}{\hat{t}'_n \hat{u}'_n} - 6\frac{M_n^2}{\hat{s}} + 2\frac{\hat{s}^2}{\hat{t}'_n \hat{u}'_n} + \frac{\hat{t}'_n \hat{u}'_n}{\hat{s}^2} - 4 \right), \qquad (50)$$

where the scale Q is identified with the mass of the final state KK excitations M_n and $\hat{v}'_n$ represents subtraction of M_n^2 from the Mandelstam variable $\hat{v} \in \{\hat{s}, \hat{t}, \hat{u}\}$ (*i.e.*, $\hat{v}'_n = \hat{v} - M_n^2$). Note that $gg \to g_n^\star g_n^\star$ is the same in the UED scenario considered here

***FORM** [20], a symbolic manipulation program, is employed in the evaluation of the squares of the amplitudes.

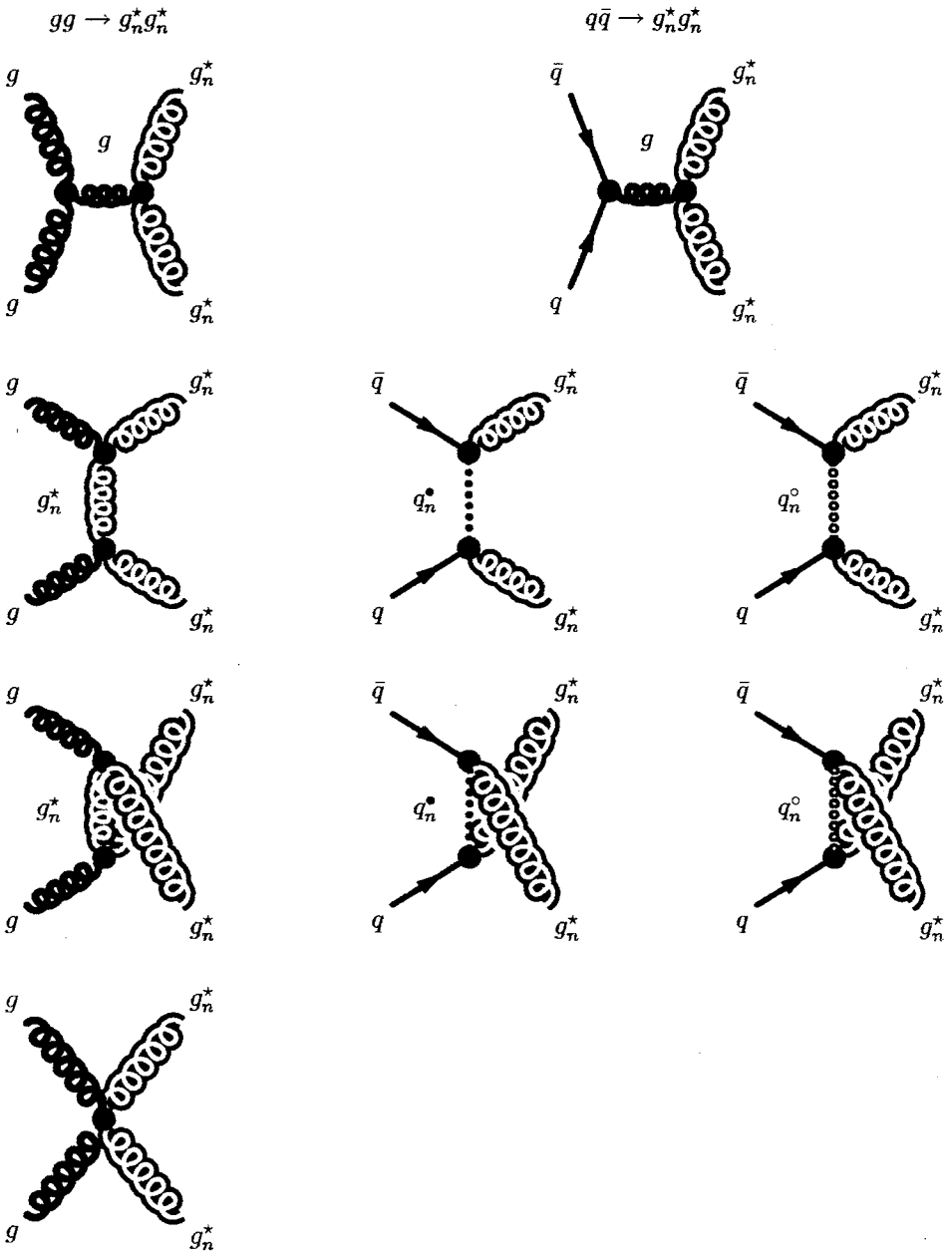

Figure 6: Feynman diagrams for case (i).

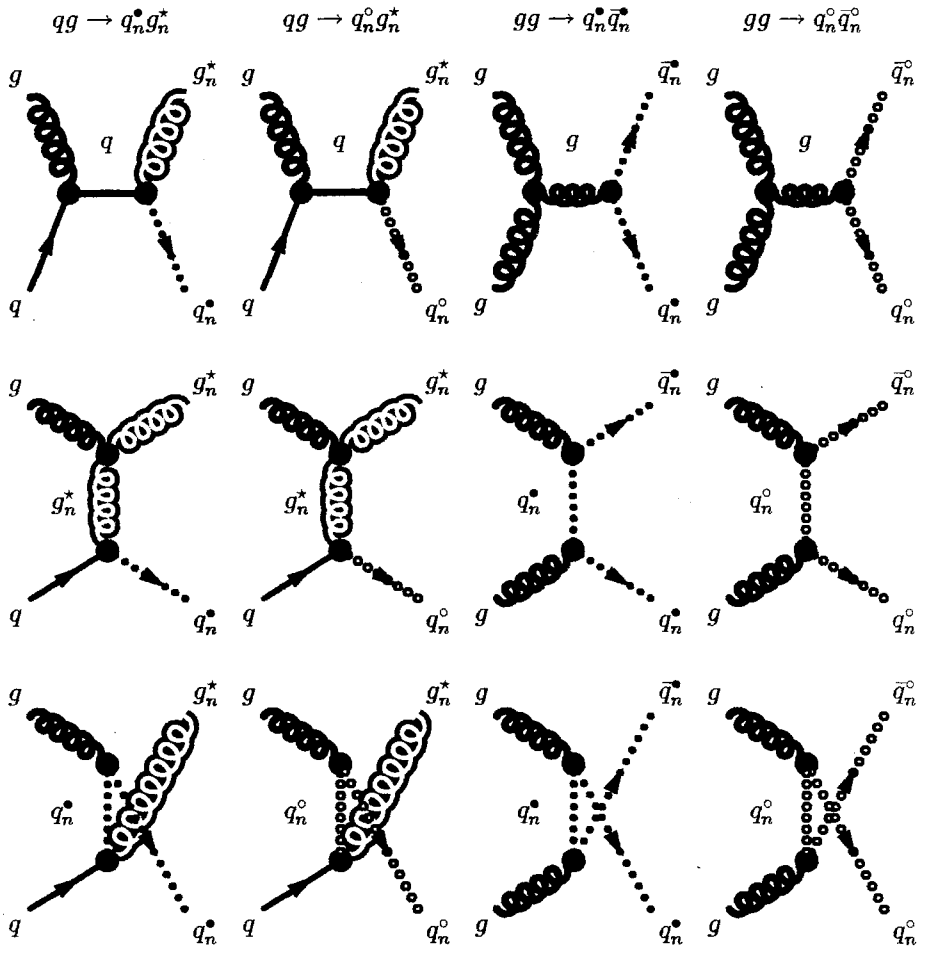

Figure 7: Feynman diagrams for case (ii) and the initial gluon contributions to case (iii)(b).

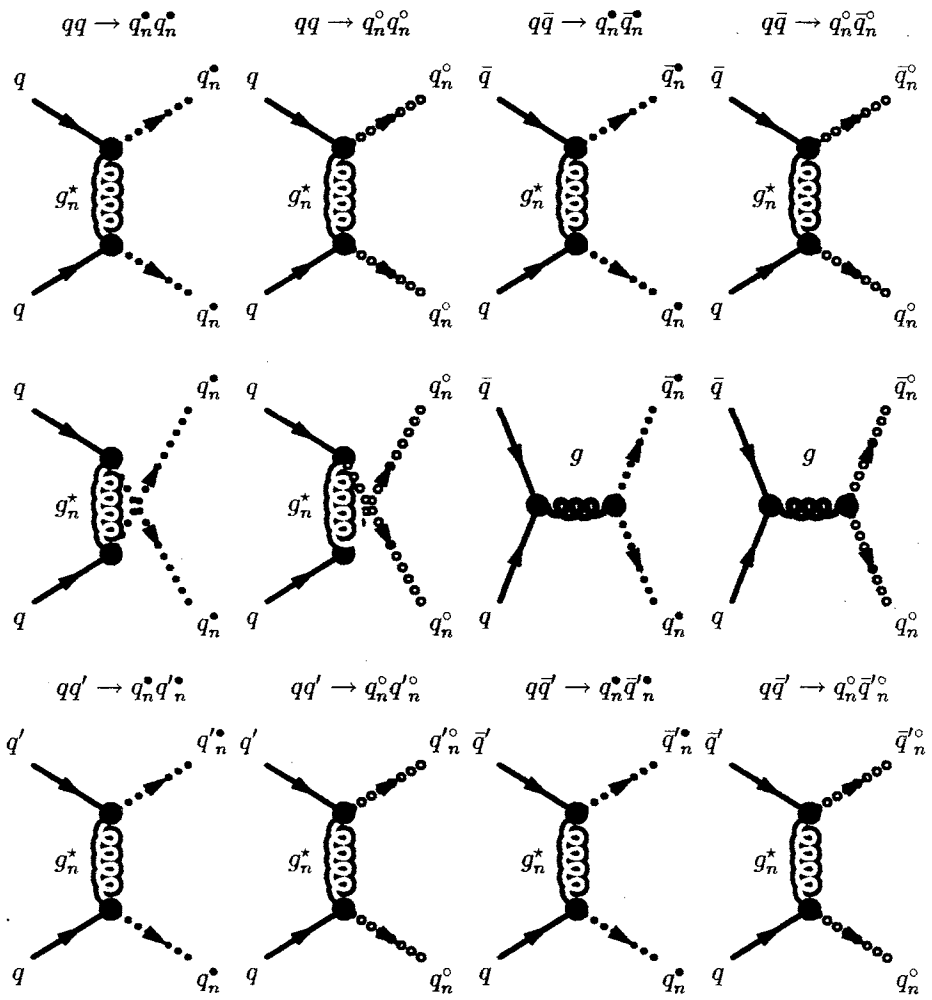

Figure 8: Feynman diagrams for case (iii)(a), the initial $q\bar{q}$ contributions to case (iii)(b) where the final states have the same flavor as the initial states, and the contributions to case (iii)(c). The $'$ indicates that q and q' are distinct flavors.

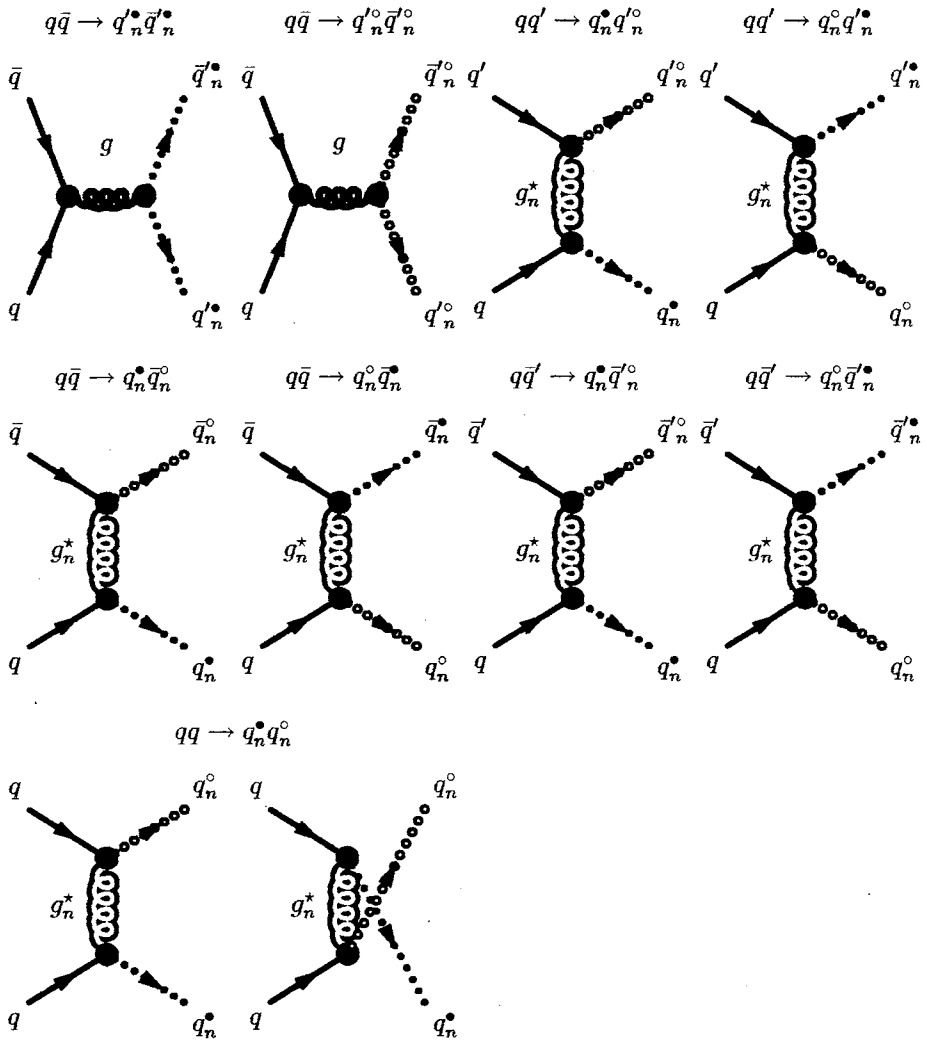

Figure 9: Feynman diagrams for case (iii)(d) and the remaining contributions to case (iii)(b). The $'$ indicates that q and q' are distinct flavors.

as well as in a model where only gluons propagate into the bulk. However, each of the remaining subprocesses is different. The amplitude-squared for $q\bar{q} \to g_n^\star g_n^\star$ is:

$$\bar{\sum}|\mathcal{M}(q\bar{q} \to g_n^\star g_n^\star)|^2 = \frac{2}{27}\pi^2\alpha_S^2(Q)\left[\frac{M_n^2}{\hat{s}}\left(4\frac{\hat{s}^4}{\hat{t}'^2\hat{u}'^2} - 131\frac{\hat{s}^2}{\hat{t}'\hat{u}'} - 108\right) + 100\frac{\hat{s}^2}{\hat{t}'\hat{u}'} - 93 + 108\frac{\hat{t}'\hat{u}'}{\hat{s}^2}\right]. \quad (51)$$

KK Quark-Gluon Production. KK quark-gluon production results from $qg \to q_n^\bullet g_n^\star$ and $qg \to q_n^\circ g_n^\star$. (Subprocesses that are simply related by particle-antiparticle replacement, such as $\bar{q}g \to \bar{q}_n^\bullet g_n^\star$, will not be enumerated.) These subprocesses involve s-channel SM quark exchange, t-channel $g_n^\star$ exchange, and u-channel KK quark exchange. The square of the matrix element for $qg \to q_n^\bullet g_n^\star$ is:

$$\bar{\sum}|\mathcal{M}(qg \to q_n^\bullet g_n^\star)|^2 = \frac{1}{36}\pi^2\alpha_S^2(Q)\left(72\frac{\hat{t}'^4}{\hat{s}^2\hat{u}'^2} - 36\frac{\hat{t}'^2}{\hat{s}\hat{u}'} + 43 - 36\frac{\hat{s}\hat{u}'}{\hat{t}'^2}\right). \quad (52)$$

The subprocess $qg \to q_n^\circ g_n^\star$ is identical to $qg \to q_n^\bullet g_n^\star$. That is, the sign of the γ_5 matrix is not important in KK quark production unless both $q_n^\bullet$ and q_n° are involved in the same subprocess, *e.g.*, in $q\bar{q} \to g_n^\star g_n^\star$ or $qq \to q_n^\bullet q_n^\circ$.

Identical Final $q_n^\bullet$ or q_n° States. Subprocesses with identical final $q_n^\bullet$ or q_n° states feature t- and u-channel $g_n^\star$ exchanges. A relative minus sign represents the antisymmetrization of fermionic wave functions that originates from the interchange of identical fermionic states between the two diagrams. Notice that although a given SM quark q and its KK counterparts have different mass, they have the same fermionic properties that produces the minus sign for the antisymmetrization of wave functions. The amplitude-squared for $q_n^\bullet q_n^\bullet$ production is:

$$\bar{\sum}|\mathcal{M}(qq \to q_n^\bullet q_n^\bullet)|^2 = \frac{1}{27}\pi^2\alpha_S^2(Q)\left[\frac{M_n^2}{\hat{s}}\left(18\frac{\hat{s}^4}{\hat{t}'^2\hat{u}'^2}+17\frac{\hat{s}^2}{\hat{t}'\hat{u}'}\right)\right.$$
$$\left.+\,30\frac{\hat{s}^4}{\hat{t}'^2\hat{u}'^2}-16\frac{\hat{s}^2}{\hat{t}'\hat{u}'}+2\right]. \qquad (53)$$

The identical result is obtained for $q_n^\circ q_n^\circ$ production.

KK Quark-Antiquark Pair Production. Double KK quark-antiquark pairs with the same flavor can arise from initial gluons or quarks. The former case involves direct-channel SM gluon exchange and cross-channel KK quark exchanges. The latter case consists of s-channel SM gluon exchange, and, in the case of initial partons of the same flavor as the final states, t-channel $g_n^\star$ exchange. For initial gluons, squaring the amplitude leads to the following expression for KK quark pair production:

$$\bar{\sum}|\mathcal{M}(gg \to q_n^\bullet \bar{q}_n^\bullet)|^2 = \frac{1}{24}\pi^2\alpha_S^2(Q)\left[\frac{M_n^4}{\hat{s}^2}\left(-80\frac{\hat{s}^4}{\hat{t}'^2\hat{u}'^2}+36\frac{\hat{s}^2}{\hat{t}'\hat{u}'}\right)\right.$$
$$-\frac{M_n^2}{\hat{s}}\left(48\frac{\hat{s}^2}{\hat{t}'\hat{u}'}+36\right) \qquad (54)$$
$$\left.-\,24\frac{\hat{s}^4}{\hat{t}'^2\hat{u}'^2}+12\frac{\hat{s}^2}{\hat{t}'\hat{u}'}-17+18\frac{\hat{t}'\hat{u}'}{\hat{s}^2}+12\frac{\hat{s}^2}{\hat{t}'^2}\right],$$

where the only difference for the case of KK top pair production is adjustment of the mass via Eq. 21. The amplitude-squared for KK quark-antiquark final states arising from SM quark-antiquark initial states, for which the flavor is the same in the initial and final states, is:

$$\bar{\sum}|\mathcal{M}(q\bar{q} \to q_n^\bullet \bar{q}_n^\bullet)|^2 = \frac{1}{54}\pi^2\alpha_S^2(Q)\left[\frac{M_n^2}{\hat{s}}\left(48-12\frac{\hat{s}}{\hat{t}'}+12\frac{\hat{s}^2}{\hat{t}'^2}\right)\right.$$
$$\left.+\,48\frac{\hat{t}'^2}{\hat{s}^2}+36\frac{\hat{t}'}{\hat{s}}+23+16\frac{\hat{s}}{\hat{t}'}+12\frac{\hat{s}^2}{\hat{t}'^2}\right]. \qquad (55)$$

This does not lead to KK top quark production since the top quark content of the colliding protons is negligible. The relative sign between the two diagrams again

incorporates the antisymmetrization of fermionic wave functions corresponding to the interchange of two fermionic states between the two diagrams. When the final states have different flavors than the initial state, only the s-channel contributes. For the lighter flavors, this is simply the s-channel part of Eq. 55:

$$\bar{\sum}|\mathcal{M}(q\bar{q}\to q'^{\bullet}_n\bar{q}'^{\bullet}_n)|^2=\frac{4}{9}\pi^2\alpha_S^2(Q)\left(2\frac{M_n^2}{\hat{s}}-2\frac{\hat{t}'\hat{u}'}{\hat{s}^2}+1\right). \tag{56}$$

Again, for top production, the only change involves correcting for the final state KK mass. The same results apply for $q^{\circ}_n\bar{q}^{\circ}_n$ production.

For double KK quark production with different flavors in the final state, the result is the same as the corresponding case with identical flavors with the appropriate channel removed. That is, $qq'\to q^{\bullet}_n q'^{\bullet}_n$ is just the t-channel contribution to $qq\to q^{\bullet}_n q^{\bullet}_n$,

$$\bar{\sum}|\mathcal{M}(qq'\to q^{\bullet}_n q'^{\bullet}_n)|^2=\frac{2}{9}\pi^2\alpha_S^2(Q)\left(-M_n^2\frac{\hat{s}}{\hat{t}'^2}+2+\frac{\hat{s}^2}{\hat{t}'^2}\right), \tag{57}$$

while $q\bar{q}'\to q^{\bullet}_n\bar{q}'^{\bullet}_n$ is also the t-channel contribution to $q\bar{q}\to q^{\bullet}_n\bar{q}^{\bullet}_n$,

$$\bar{\sum}|\mathcal{M}(q\bar{q}'\to q^{\bullet}_n\bar{q}'^{\bullet}_n)|^2=\frac{1}{18}\pi^2\alpha_S^2(Q)\left(4M_n^2\frac{\hat{s}}{\hat{t}'^2}+4\frac{\hat{s}^2}{\hat{t}'^2}+8\frac{\hat{s}}{\hat{t}'}+5\right), \tag{58}$$

and similarly for q°_n final states.

Mixed KK Final States. Finally, it is possible to produce the mixed KK final states involving one $q^{\bullet}_n$ and one q°_n. The projection operators conspire to nullify the interference term in $qq\to q^{\bullet}_n q^{\circ}_n$. The differing signs of the γ_5's also affect the t- and u-channel contributions. The amplitude-squared for this subprocess is:

$$\begin{aligned}\bar{\sum}|\mathcal{M}(qq\to q^{\bullet}_n q^{\circ}_n)|^2=\frac{1}{9}\pi^2\alpha_S^2(Q)\Bigg[&-\frac{M_n^2}{\hat{s}}\left(6\frac{\hat{s}^4}{\hat{t}'^2\hat{u}'^2}+4\frac{\hat{s}^2}{\hat{t}'\hat{u}'}\right)\\&+10\frac{\hat{s}^4}{\hat{t}'^2\hat{u}'^2}-8\frac{\hat{s}^2}{\hat{t}'\hat{u}'}+5\Bigg].\end{aligned} \tag{59}$$

The six remaining mixed subprocesses, $q_n^\bullet \bar{q}_n^\circ$, $q_n^\circ \bar{q}_n^\bullet$, $q_n^\bullet q'^\circ_n$, $q_n^\circ q'^\bullet_n$, $q_n^\bullet \bar{q}'^\circ_n$, and $q_n^\circ \bar{q}'^\bullet_n$, all are represented by the same t-channel diagram and have the same form as the t-channel contribution to Eq. 59:

$$\bar{\sum} |\mathcal{M}(q\bar{q}' \to q_n^\bullet \bar{q}'^\bullet_n)|^2 = \frac{1}{18}\pi^2 \alpha_S^2(Q) \left[-4\frac{M_n^2}{\hat{t}'}(1 + \frac{\hat{u}'}{\hat{t}'}) + 1 + 4\frac{\hat{u}'^2}{\hat{t}'^2} \right] . \qquad (60)$$

It is not possible to produce mixed KK final states from initial gluons, nor is it possible to produce mixed KK final states of a different flavor from initial $q\bar{q}$ pairs.

Unitarity. These amplitude-squared formulae do not contain any terms that grow with energy, and the matrix elements for these subprocesses are tree-unitary. This has also been observed for the case in which only the gauge bosons propagate into the bulk [12, 24]. Note that the matrix elements of the individual diagrams with external gluons are not tree-unitary: There are delicate cancellations involved between individual diagrams, which ensures unitarity for the total amplitude. As an example, consider the subprocess, $q\bar{q} \to g_n^\star g_n^\star$, which has both $q_n^\bullet$ and q_n° propagators. The amplitude-squared for this reaction would not be tree-unitary if there were just a single tower of KK excitations of the quarks, or if the two towers $q_n^\bullet$ and q_n° did not couple left- and right-handedly to the SM quarks. This is another example of tree-unitarity for a class of massive vector boson theories other than the known spontaneously broken gauge theories [23].

EW Interactions

Survey of Processes. It is easier to distinguish between the EW and QCD interactions by restricting the number of jets to be less than two. The subsequent decays

of the produced KK excitations are simpler to treat for the lighter particles. Also, the SM background can be expected to be more prominent when there is a SM $2 \to 2$ process with a Z boson that can decay to neutrinos. For example, consider $e^{+\star}e^{-\star}$ production where there is a mechanism of new physics that permits their further decay to e^+e^- plus two gravitons (missing energy). There is a SM background for this experimental signature at the same order, which is ZZ production where one Z decays into e^+e^- and the other decays into neutrinos (missing energy). Compare this example to $q^\circ\gamma^\star$ production where the same new physics mechanism leads to their further decay into $q\gamma$ plus missing two gravitons. The leading order SM background for this experimental signature is at least level higher: $q\gamma Z$ production. This is offers significant improvement in the signal-to-background ratio. These reasons serve as the motivation for investigating single and double photon production.

Single Photon Production. The production of a single KK photon and KK quark is similar to KK quark-gluon production. The differences lie in the overall strengths of the interactions and the fact that only the gluon features triple and quartic self-interactions. The amplitude-squared for KK photon-quark production is:

$$\bar{\sum}|\mathcal{M}(qg \to q_n^\bullet\gamma^\star)|^2 = \frac{1}{48}\pi^2\alpha(Q)\alpha_S(Q)\left[-3\hat{s}^3\hat{u}' - 2\hat{s}^2\hat{u}'^2 - 3\hat{s}\hat{u}'^3\right], \qquad (61)$$

where $\alpha(Q)$ is the running electromagnetic coupling. KK photon-gluon production is similar in the same way to KK double gluon production. The modulus square of the matrix element for this process is:

$$\bar{\sum}|\mathcal{M}(q\bar{q}\to g_n^\star\gamma^\star)|^2=\frac{1}{72}\pi^2\alpha(Q)\alpha_S(Q)\left[M_n^8(192)\right.$$
$$+M_n^6(-320\hat{t}-320\hat{u})+M_n^4(152\hat{t}^2+464\hat{t}\hat{u}+152\hat{u}^2)$$
$$+M_n^2(-32\hat{t}^3-160\hat{t}^2\hat{u}-160\hat{t}\hat{u}^2-32\hat{u}^3) \qquad (62)$$
$$\left.+40\hat{t}^3\hat{u}-16\hat{t}^2\hat{u}^2+40\hat{t}\hat{u}^3\right]\,.$$

Double Photon Production. The production of two KK photons is almost identical to the production of one KK gluon and one KK photon. The only difference is in the overall strength of the interactions. The amplitude-squared for this process is simply given by Eq. with a corresponding alteration of the overall factor to represent the difference between the electromagnetic and strong interactions (in addition to an overall factor for the different group generators that appears in the modulus-square of the vertex factors as well as a statistical factor of one-half for identical final states).

IV

DECAYS

Kaluza-Klein Number

Fermi-Phobic Model

Decay Mechanism. The projection of momenta along extra dimensions is conserved in scattering processes. The SM wall can balance momentum in extra dimensions by explicit tree-level violation of KK number conservation, permitting the exchange of a single KK excitation. KK gauge bosons can thus decay into fermion-antifermion pairs.

Decay Rates. At tree-level, the $g_n^\star$ decays into $q\bar{q}$ pairs with (total) width $\Gamma_n = 2\,\alpha_s(Q)m_n$. The KK photon decay is very similar to the KK gluon decay. The KK photon decays to leptons in addition to quarks, and the coupling strength is different because the electric charge differs from the strong charge, but the structure of the matrix-element modulus-square is the same. The $\gamma_n^\star$ decays to fermion pairs with total width $\frac{14}{3}\alpha(m_{\gamma_n^\star})m_{\gamma_n^\star}$. The $W_n^\star$ and $Z_n^\star$ have the same analytic expression for the partial decay rates as the W and Z except for a factor of $2\frac{m_{W_n^\star}}{m_W}$ for the $W_n^\star$ and similarly for the $Z_n^\star$; also, the KK excitations are heavy enough to include the top quark in the decay rates.

UED Model

Stability. As previously discussed, the lowest-lying KK excitations of the light fermions and massless gauge fields may very well be stable. This is a consequence of

KK number conservation (Eq. 4), which is valid at all vertices and thus also at the tree-level. KK number is broken at the loop-level, but the lightest KK excitations can not decay even at the loop level[††] unless some new physics mechanism is introduced. The KK excitations of massive gauge bosons and heavier generation fermions can decay to lighter KK states and SM fields at tree-level. For any SM decay with a massless final state, such as $Z \rightarrow \nu\bar{\nu}$, there are corresponding decays involving their KK excitations, such as $Z_1^\star \rightarrow \nu_1^\bullet \bar{\nu}$. When the final states are massive the decay may be kinematically forbidden, depending on the compactification scale: For example, the $t_1^\bullet$ can not decay to $W^+ b_1^\bullet$ for a 400 GeV compactification scale, but it can decay to $W_1^{+\star} b$. At the tree-level, KK number conservation results in increasing kinematic suppression of all decays involving KK excitations of massive SM fields with increasing compactification scale. Note also that the lowest-lying KK excitations of the quarks and gluons can not decay to their SM counterparts via graviton emission unless KK number is violated in such interactions. Long-lived refers to lifetimes long enough such that the final state decay occurs beyond the detector.

KK Number Violation. Decays are possible if there is a source of KK number violation, as in the fermi-phobic and original ADD model where any fields constrained to the SM wall appear in the Lagrangian with a delta function. In the universal model, no fields are constrained to the wall, such that no delta functions are present to violate KK number conservation and instigate the decays of KK excitations. Yet it is desired

[††]Loop corrections may potentially create splitting between the masses of quark and massless gauge boson KK excitations, allowing for decays such as $q_n^\bullet \rightarrow q g_n^\star$ or $q_n^\bullet \rightarrow q\gamma^\star$. These decays will be kinematically suppressed, and assumed to occur beyond the detector.

to implement a decay scheme to naturally evade cosmological constraints. This is done by introducing a new physics mechanism that violates KK number conservation. The specific source of new physics can result in a form factor that appears at the KK vertices, which disturbs the mathematics that normally preserves KK number in the integration over the compactified dimension.

UED Model

Fat Brane Scenario

Decay Mechanisms. The lowest-lying KK excitations of the light fermions and the massless gauge bosons can decay into SM fields via new physics mechanisms that produce a violation in KK number conservation. Various decay schemes have been considered in the literature [14], [13], [15]. However, provided that the KK excitations decay within the detector, the effect of a specific decay mechanism on the final state distributions presented here can be expected to be small.

Fat Brane Concept. For purposes of illustration, the decay properties of KK excitations in the fat brane scenario proposed in Ref. [14] shall analyze in some detail . In this scenario, the "small" universal extra dimension is assumed to be the thickness of the D_4 brane in which the SM particles propagate. In turn, this brane is embedded in a $4+N$ dimensional space, in which gravity propagates. (In order to avoid drastically modifying Newton's law at the solar system scale, it is necessary to require $N \geq 2$.) The gravity extra dimensions (call them $\{z_i\}$) are taken to be symmetric, with a compactification radius r much larger than the thickness of the fat brane R. The orbifold structure of the UED space in which the SM fields propagate can be imposed

by using boundary conditions on the fat brane. The non-gravitational interactions are identical to those presented in the Appendices. The differences in this model lie in the interactions between gravity and the KK excitations of the SM fields, where KK number violation in such interactions will mediate the decays. The thick brane absorbs the unbalanced momentum that results from the KK number violation.

Decay Rates

QCD Spectrum. The effective 4D interactions of the graviton fields with the SM fields and their KK excitations are obtained by the 'naive' (straightforward) generalization of the results in Ref. [4]. The Feynman rules for the couplings of the graviton fields to the UED fields are related to the corresponding couplings of the graviton fields to the SM fields by the form factor $\mathcal{F}_n(x_y)$ as introduced in Ref. [14, 15]. For example, the $q_n^{\bullet}$-q-$G_{\vec{k}}$ coupling is:

$$\Lambda_{q_n^{\bullet}\text{-}q\text{-}G_{\vec{k}}} = \mathcal{F}_n(x_y)\Lambda_{q\text{-}q\text{-}G_{\vec{k}}}\,, \tag{63}$$

where $G_{\vec{k}}$ is the KK excitation of the graviton corresponding to mode $\vec{k}$ and $x_y \equiv m_y R = 2\pi k_y R/r$. Note that n is the mode of the KK quark field, while k_y is the mode of the KK graviton field along the y direction. Thus, m_y is the contribution of the y dimension to the graviton mass. As with the non-gravitational interactions, the KK quark field components associated with odd Z_2 parity ($Q_R(x)$, $U_L(x)$, and $D_L(x)$) do not interact with the SM quark fields because of the presence of the projection operators. Thus, these KK fields associated with odd Z_2 parity can not decay to SM quarks and gravitons as indicated in Ref. [15]. The form factor, $\mathcal{F}_n(x)$, does not include the sine terms, and depends on the component of the graviton mass arising

from the universal compact dimension only, k_y:

$$\mathcal{F}_n(x_y) = \frac{\sqrt{2}}{\pi R}\int_0^{\pi R} dy \exp(\frac{i2\pi k_y y}{r})\cos(\frac{ny}{R})\,. \tag{64}$$

The result of this analysis for the modulus-square of form factor,

$$|\mathcal{F}_1(x_y)|^2 = \frac{4}{\pi^2}\frac{x_y^2}{(1-x_y^2)^2}\left[1+\cos(\pi x_y)\right]\,, \tag{65}$$

differs by the sign of the cosine term from the one in Ref. [15], which is potentially significant, since it affects the leading behavior of the form factor in the critical regions: x_y near zero (decay to light gravitons) and unity (decay to heavy gravitons).

The total decay width is obtained by summing over all possible graviton towers the partial decay width $\Gamma_n(x_y, x_z)$, where x_a refers to all of the extra dimensions, x_y denotes the universal direction, and x_z is exclusive to gravity: $x_a^2 = x_z^2 + x_y^2$. The form-factor appears as a multiplicative constant in the partial width:

$$\Gamma_n(x_y, x_z) = |\mathcal{F}_n^2(x_y)|\;\Gamma_n'(x_a)\,. \tag{66}$$

Replacing the KK sum with an integral over the density of graviton states [4], the following expression is obtained:

$$\Gamma_{tot} = \sum_{G,\Phi}\frac{2\pi^{\frac{N-1}{2}}\;M_P^2\;M^N}{\Gamma(\frac{N-1}{2})\;\;M_D^{N+2}}\int_{2\pi R/r}^{1} dx_y\;|\mathcal{F}_n^2(x_y)|\int_0^{\sqrt{1-x_y^2}} x_z^{N-2}dx_z\;\Gamma_n'(x_a)\,. \tag{67}$$

Here, M_P is the conventional 4D Planck scale, while M_D is the $(4+N)$-dimensional Planck scale and should not be more than one or two orders of magnitude above $1/R$ [21]. Note that N is the number of extra compact dimensions seen by the graviton, as opposed to the number of universal dimensions, which has been taken to be one.

For completeness, given here are the partial decay widths appearing in Eq. 67. These results are based on the three-point vertex Feynman rules given in Ref. [4],

with the masses of all particles (except gravitons) set to zero.[‡‡] The decay of the $q_n^\bullet$ (or q_n°) into a SM quark and a massive spin 2 graviton G^a has partial width, apart from the overall form factor, given by:

$$\Gamma'_n(q_n^\bullet \to qG^a) = \frac{\kappa^2}{768\pi}\frac{M_n^3}{x_a^4}\left[\left(1-x_a^2\right)^4\left(2+3x_a^2\right)\right] . \tag{68}$$

The $q_n^\bullet$ can also decay into one of $N(N-1)/2$ massive spin-0 particles, ϕ_{ij}^a:

$$\Gamma'_n(q_n^\bullet \to q\phi_{ij}^a) = \delta_{ij}\frac{9\kappa^2\omega^2}{256\pi}M_n^3(1-x_a^2)^2 , \tag{69}$$

where $\omega = \sqrt{\frac{2}{3(N+2)}}$. Finally, the $g_n^\star$ can only decay into a SM gluon via massive spin 2 graviton emission:

$$\Gamma'_n(g_n^\star \to gG^a) = \frac{\kappa^2}{96\pi}\frac{M_n^3}{x_a^4}\left[\left(1-x_a^2\right)^2\left(1+3x_a^2+6x_a^4\right)\right] . \tag{70}$$

The decay widths of the $q_1^\bullet$ (or q_1°) and $g_1^\star$, integrated over the density of graviton states with the form factor as in the prescription of Eq. 67, are illustrated in Fig. 10. The distributions of the graviton mass and missing energy (graviton energy) in the rest frame of the decaying particle are shown in Fig. 11. It is interesting to note that, in this scenario, when gravity propagates in two extra-dimensions ($N = 2$), the decays of KK quark or gluon excitations will be mediated mostly by very light gravitons, while for $N \geq 3$ the heavy graviton (mass of order μ) contribution will dominate (see the top of Fig. 11). As a consequence, for $N = 2$ the missing energy distribution will have a peak at half the KK excitation mass, while with increasing N the distribution will shift toward larger values. Note also that all of these decays will occur within

[‡‡]This does not mean that the KK mass of the particle decaying is neglected. Rather, this is a consequence of the fact that the mass terms in the Feynman rules in Ref. [4] come from mass terms in the Lagrangian that are absent in the 5-dimensional theory.

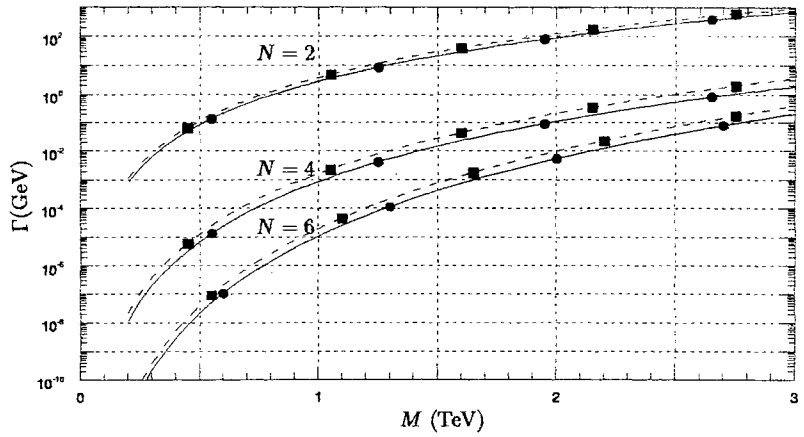

Figure 10: The decays of the $q_1^{\bullet}$ or q_1° (solid) and $g_1^{\star}$ (dashed) into SM fields via graviton emission (spin 2 and scalar combined) are shown as a function of the compactification scale $\mu = M = 1/R$ for $M_D = 5$ TeV. The pairs of curves correspond to 2, 4, and 6 extra dimensions from top to bottom, respectively.

the detectors in the range of parameter space that is explored and is depicted here.

EW Spectrum. The KK excitations of the light leptons and EW gauge bosons decay to the corresponding SM particles and gravitons in exactly the same manner as the KK excitations of the quarks and gluons in the fat brane scenario. This is because the underlying interaction is gravitational, which only depends on the spin of the decaying particle. Thus, the analytical expression for the decay rate of the KK electron, for example, is the same as that for the KK quark except for obvious overall factors that represent the difference between the strong and electromagnetic forces. Similarly, the KK photon decays analogously to the KK gluon. However, the heavier leptons and massive gauge bosons have more decay channels, as in the case of the top quark. For example, the $Z^{\star}$ can decay to a Z and a graviton, or it may decay into $e^{+\star}e^{-}$ which subsequently becomes $e^{+}e^{-}$ and an additional graviton.

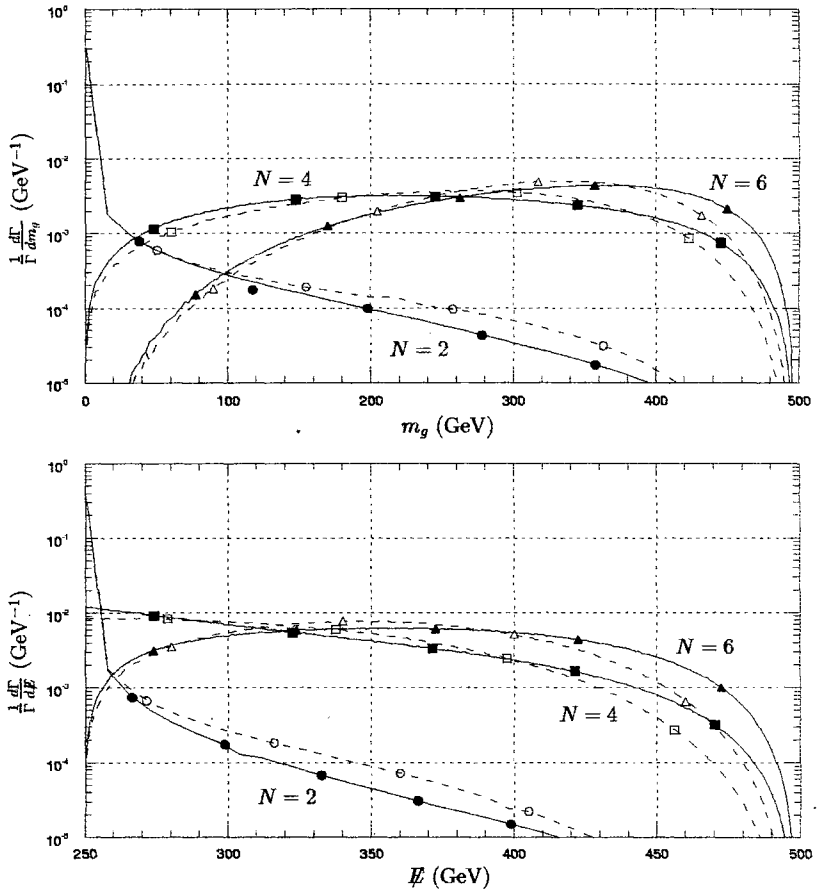

Figure 11: The graviton mass distribution (top) and missing energy distribution (bottom) of the $q_1^\bullet$ or q_1° (solid) and $g_1^\star$ (dashed) are illustrated for $\mu = 500$ GeV and $M_D = 5$ TeV. The pairs of curves correspond to 2, 4, and 6 extra dimensions.

V

RESULTS

Fermi-Phobic Model

QCD Interactions

Dijet Production. The CTEQ distribution functions [25] for the parton luminosity are evaluated at $Q = p_T$, and impose the following cuts: The transverse momentum p_T is constrained to lie above some minimum p_T^{min}, while the rapidity is restricted to satisfy $\mid y \mid \leq 2.5$. The total cross section can also be separated into the SM cross section and the $g^\star$ cross section, which is due to the contributions of Fig. 3: $\sigma = \sigma_{SM} + \sigma_{KK}$. Although σ_{KK} includes the interference terms between g's and $g^\star$'s, it usefully represents the amount by which the total cross section exceeds the SM background. The KK contributions, along with the SM background, are shown in Fig.'s 12–13 for compactification scales in the range 1 TeV $\leq \mu \leq$ 10 TeV and for transverse momentum as high as $p_T^{min} \leq 4$ TeV.

The KK effect is actually quite large: For sufficiently high p_T^{min} ($\sim$ 2 TeV), the effect of the virtual exchanges of the $g^\star$'s actually exceeds the SM background for compactification scales below 7 TeV. The effect becomes even more pronounced for yet higher p_T^{min}, where the KK contribution becomes several factors larger than the SM cross section. The trend continues beyond the 4 TeV shown, but the cross section is too small beyond this point to observe more than a couple of events per year at the anticipated integrated luminosity of the LHC (2×10^5 pb^{-1}). Final quark states

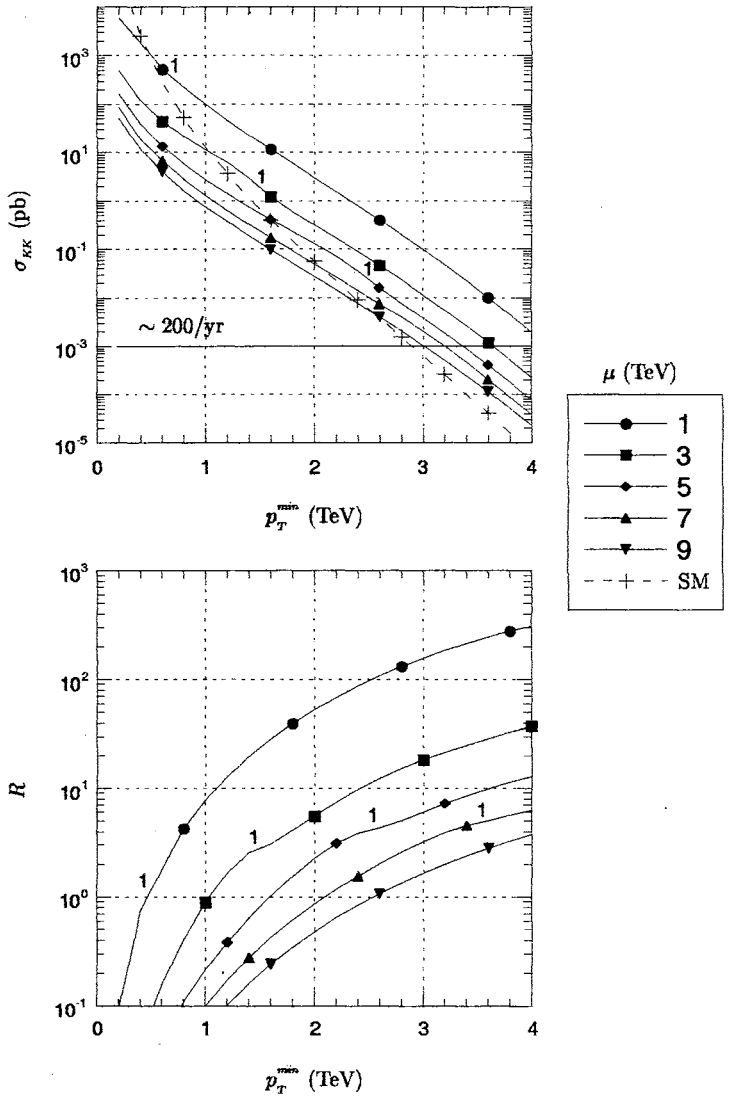

Figure 12: The contributions of the virtual exchanges of g^*'s to the LHC dijet production cross section, $\sigma_{KK} = \sigma - \sigma_{SM}$, (top) and the ratio of the KK contribution to the SM background, $R = \sigma_{KK}/\sigma_{SM}$, (bottom) are illustrated as a function of the minimum transverse momentum p_T^{min} for fixed values of the compactification scale μ. The solid horizontal line represents $\sim$ 200 events/yr at the projected integrated luminosity. Discernible bumps in regions for which $p_T^{min} = k\mu/2$ are indicated by the corresponding value of $k \in \{1, 2, \ldots\}$.

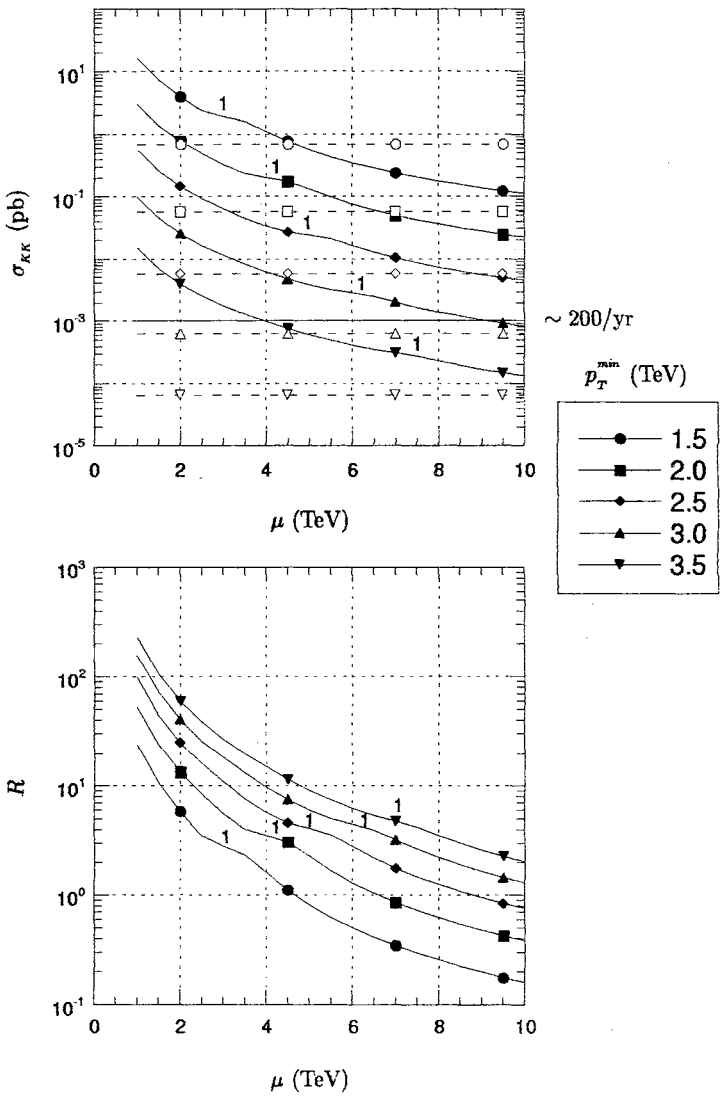

Figure 13: Same as Fig. 12, but as a function of the compactification scale μ for fixed values of the minimum transverse momentum p_T^{min}. The horizontal dashed lines represent the SM background.

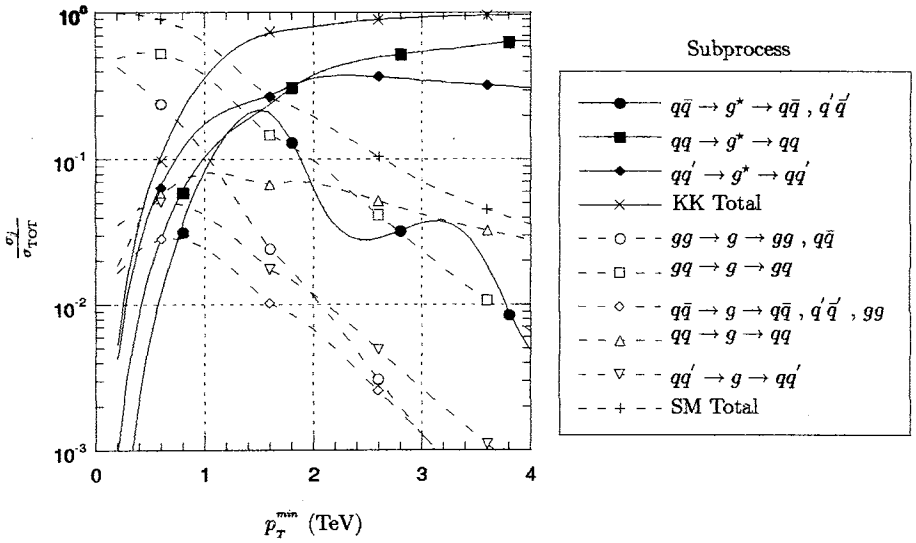

Figure 14: The partial contributions to the total dijet cross section are shown as a function of p_T^{min}, for $\mu = 3.5$ TeV.

due to the decay of a very massive $g^\star$ have very high p_T, thereby enhancing the ratio $R \equiv \sigma_{KK}/\sigma_{SM}$ for high p_T^{min}, which is where the $g^\star$ contribution actually exceeds the SM contribution. When $p_T^{min} = k\mu/2$ for $k \in \{1, 2, \ldots\}$, there is a slight disturbance in the cross section plots, which is expected since this corresponds to an on-shell $g^\star$ contribution. Naturally, the disturbance is only discernible for small values of k. These discernible regions are indicated on the plots by the corresponding values of k.

The partial contributions of the various subprocesses to the full dijet KK (for a representative value of $\mu = 3.5$ TeV) and SM cross sections are illustrated in Fig. 14. At low p_T, the virtual $g^\star$ effect is greatest for subprocesses with two different initial quarks, while, at high p_T, it is largest for subprocesses with identical initial quarks.

Fig. 15 shows the dijet differential cross section $d\sigma/dm$ as a function of the invariant mass m of the final state q-$\bar{q}$ pair: The peaks are subtle, and positioned well below the SM background. The signal in the two-jet invariant mass distribution is well below the SM background unless the invariant mass is very large ($m > 5$ TeV).

However, at the LHC, the cross sections are not large enough for the signal to be observable in this range of m. There are two reasons why the dijet invariant mass distribution does not give a good signal. First, the widths of the $g^\star$'s are large such that the peaks corresponding to $m = \mu$ are not sharp nor tall enough. Secondly, most of the cross section for a given invariant mass comes from pairs which have relatively low p_T for which the SM background is very large. The decay of the resonant KK gluon, $g^\star$, gives rise to high p_T for each of the jet pairs. It is only when the final states where each of the jets have high p_T are considered that the KK contributions exceed the SM background. In the invariant mass distribution, such high p_T contributions constitute only a very small part of the cross sections observable at the LHC energy.

Depicted in Fig. 16 are the effects produced by variation of the somewhat arbitrary choice of $Q = p_T^{min}$ for the SM background. The relative uncertainty in the SM background can be quite high, say 40 %, due to the ambiguity in the choice of Q, and other factors such as the choice of parton distributions. However, since the signal and the background are each calculated at tree-level, the uncertainties should somewhat cancel in the ratio, R. Thus, R provides a good measure of the relative KK effect. It is pointed out that due to these uncertainties and the fact that one can not directly measure R, when working at tree-level it is necessary to look for signals that disagree with the SM by much more than 50%, probably as much as 100%, to be sure that a signal for new physics is indeed what is observed. Therefore, the detection of KK excitations of the gluons is most favorable for regions of (p_T^{min}, μ)-space where the KK contribution is at least comparable to the SM background, and above the horizontal line (in Fig.'s 12–13) that marks an anticipated couple of hundred events per year.

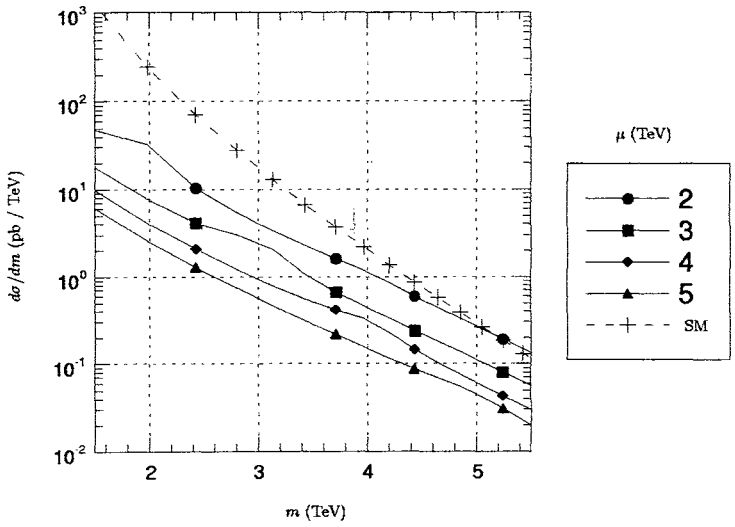

Figure 15: The differential cross section $d\sigma/dm$ is shown as a function of the invariant mass m of the q-$\bar{q}$ pair. The peaks that are predicted to occur when the invariant mass m matches the compactification scale μ are subtle and located well below the SM signal.

For comparison, Fig.'s 17–18 also give the $g^\star$ cross section and its relation to the SM background for the Fermilab Tevatron $p\bar{p}$ collider running at $\sqrt{s} = 2$ TeV. The KK effect is much smaller than for the LHC because of the considerably more restrictive constraints on the transverse momentum. The $g^\star$ cross section is only comparable to the SM for compactification scales μ as high as about 2 TeV, and the relative uncertainty in the total dijet cross section must be quite precise in order to see a sizeable discrepancy for $\mu \sim 3$ TeV.

Single On-Shell $g^\star$ Production. The various cuts are performed by defining the two 4-momenta of the decaying particles in their center of mass frame in terms of Ω_4 (each decaying particle has momentum $m_n/2$) and boosting the two 4-momenta to the lab frame. In addition to the $g^\star$ cross section, the SM three-jet background is calculated following the outline of Ref. [26].

In addition to the cuts applied for dijet production, for three or four jets, the final states are constrained to be separated by a cone of radius $R = \sqrt{(\Delta\phi) + (\Delta\eta)} = 0.4$,

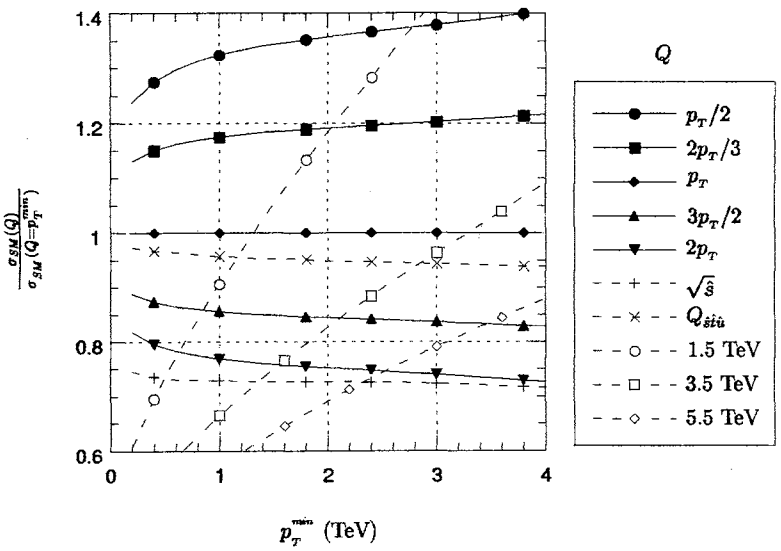

Figure 16: The effect that variation of the choice of Q has on the SM dijet background is shown as a function of the minimum transverse momentum, p_T^{min}. Here $Q_{\hat{s}\hat{t}\hat{u}} = \sqrt{\frac{\hat{s}\hat{t}\hat{u}}{\hat{s}^2+\hat{t}^2+\hat{u}^2}}$, and values in TeV (*e.g.*, 3.5 TeV) correspond to the choice of (constant) Q equal to a compactification scale at that particular scale.

where ϕ is the azimuthal angle and η is the pseudorapidity, which is related to the polar angle θ via $\eta = -\ln\tan(\theta/2)$. The single on-shell $g^\star$ production cross sections, along with the SM background, are plotted in Fig.'s 19–20 for 1 TeV $\leq \mu \leq$ 5 TeV and $p_T^{min} \leq 2$ TeV. High p_T cuts have a similar effect to that described for dijet production except that the $p_T^{min} = k\mu/2$ disturbances are much larger than the dijet case, which should be expected since the $g^\star$ is produced on-shell in the three-jet case considered here. Such discernible disturbances are indicated by the corresponding values of $k \in \{1, 2, \ldots\}$. Again the p_T cuts are terminated when the number of anticipated events is quite scarce ($\sim$ 1/yr). Although it is not as extreme as in the dijet case, the single on-shell $g^\star$ results also exceed the SM background for very high p_T^{min}. The partial contributions of the various subprocesses to the $g^\star$ (for a representative value of $\mu = 3.5$ TeV) and SM cross sections are shown in Fig. 21.

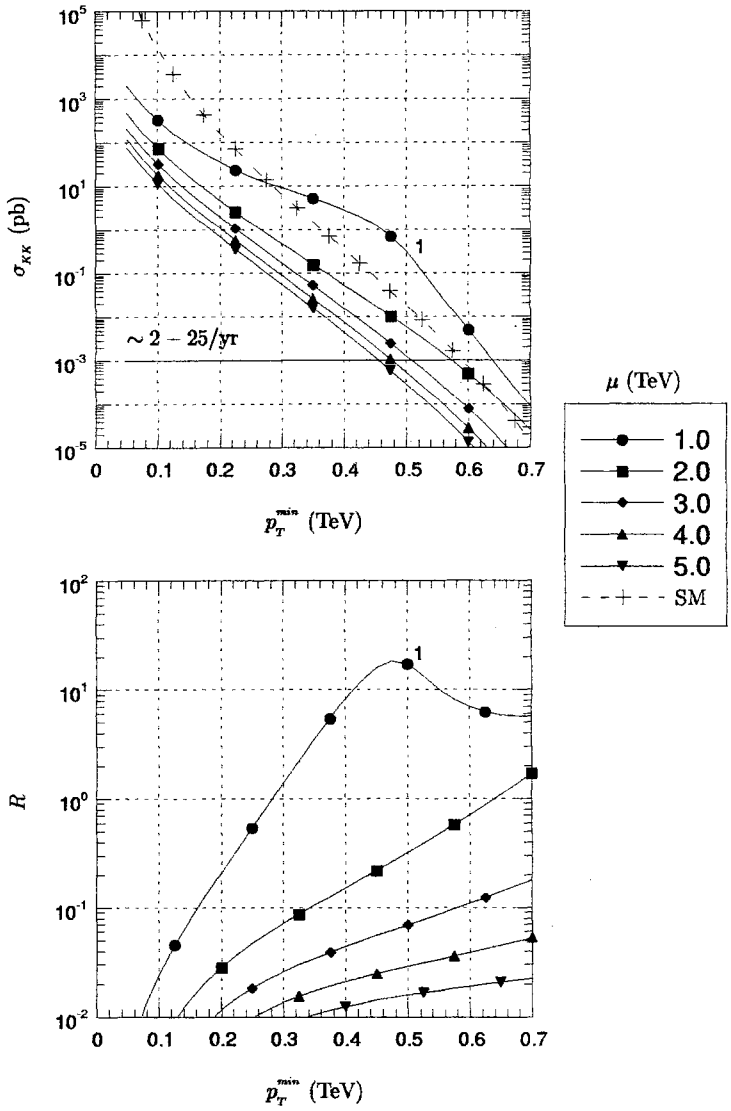

Figure 17: The contributions of the virtual exchanges of $g^\star$'s to the Tevatron dijet production cross section, $\sigma_{KK} = \sigma - \sigma_{SM}$, (top) and the ratio of the KK contribution to the SM background, $R = \sigma_{KK}/\sigma_{SM}$, (bottom) are illustrated as a function of the minimum transverse momentum p_T^{min} for fixed values of the compactification scale μ. The solid horizontal line represents ~ 2 (25) events/yr at the projected initial (final) Run 2 integrated luminosity. Discernible bumps in regions for which $p_T^{min} = k\mu/2$ are indicated by the corresponding value of $k \in \{1, 2, \ldots\}$.

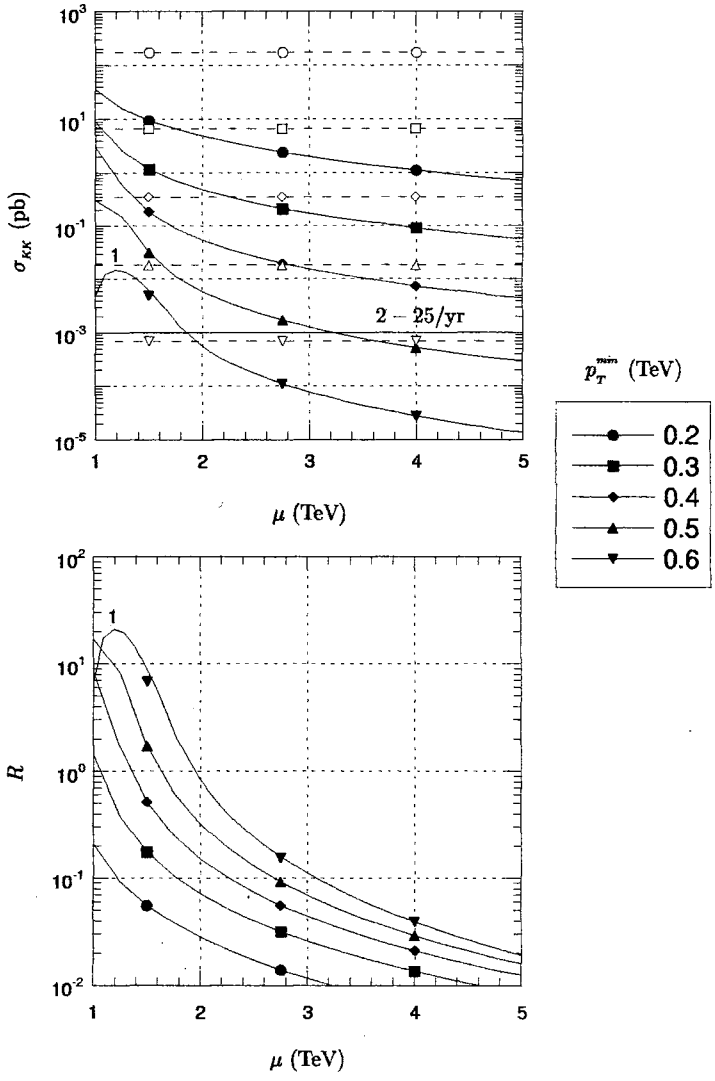

Figure 18: Same as Fig. 17, but as a function of the compactification scale μ for fixed values of the minimum transverse momentum p_T^{min}. The horizontal dashed lines represent the SM background.

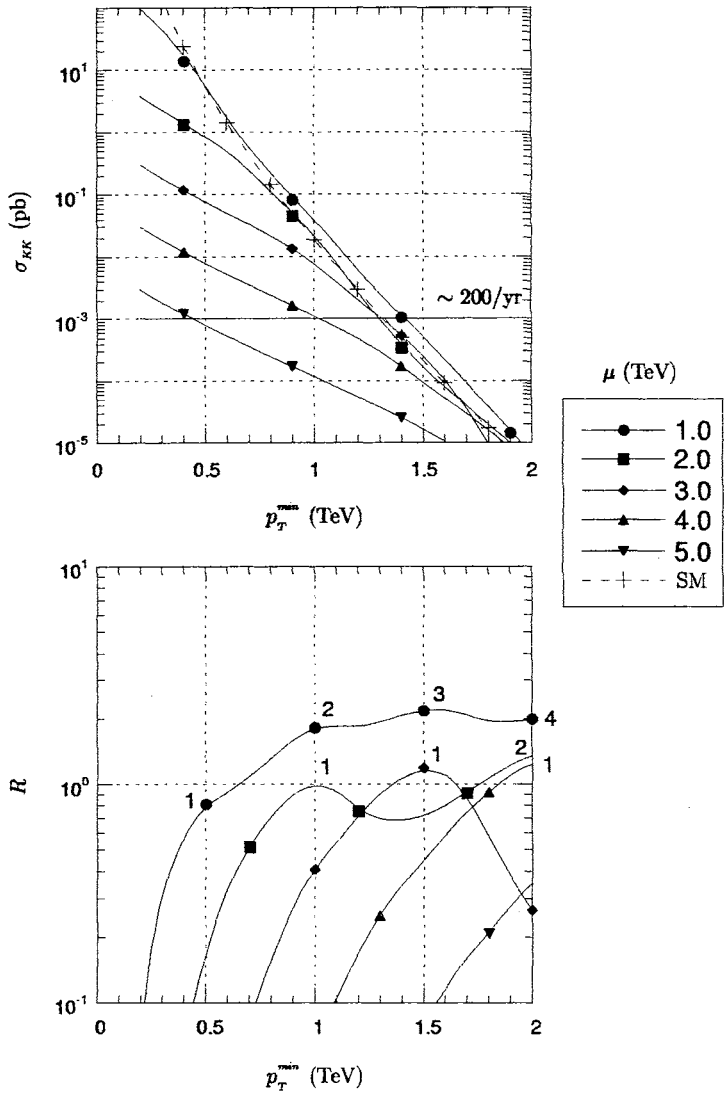

Figure 19: The contributions of the single on-shell production of g^*'s to the three-jet cross section at the LHC, $\sigma_{KK} = \sigma - \sigma_{SM}$, (top) and the ratio of the KK contribution to the SM background, $R = \sigma_{KK}/\sigma_{SM}$, (bottom) are illustrated as a function of the minimum transverse momentum p_T^{min} for fixed values of the compactification scale μ. The solid horizontal line represents $\sim$ 200 events/yr at the projected integrated luminosity. Discernible bumps in regions for which $p_T^{min} = k\mu/2$ are indicated by the corresponding value of $k \in \{1, 2, \ldots\}$.

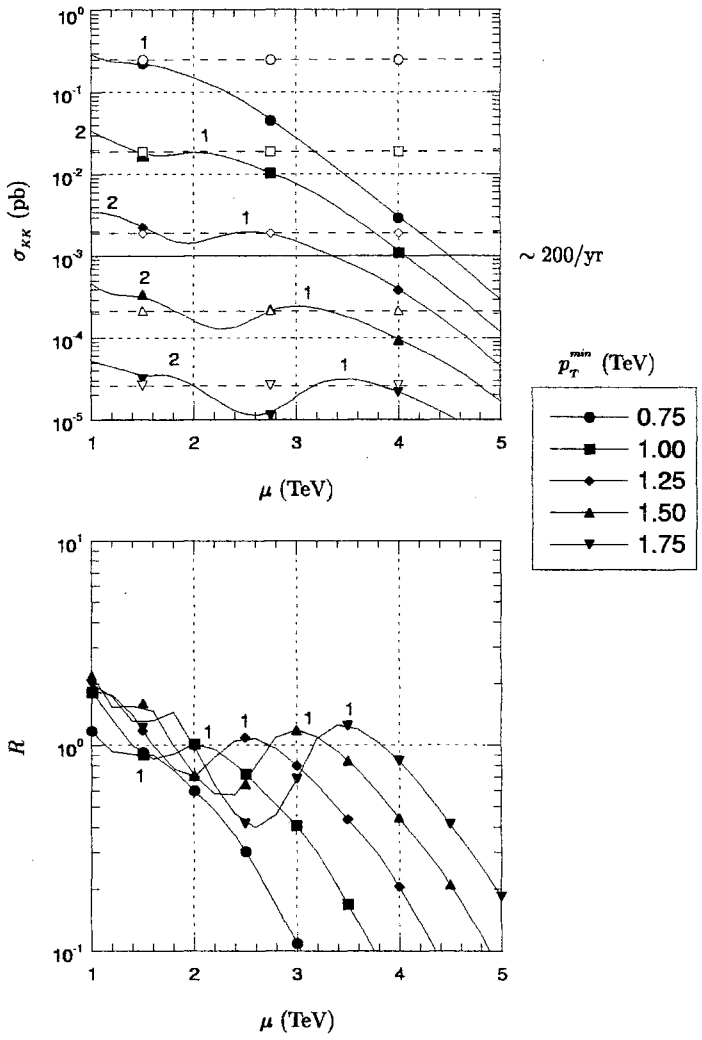

Figure 20: Same as Fig. 19, but as a function of the compactification scale μ for fixed values of the minimum transverse momentum p_T^{min}. The horizontal dashed lines represent the SM background.

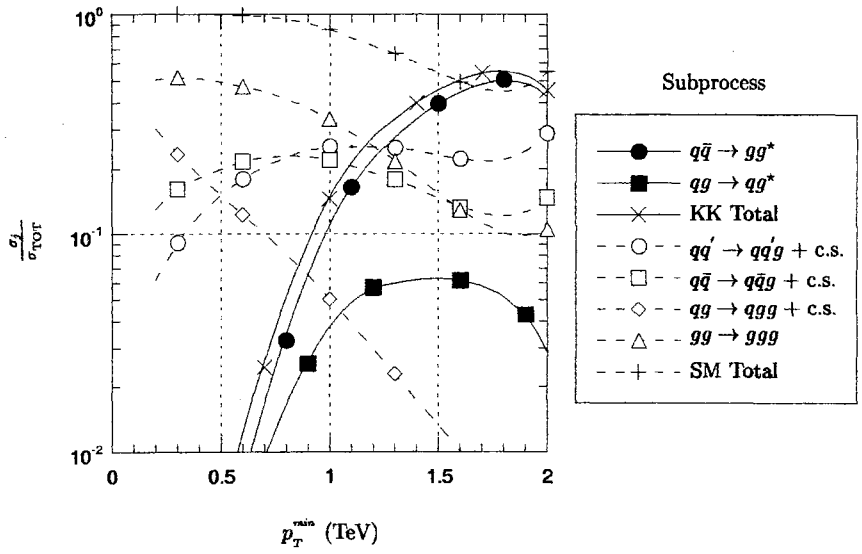

Figure 21: The partial contributions to the total three-jet cross section are shown as a function of p_T^{min}, for $\mu = 3.5$ TeV. Here, c.s. represents all subprocesses that are related by crossing symmetry.

The $qg \to qg^\star$ subprocess dominates over the range of interest, and $q\bar{q} \to gg^\star$ only contributes to the KK dijet cross section significantly for low p_T. The effect of varying Q in the SM for three jets resembles the effect for two jets to a large degree (Fig. 22).

The calculation of the background for these three-jet final states is somewhat of an overestimate. For this signal, two of the jets come from the decay of an on-shell $g^\star$. Upon imposing the condition that two of the jets cluster around the $g^\star$ mass for the SM background, the background to the signal ratio will be less. This was not imposed since it is not certain whether that will be possible to implement experimentally in the actual detection of the jets. If that is experimentally feasible, the background to signal ratio will be less.

Double On-Shell $g^\star$ Production. The same cuts are employed that were utilized for the single $g^\star$ case. Illustrated in Fig. 23 are the four-jet KK cross sections for 1.0 TeV $\leq \mu \leq$ 3.5 TeV , and $p_T^{min} \leq 1.5$ TeV. High p_T cuts have a similar effect to that

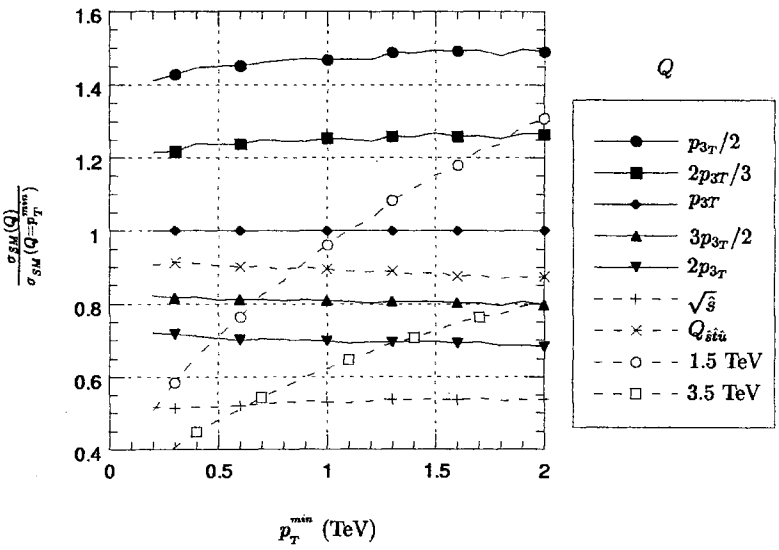

Figure 22: The effect that variation of the choice of Q has on the SM three-jet background is shown as a function of the minimum transverse momentum, p_T^{min}. Here, p_{3T} is the transverse momentum of one of the jets, $Q_{\hat{s}\hat{t}\hat{u}} = \sqrt{\frac{\hat{s}\hat{t}\hat{u}}{\hat{s}^2+\hat{t}^2+\hat{u}^2}}$, and values in TeV (*e.g.*, 3.5 TeV) correspond to the choice of (constant) Q equal to a compactification scale at that particular scale.

described for single $g^\star$ production. The KK cross section is considerably smaller for double $g^\star$ production as compared to the single $g^\star$ case, which itself is much smaller than the dijet case: For double $g^\star$ production, the KK cross section is too small to expect more than a couple of events per year for a compactification scale in excess of 3.5 TeV, regardless of the SM four-jet background. The subprocess with initial quarks is about a factor of 6 larger than the contribution from initial gluons, which can be explained by the fact that it is partially magnified by the factors of $\sqrt{2}$ in the q-$\bar{q}$-$g^\star$ vertices. Also, the production of two $g^\star$'s with different modes is negligible compared to the case when they have identical modes because there can not be a gluon propagator in the s-channel in the former case.

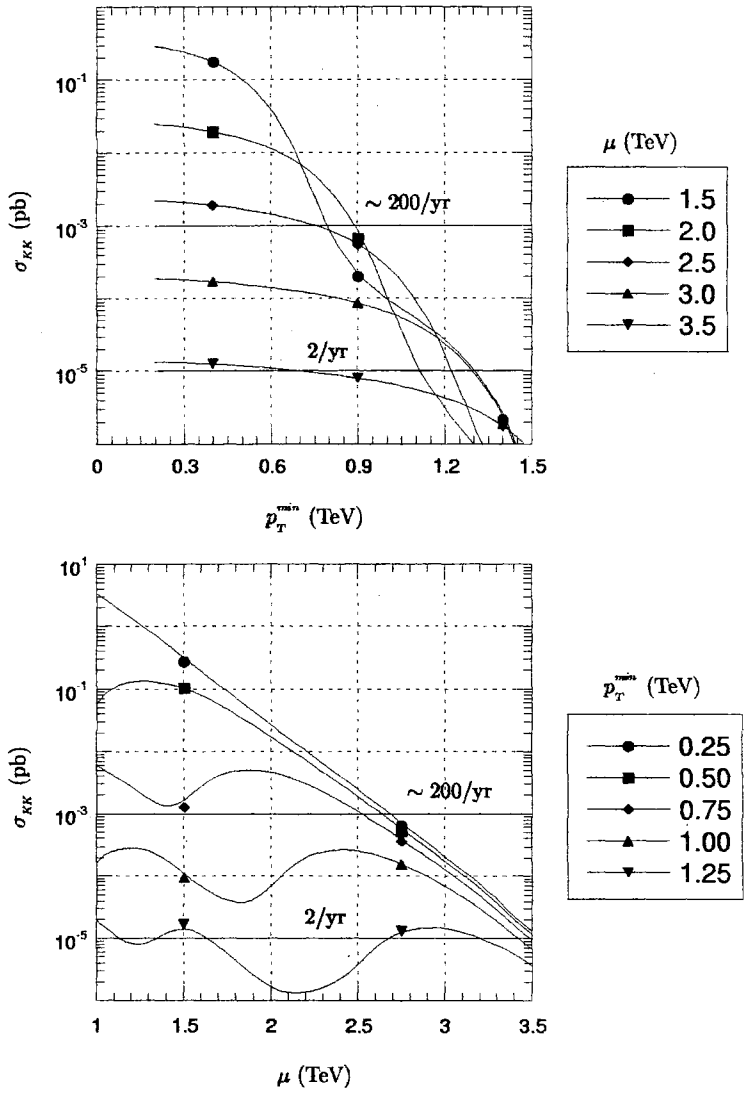

Figure 23: The contributions of the double-on shell production of g^*'s to the four-jet cross section at the LHC, $\sigma_{KK} = \sigma - \sigma_{SM}$, are illustrated as a function of the minimum transverse momentum p_T^{min} for fixed values of the compactification scale μ (top) and as a function of μ for fixed p_T^{min} (bottom).

EW Interactions

Muon Pair Production and Bhabha Scattering. Muon pair production is among the best prospects for the indirect observation of KK excitations of the EW gauge bosons in e^+e^- processes because it can be measured with relatively high precision at present and upcoming colliders while still producing rather substantial deviations from the SM cross section in comparison with other processes. Muon pair production has already been investigated elsewhere in the literature [10] for the purpose of setting present and future e^+e^- collider bounds. This process is primarily included here as a standard by which to compare the results for other processes, but it also serves as a check on these calculations. The first 100 KK excitations are included in this analysis for purely direct-channel processes and 25 KK excitations for processes with both direct- and cross-channel Feynman diagrams; in addition, e^+e^- collider energies are considered from LEP2 energies to 1.5 TeV and compactification scales up to 10 TeV.

The cross section for muon (or tau) pair production is easily obtained via replacement of the usual SM propagator terms by the effective propagator terms of Eq. 48. Because the compactification scale μ is a TeV or more and feasible values of $\sqrt{s}$ for colliders in the present and not-too-distant future range up to about a TeV, the primary effect of the KK excitations of the EW gauge bosons arises from the interference of the $n = 0$ (SM) mode terms with the $n > 0$ (KK) mode terms. Since $(s - m^2_{X_{n>0}}) < 0$ for the ranges of $\sqrt{s}$ and μ that are considered, the overall effect of the KK excitations is a reduction in the muon (or tau) pair production cross section

as compared to the SM. This effect is illustrated in Fig. 24, where the ratio

$$R \equiv \frac{\sigma}{\sigma_{SM}} = \frac{\sigma_{SM} + \sigma_{KK}}{\sigma_{SM}} \tag{71}$$

is plotted for variation of compactification scale μ and collider energy $\sqrt{s}$ in the ranges 1 TeV $\leq \mu \leq$ 10 TeV and 0.3 TeV $\leq \sqrt{s} \leq$ 1.5 TeV. It is clear that a very precise measurement of the cross section ($\lesssim 6\%$ uncertainty) is needed in order to observe a KK effect at a LEP2 collider running at $\sqrt{s} = 200$ GeV for $\mu \geq 2$ TeV. However, the effect increases significantly for larger collider energies: For example, a compactification scale of 4 TeV produces an effect of only a few percent at LEP2 energies, while it reduces the cross section by more than 30% at a TeV-scale e^+e^- high-energy collider.

Bhabha scattering involves the cross-channel exchanges of the γ and Z as well as the direct-channel exchanges of muon pair production. Again the primary effect can be attributed to the interference of the $n = 0$ mode with the $n > 0$ modes. However, although this interference causes a reduction in the direct-channel cross section (*i.e.*, muon pair production), it has the opposite effect in the cross-channel. These competing effects lead to a smaller overall effect of the KK excitations on Bhabha scattering as compared to muon pair production. This overall enhancement of the SM cross section is depicted in Fig. 25 for the same range of parameters as in the muon case. The enlargement of the SM cross section is less than 10% for $\mu > 3$ TeV or $\sqrt{s} < 900$ GeV. This makes Bhabha scattering considerably less attractive for observable effects of the KK states as compared to muon production.

Dijet Production. The full dijet final state cross section is given by summing

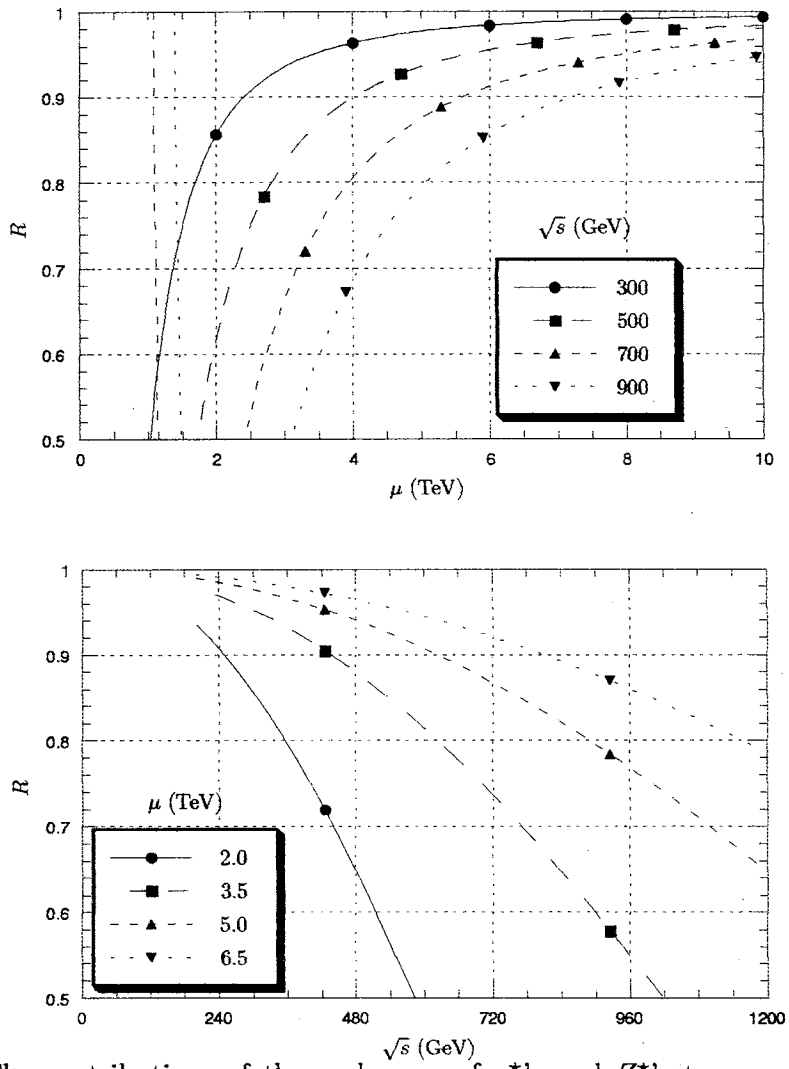

Figure 24: The contributions of the exchanges of $\gamma_n^\star$'s and $Z_n^\star$'s to muon (or tau) pair production are illustrated as a function of the compactification scale μ for fixed values of the collider energy $\sqrt{s}$ (top), and as a function of $\sqrt{s}$ for specific choices of μ (bottom).

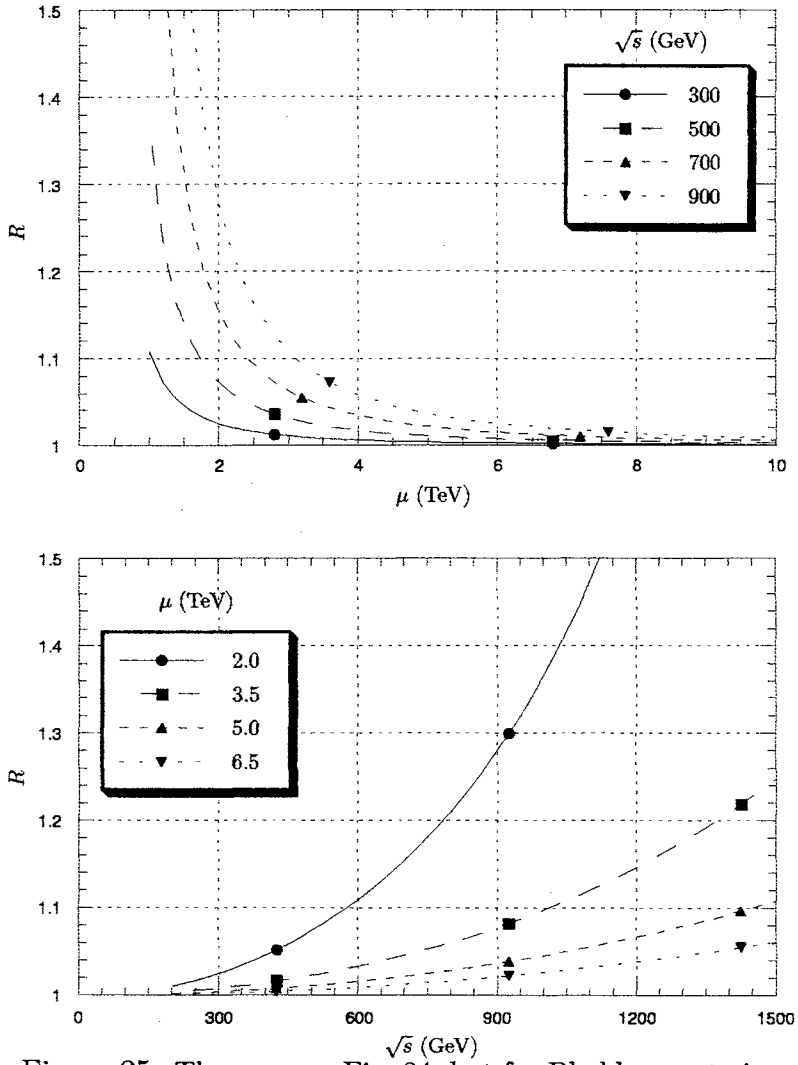

Figure 25: The same as Fig. 24, but for Bhabha scattering.

$e^+e^- \to q\bar{q}$ over all quark flavors for which $s > 4m_q^2$. Thus, top quark production is only included for $\sqrt{s} > 350$ GeV. The standard top quark corrections are included in the cross section formulae, since the top quark mass is significant compared to $\sqrt{s}$ for LEP energies, but note that the top quark mass is negligible in comparison to TeV-scale KK excitations. The KK excitations result in the same effective s-channel propagator expressions as in the case of muon pair production (Eq. 48). As a result, the ratio R is virtually identical in the two cases. The KK effect on dijet final state production is plotted in Fig. 26. As for muon production, a compactification scale of 3.5 TeV results in a reduction by 50% at a TeV-scale collider, by 12% for $\sqrt{s} = 500$ GeV.

Higgs Production. First, consider the associated SM production of the Higgs boson: $e^+e^- \to ZH$. Here, the Z boson is taken to be produced on-shell. As discussed previously, the KK contribution is either zero or strongly suppressed due to KK number non-conservation unless the Higgs boson is confined to the SM three-brane. The Z-Z_n^*-H coupling is non-zero in this situation because the corresponding term in the 5D Lagrangian density contains a delta function to constrain the Higgs boson to the SM wall. Therefore, the focus is on this scenario here. The effect of the KK excitations of the Z is described by the replacement of the SM direct-channel Z boson propagator by the effective propagator given in Eq. 48. Although the Higgs mass is important in limiting the available collider energy range and determining the numerical value of the SM cross section, it does not affect the ratio of the total cross section given by the sum of the SM and KK contributions to the SM cross section. In fact, since there is only one diagram involved, the ratio R is given by the effective

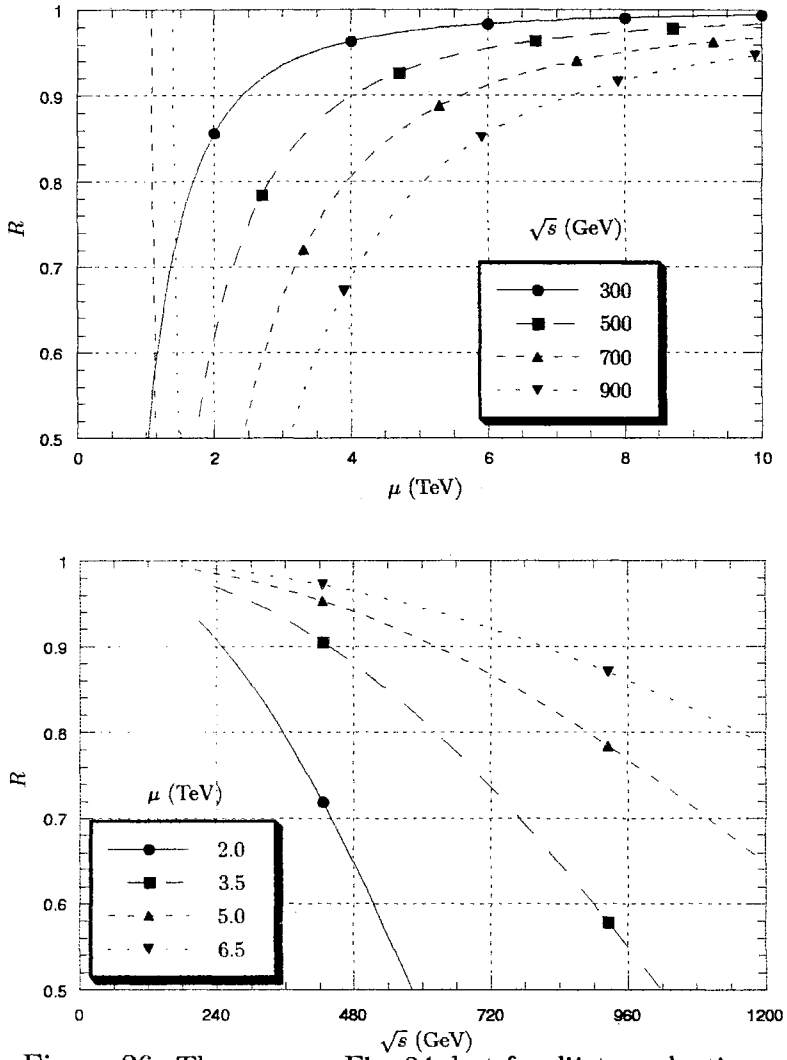

Figure 26: The same as Fig. 24, but for dijet production.

propagator from Eq. 48:

$$R = |D^{\star}_{eff}(Z,s)|^2 = \frac{1}{2}\sum_{m,n=0}^{\infty} c_{Z_m} c_{Z_n} \frac{s'_{Z_m} s'_{Z_n} + m_{Z_m}\Gamma_{Z_m} m_{Z_n}\Gamma_{Z_n}}{(s^2_{Z_m} + m^2_{Z_m}\Gamma^2_{Z_m})(s^2_{Z_n} + m^2_{Z_n}\Gamma^2_{Z_n})} \qquad (72)$$

Thus, not only is the ratio R independent of the Higgs mass, it is also independent of the Higgs model (to the point where there are only exchanges of Z or $Z^{\star}_n$ bosons). For example, the ratio R is the same in the SUSY Higgs doublet case of $e^+e^- \rightarrow Ah$ as in the SM case of $e^+e^- \rightarrow ZH$. However, the total cross section depends on the Higgs model, and this plays a strong role in determining if the total cross section is significant enough to observe the Higgs boson(s) (and if so, if it is large enough to see a KK effect).

The KK effect on Higgs production for processes (such as the SM and SUSY Higgs doublet cases discussed above) in which there are only exchanges of Z or $Z^{\star}_n$ bosons is shown in Fig. 27, where R is graphed as a function of the compactification scale μ and collider energy $\sqrt{s}$ for the same range of parameters as in the case of muon pair production. Although there are no photon exchanges in the Higgs case, the effect of KK excitations of the Z boson on Higgs production is almost identical to the KK effect on muon pair production. Lowest-lying KK excitations of the Z boson with masses of about 5 TeV cause a 20% reduction compared to the SM cross section for a collider energy of 1 TeV, whereas the reduction is only 5% at $\sqrt{s} = 500$ GeV, and only 2% at the LEP2 energies. However, a compactification scale of 3.5 TeV produces at least a 10% effect at collider energies beginning at 400 GeV; the reduction is about half for a 1 TeV energy collider. This reduction in the overall cross section as compared to the SM cross section also has a significant effect on the Higgs

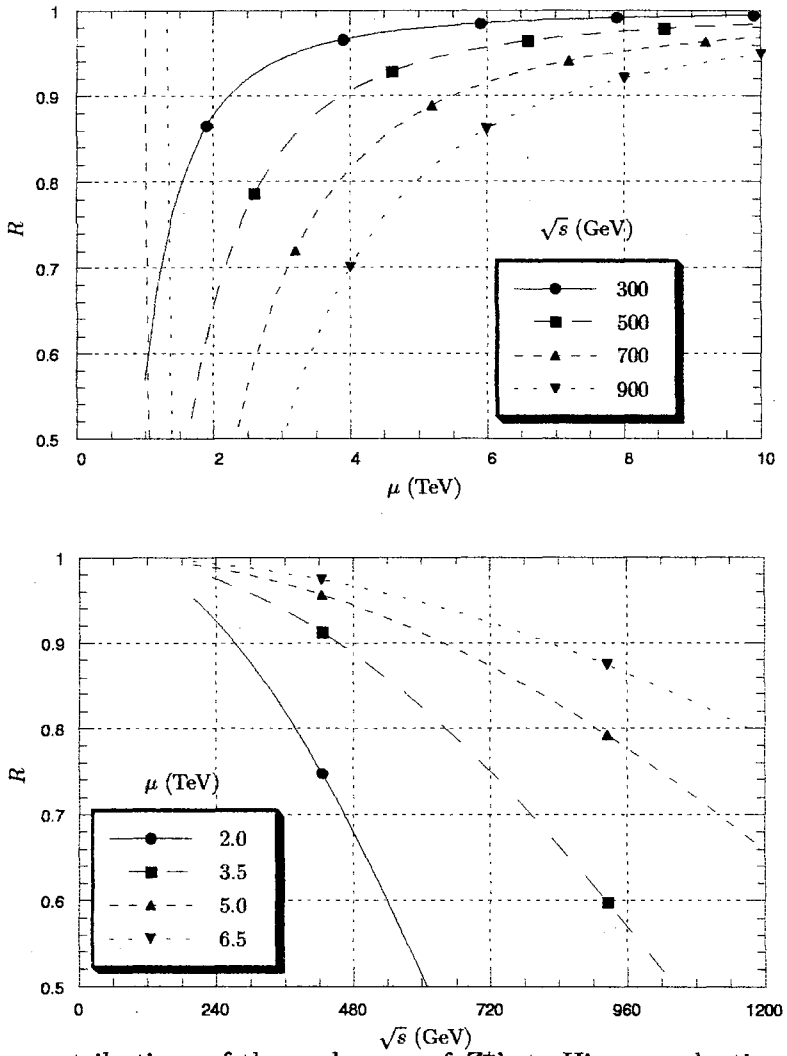

Figure 27: The contributions of the exchanges of $Z_n^\star$'s to Higgs production are illustrated as a function of the compactification scale μ for fixed values of the collider energy $\sqrt{s}$ (top), and as a function of $\sqrt{s}$ for specific choices of μ (bottom).

mass bound, and this is Higgs model-dependent.

Neutrino Pair and Single Photon Production. First consider the case of neutrino pair production, $e^+e^- \to \sum_\ell \nu_\ell \bar{\nu}_\ell$. The production of muon or tau neutrino pairs only consists of direct-channel Z and $Z_n^\star$ exchanges described by the effective propagator modulus-squared of Eq. 48, whereas the production of electron neutrino pairs also includes the cross-channel exchanges of W's and $W_n^\star$'s. The modulus-squared of the effective propagator for this t-channel production involving W's and $W_n^\star$'s is the same as the s-channel production involving Z's and $Z_n^\star$'s with the replacements $Z \to W$ and $s \to t$. Similarly, the s-t interference is given by Eq. 49 with the replacement $\gamma \to W$.

As in the case of Bhabha scattering, the effect of the direct-channel exchanges of the Z's and $Z_n^\star$'s to reduce the cross section and the competing effect of the cross-channel exchanges of the W's and $W_n^\star$'s to increase the cross section as compared to the SM results in a considerably smaller effect than processes such as muon pair production and dijet production where there are only s-channel exchanges of the EW gauge bosons. Although the s-channel KK effect to increase the cross section is larger than the t-channel KK counter-effect percentage-wise, the SM t-channel is dominant for neutrino pair production, which causes a slight increase in the cross section as compared to the SM. This is illustrated in Fig. 28, where the same ranges of the collider energy $\sqrt{s}$ and compactification scale μ are employed as in the case of muon pair production. The KK effect is smaller for neutrino pair production than for Bhabha scattering; also, there appears to be far less dependence on the variation of the collider energy. The result is a KK effect of less than 7% even for a collider energy

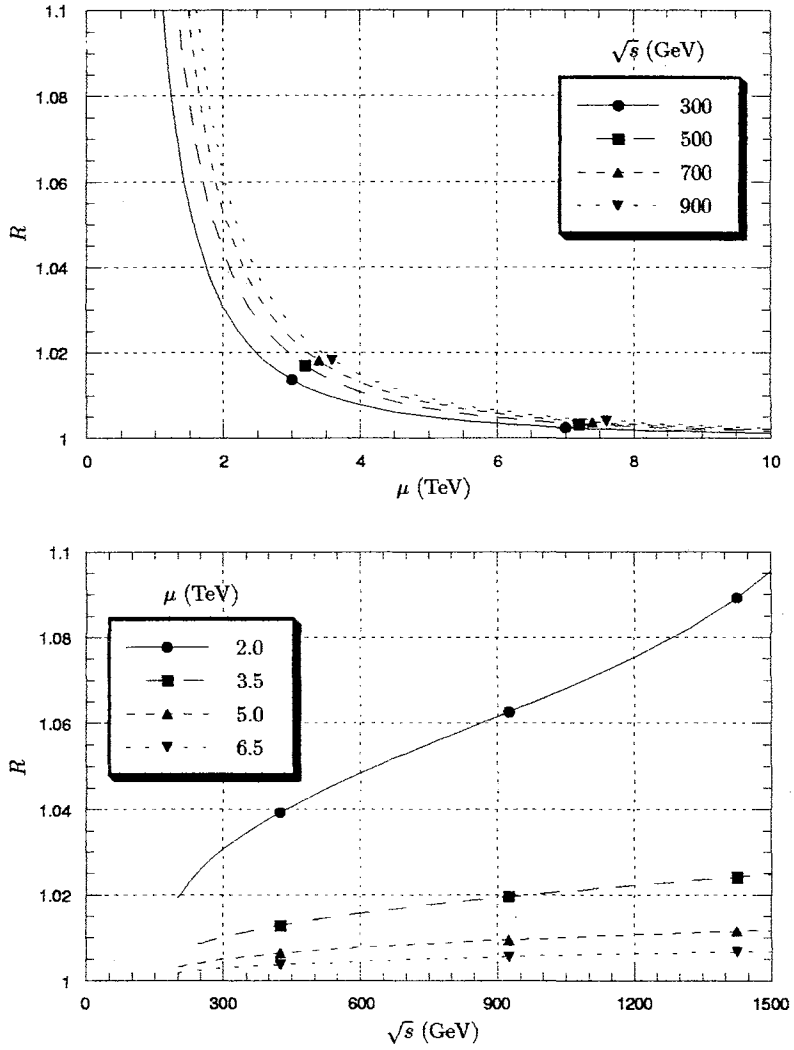

Figure 28: The contributions of the exchanges of $W_n^\star$'s and $Z_n^\star$'s to neutrino pair production are illustrated as a function of the compactification scale μ for fixed values of the collider energy $\sqrt{s}$ (top), and as a function of $\sqrt{s}$ for specific choices of μ (bottom).

as high as a TeV.

Single photon production via $e^+e^- \to \nu\bar{\nu}\gamma$ is somewhat more complicated. Single photon production was considered in Ref. [27] in the context of Z' physics, where only the lowest-lying KK excitations of the W and Z bosons were included. Here, their results are extended to include the 25 lowest-lying states, but concede that the effect depends almost exclusively on the first few states, and primarily on the first. The diagrams for single photon production are the same as for neutrino pair production with a photon radiating off the incoming electron or positron or the internal W or $W_n^\star$. The effect of the KK excitations results in the same direct-channel effective propagator as the neutrino production case, and the same cross-channel effective propagator when the photon radiates off the incoming electron or positron. However, for the case where the photon radiates off the internal W or $W_n^\star$, a difference arises from the coupling of the photon to W's and $W_n^\star$'s. The γ-W-$W_n^\star$ and γ-$W_m^\star$-$W_{n\neq m}^\star$ couplings are forbidden due to KK number non-conservation, as discussed in Section 2. On the other hand, the diagram with the γ-$W_n^\star$-$W_n^\star$ coupling has two propagators with KK excitations of the W boson, which are quite massive (TeV-scale). This suppresses the KK contribution from this diagram in comparison to the contributions of the diagrams in which the photon radiates off either of the incoming particles.

The overall KK effect on single photon production is very much similar to the KK effect on neutrino pair production. Graphically, the total KK contribution is shown in Fig. 29. Again, the enlargement of the SM cross section is very small. The single photon and neutrino pair production KK effects are almost identical for large collider energies ~ 1 TeV, but the single photon case is more dependent on the

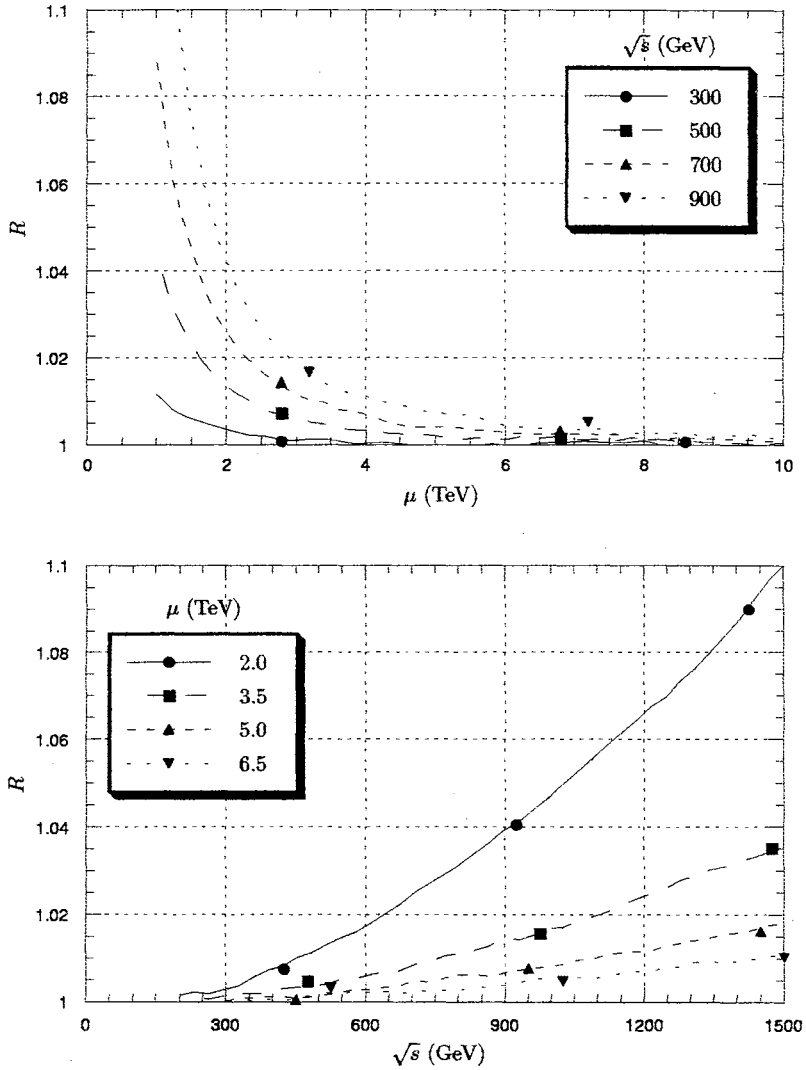

Figure 29: The same as Fig. 28, but for single photon production.

collider energy, resulting in an even smaller effect for LEP energies than the neutrino pair case. Again, the compactification scale must be quite small $\lesssim 2$ TeV in order to see even a 5% effect for a collider with very high energy (TeV-scale).

UED Model

QCD Interactions

Stable KK Final States. For stable KK final states, the production cross sections for the set of subprocesses $\{j\}$ enumerated previously are related to the squares of the amplitudes tabulated therein via:

$$\sigma_{KK}^{tot} = \frac{1}{4\pi} \sum_j \sum_n \int_{\rho_n}^1 dx_A \int_{\rho_n/x_A}^1 dx_B f_{a/A}(x_A, Q) f_{b/B}(x_B, Q) \int_{-1}^1 dz \frac{\bar{\sum} |M_j|^2}{S!} \frac{1}{\hat{s}} \sqrt{1 - \frac{4M_n^2}{\hat{s}}}, \tag{73}$$

where S is a statistical factor (the number of identical final states) and $\rho_n = 4M_n^2/s$. The first summation is over the subprocesses $\{j\}$ tabulated in the previous section, while the second summation runs over all n for which pairs of final states with mass M_n can be produced for a given collider energy $\sqrt{s}$. The higher ($n > 1$) states produce only a slight effect (at the 1% level) due to their large mass.* The cross sections for the higher modes are easily computed from the cross section expression for the first mode by simply replacing the mass of the first mode with that of the higher mode, which includes adjusting the scale Q to correspond to the higher mass.

*Furthermore, $Q = m_n$ for the $n > 1$ modes exceeds the compactification scale μ, for which the running of $\alpha_S(Q)$ transforms from a logarithmic to a power law behavior [21]. This has the effect of reducing the contributions of the higher order modes [22] to the total cross sections even further.

The cross sections in Eq. 73 are evaluated with the CTEQ5 distribution functions [25] and $Q = M_n$ in the parton luminosity. In Fig. 30, the cross section is presented for the production of two stable KK final states for a given first excited KK mass $M = \mu = 1/R$ at the Tevatron proton-antiproton collider. In addition to the total cross section, the contributions of KK gluon pair, KK quark-gluon, and KK quark pair production are plotted. For the case of double KK quark production, the final state consists of light quark KK excitations, but not the top quark, which can decay (*e.g.*, $t_1^\circ \to W_1^{+\star} b$). The production of KK quark pairs is dominant (not as much because the cross section for a specific process is much higher, but because there are many more processes involved), while the KK gluon pair and KK quark-gluon production rates are comparable.

Stable, slowly moving KK quarks produced at colliders will hadronize, producing high-ionization tracks. The production of heavy, charged stable particles will produce a clear signal of new physics. They will appear as a heavy replica of the light SM quarks, with both up- and down-type quark charges, but with two KK quarks corresponding to each SM quark.

At the Tevatron Run I, searches for heavy stable quarks [28] have set an upper limit of about 1 pb on the production cross section of such particles (for a mass range between 200 and 250 GeV). Using a naive extrapolation of the limits presented in Ref. [28] to higher mass values, a lower bound is estimated on the first excited KK mass of about 350 GeV (in agreement with Ref. [13]). For the projected initial (final) Run II ($\sqrt{s} = 2$ TeV) integrated luminosity, which will yield 2 (15) events for each 10^{-3} pb of cross section, 100 events would be produced for a compactification scale of

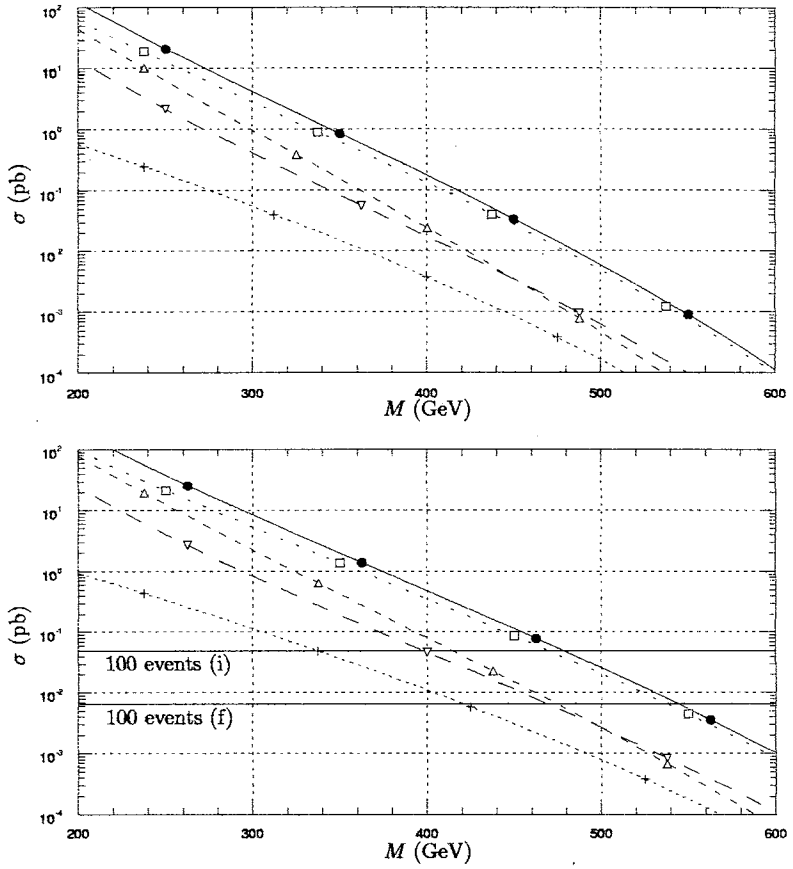

Figure 30: The cross section for the production of two stable KK final states is shown as a function of the KK mass for Tevatron Run I (top) and II (bottom). The solid curve corresponds to the total contribution, while the dashed lines represent the partial contributions of KK quark pair ($\Box$), KK quark-gluon ($\triangle$), and KK gluon pair ($\triangledown$) production. Also shown is top production ($+$), which features a different collider signature (namely, the top will subsequently decay into additional states). Solid horizontal lines mark 100 events at the initial and final projected luminosities for Run II.

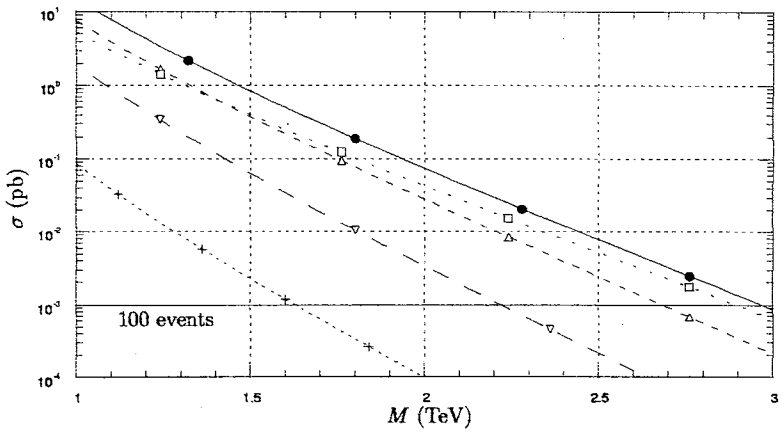

Figure 31: The same as Fig. 30, but for the LHC. The solid horizontal line represents 100 annual events at the projected luminosity.

450 GeV (550 GeV). In order to set definite limits on the mass of KK excitations at Run II, an analysis similar to the one performed for Run I is needed. An estimate of the Run II reach can be made by assuming that the limit on the heavy stable quarks production cross-section is driven by statistics. In this case, an improvement of around a factor of 10 can be expected in this limit, to 0.1 pb. Then, the nonobservation of heavy stable quarks would raise the lower bound for the mass of the first KK mode in the universal scenario to around 450 GeV.

Much better prospects for the discovery of KK fields may be found at the LHC proton-proton collider, where the anticipated annual luminosity is 10^5 pb^{-1}. The cross-sections for the production rate of two stable KK excitations at the LHC energy are illustrated in Fig. 31. A dedicated study is required to find the exact reach of the LHC in this case, but, by requiring at least 100 events to be produced, it can be estimated that the LHC will discover the first stable KK excitations if their mass is smaller than about 3 TeV.

Thus, stable KK quarks and gluons of the UED scenario will either be discovered at the Tevatron Run II or the LHC, or the lower bound on their masses will be raised to around 450 GeV or 3 TeV, respectively. However, cosmological constraints require new physics to explain the existence of stable KK excitations in this mass range. This cosmological restriction can be lifted via a new physics mechanism that causes the lowest-lying KK excitations to have a lifetime that is short compared to the cosmological scale. This possibility is now the focus.

Decaying KK Final States. The collider signature for the production and decay of gluon or light quark (except the top) KK excitations in this model is SM dijet production with missing energy carried off by the gravitons. This production rate is related to the cross sections for the stable case and the differential branching fractions of the decaying KK states via:

$$d\sigma_{tot} = \sum_{A,B} d\sigma_{prod}(p\bar{p} \to A\ B)\ \frac{d\Gamma_A}{\Gamma_A}\ \frac{d\Gamma_B}{\Gamma_B}. \tag{74}$$

The sum is over the KK intermediate states, denoted by A and B. The spin correlations are not taken into account. The top case will be discussed separately.

Consider the following two distributions of experimental interest in Fig. 32: the two-jets + missing energy cross-section as a function of the minimum transverse momentum, p_T^{min}, of the jets (top), and the cross-section as a function of the missing transverse momentum, $|\ \not{\vec{p}}_T\ |$ (bottom). The dependence of these distributions on the number of extra dimensions in which gravity propagates (or on the decay mechanism) is encoded in the mass distributions of the gravitons which mediate this decay. For example, if the quark (or gluon) KK excitations decay mostly to light

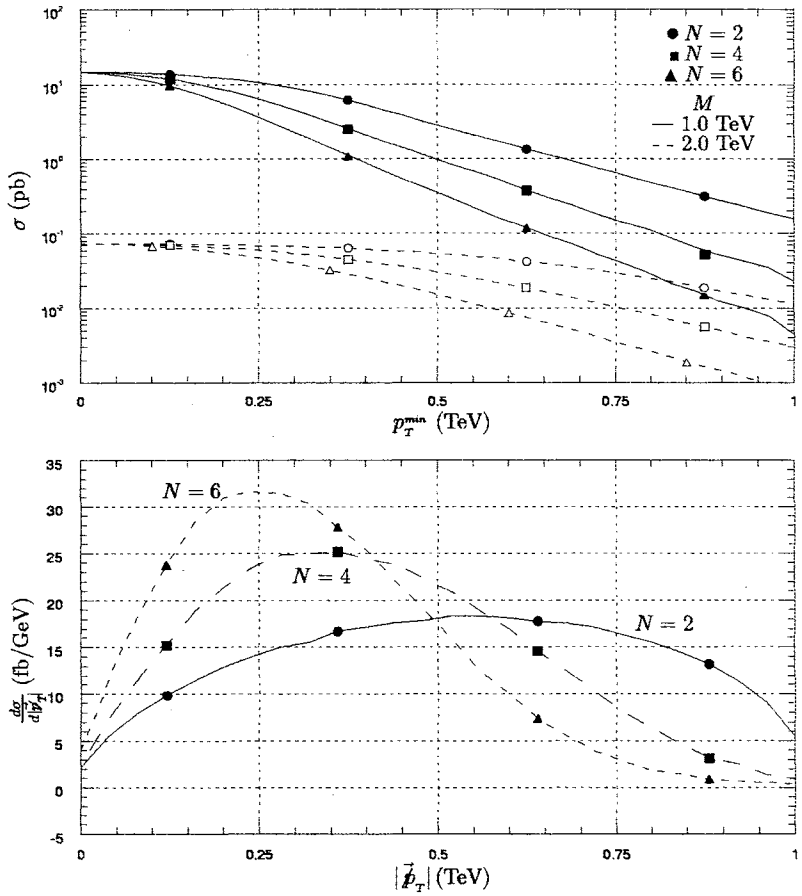

Figure 32: The total cross section for the dijet production plus missing energy from decaying KK final states (top) and the missing transverse momentum $|\not{\vec{p}}_T|$ distribution (bottom) are shown for 2, 4, and 6 extra dimensions. The compactification scale is 1 TeV in the bottom figure, while 1 and 2 TeV are shown in the top figure. No cuts are implemented in these graphs, such that the total area under each curve is equal in the bottom graph. (However, all cuts are implemented in the following figures.)

gravitons, the distributions will look like the curves corresponding to $N = 2$ in Fig. 32. Conversely, in the case when the KK particles decay to heavy gravitons, these will take almost all available momentum, leaving very little for the two observable jets. Hence, the cross section drops faster with increasing minimum transverse momentum, p_T^{min}, and the missing transverse momentum, $|\not{\vec{p}}_T|$, distribution shifts toward zero with the increase in N. Signals for decays mediated by a different mechanism will fit somewhere among these curves, depending on what fraction of the decays favor light versus heavy gravitons.

The dependence of the cross section on the mass of the KK excitations for different p_T cuts is shown in Fig. 33 for the Tevatron Run II and Fig. 34 for the LHC. For illustration, the values of $N = 2$ and $N = 6$ for the number of extra dimensions have been used. Note that the case $N = 6$ is the least favorable to direct observation, since the heavier the graviton mass, the lower the transverse momentum of the quark or gluon jets will be. Beside the cuts specified in the figure, the additional requirement is imposed that the rapidity be limited to the range $|y| \leq 2.5$, and the two observable jets be separated by a cone of radius larger than $R = \sqrt{(\Delta\phi)^2 + (\Delta\eta)^2} = 0.4$, where ϕ is the azimuthal angle and η is the pseudorapidity, which is related to the polar angle θ via $\eta = -\ln\tan(\theta/2)$. Requiring for direct observation at least 100 events with $p_T > 50$ GeV at the Tevatron and $p_T > 400$ GeV at the LHC, respectively, it is seen that the Tevatron reach extends to about 550 GeV, while at the LHC KK excitations can be discovered in this model for values of the compactification scale as high as 3 TeV. It is assumed here that cuts on missing transverse momentum (Fig. 35) are used to greatly reduce the SM background.

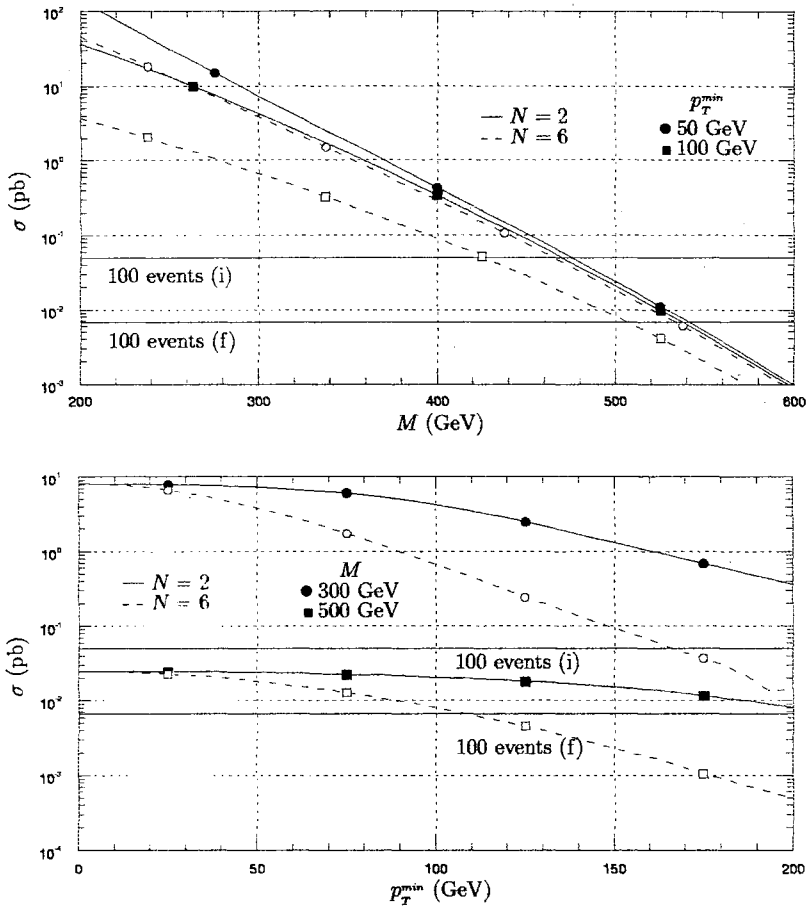

Figure 33: The total cross section for the dijet production plus missing energy from decaying KK final states at the Tevatron Run II energy is illustrated as a function of μ for fixed p_T^{min} (top) and as a function of the minimum transverse momentum p_T^{min} for fixed values of the compactification scale μ (bottom). Solid horizontal lines mark 100 events at the initial and final projected luminosities. In this and the following figures, cuts on the p_T, rapidity, and separation of the jets are implemented.

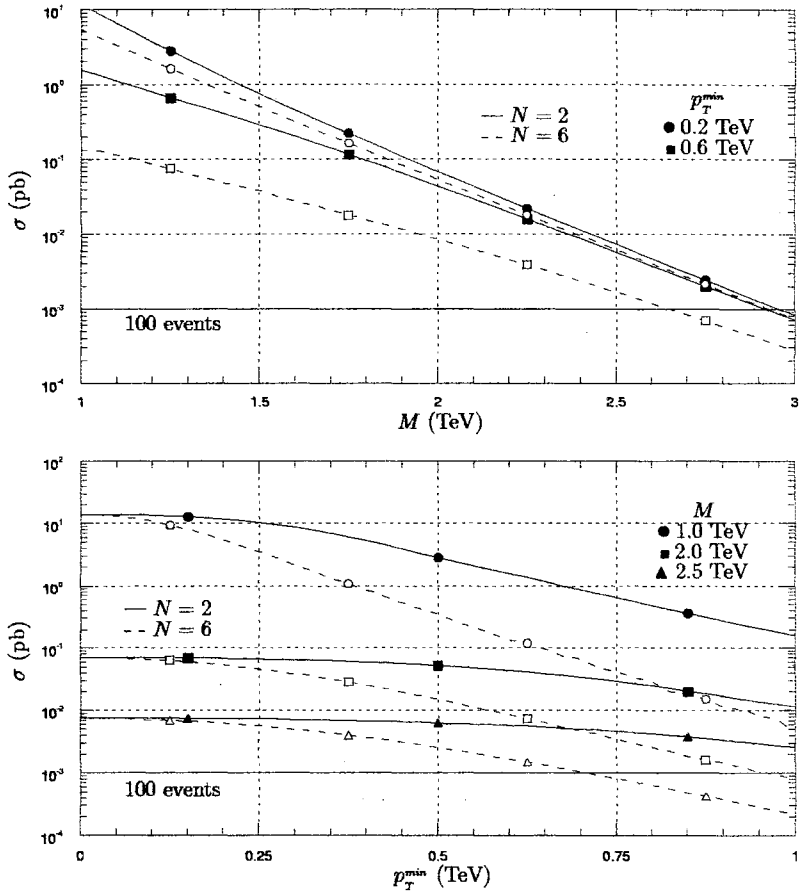

Figure 34: The same as Fig. 33, but for the LHC. The solid horizontal line marks 100 annual events at the projected luminosity.

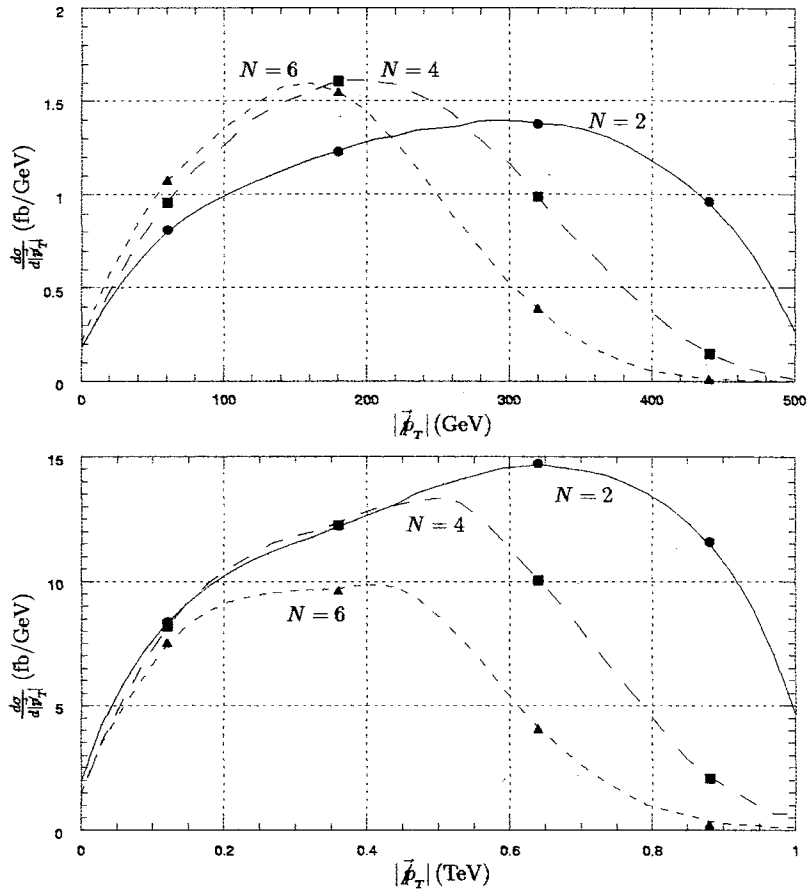

Figure 35: The missing transverse momentum distribution is illustrated for Run II of the Tevatron (top) and the LHC (bottom). The three curves represent 2, 4, and 6 extra dimensions. By $|\vec{p}_T|$ is denoted the vectorial sum of the transverse momentum of the two emitted gravitons (which is equal and opposite to that of the quarks). The compactification scale and minimum transverse momentum are 400 GeV and 50 GeV for the Tevatron and 1 TeV and 200 GeV for the LHC, respectively.

p_T^{min} (GeV)	Background (events)	Signal (events) $M = 1$ TeV $N = 2$	$M = 1$ TeV $N = 6$	$M = 2$ TeV $N = 2$	$M = 2$ TeV $N = 6$	$M = 3$ TeV $N = 2$	$M = 3$ TeV $N = 6$
100	3×10^6	1×10^6	9×10^5	7×10^3	6×10^3	84	80
200	2×10^5	9×10^5	2×10^5	6×10^3	4×10^3	80	65
300	9×10^3	4×10^5	4×10^4	5×10^3	3×10^3	73	50
400	1×10^3	1×10^5	2×10^3	4×10^3	1×10^3	65	34
500	2×10^2	5×10^4	2×10^2	3×10^3	4×10^2	58	20
600	4×10	6×10^2	3×10	2×10^3	1×10^2	50	10

Table 2: SM background [29] and UED signals with $p_T > p_T^{min}$ and $|\not{\vec{p}}_T| > 2p_T^{min}$ for 10^5 pb^{-1} at the LHC.

Presented here are some comments on the SM background. There are many SM processes which can give rise to a dijet signal with missing energy. Some examples include WZ, ZZ, $q\bar{q}Z$, and $t\bar{t}$ production, where neutrinos arising from Z and W, for example, carry off the missing energy; also $2 \to 2$ QCD processes with missing energy due to the mis-measurement of jet energies. Of course, cuts on the minimum p_T of the jets and on the missing transverse energy can be implemented to greatly improve the signal-to-background ratio. A complete analysis of SM backgrounds (including the optimization of cuts) is beyond the purpose of this paper. However, for illustration, consider the specific cuts in Table 2. For example, for $p_T^{min} = 600$ GeV and $|\not{\vec{p}}_T| > 1200$ GeV at the LHC, the SM background has been evaluated in Ref. [29] to be ~ 40 events for 10^5 pb^{-1} luminosity, while the signal would be 600, 2000, and 50 events for $N = 2$ and compactification scale $M = 1$, 2, and 3 TeV, respectively. For $N = 6$, the signal would be 30, 130 and 10 events, for the same values of M. The signal is larger or comparable with the background in almost all of these cases ($N = 6$, $M = 3$ TeV is borderline). Moreover, these cuts can be optimized in order to enhance the signal-to-background ratio: For example, in the case of $M = 1$ TeV,

the 1200 GeV cut on the missing transverse energy is too hard (this is why so few events remain), and by relaxing it the signal can be increased substantially.

Finally, consider the production and decay of KK excitations of the top quark. As seen from Fig.'s 30–31, the cross-section for this process is less than 1% than the total KK excitation production cross-section. However, if the mass of first KK tower is smaller than about 1 TeV, there will be of order 10^4 KK top pair events produced at the LHC. Unlike the light quark KK excitations, the $t^\bullet$ can also decay to $W^{+\star}b$. For $\mu < 1$ TeV, the decay to $W^{+\star}b$ is dominant (unless $N = 2$; in this case, it is necessary to demand that $\mu < 0.4$ TeV). Furthermore, the $W^{+\star}$ can decay either into W + graviton, in which case the signal for this process will be $b\bar{b}W^+W^-$ in the final state, plus missing energy; or into $d^\bullet u$, for example, in which case the signal could be two b jets plus four light quark jets plus missing energy.

EW Interactions

Stable KK Final States. The cross section for the production of two stable KK final states for a given first excited KK mass $M = \mu = 1/R$ at the LHC is illustrated in Fig. 36 for a variety of EW processes. The contributions of KK photon pair, photon-quark, and photon-gluon production are plotted. The heavier KK excitations, such as the Z boson, will subsequently decay into lighter KK states. The production of a KK photon and KK jet is dominant compared to double KK photon production because the former has a strong coupling from the gluon that is present in the interaction. The production of heavy, charged stable particles will produce a clear signal of new physics.

Decaying KK Final States. The dependence of the single and double photon cross sections on the mass of the KK excitations for $\delta = 6$ is also shown in Fig. 36 for the LHC. Requiring for direct observation at least 100 events with $p_T > 400$ GeV at the LHC, the LHC can probe up to 1300–1400 GeV for KK excitations in EW processes. Implementing additional cuts on missing transverse momentum, the EW processes offer the potential for a cleaner signal against the SM background (compared to dijet production).

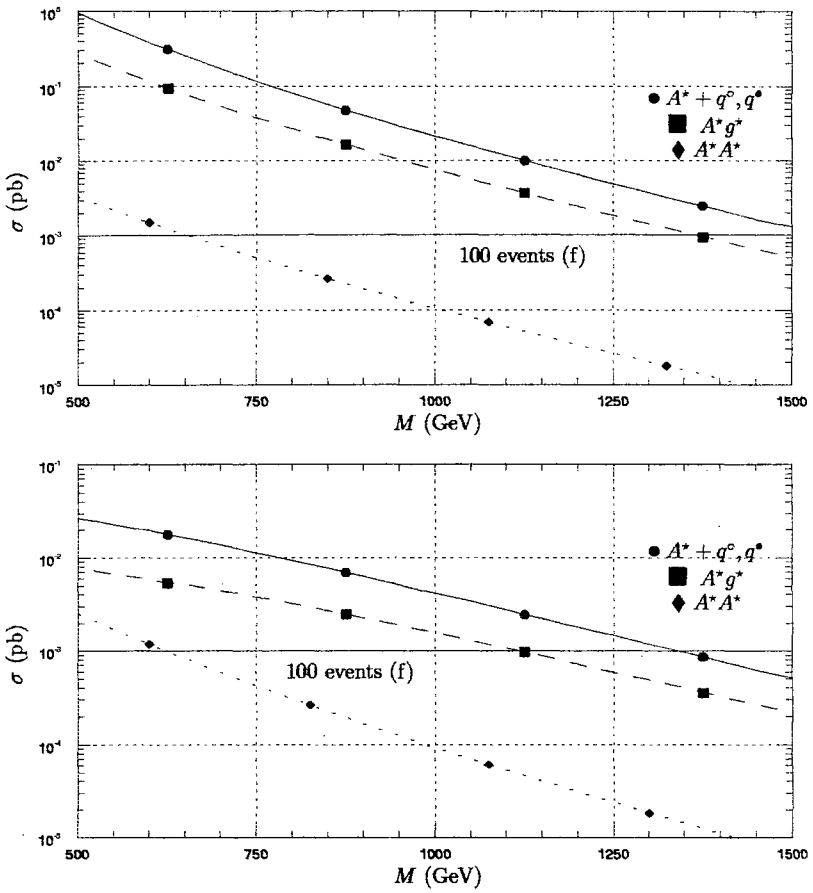

Figure 36: The cross section for the production of two stable (top) and decaying (bottom) KK EW final states is shown as a function of the KK mass for the LHC. The contributions of KK photon-quark (•), photon-gluon (■), and photon pair (♦) production are shown. The solid horizontal line marks 100 annual events at the projected luminosity.

VI

CONCLUSIONS

Fermi-Phobic Model

QCD Interactions

Results. In this work, the phenomenology of a class of string-inspired models has been investigated in which the SM gauge bosons can propagate into one TeV-scale extra dimension. Specifically, the effects that the KK excitations of the gluons have on multijet final states have been calculated at very high energy hadronic colliders such as the LHC or upgraded Tevatron Run 2.

At the LHC ($\sqrt{s} = 14$ TeV), a large enhancement was found, relative to the SM, of the dijet cross sections at high p_T, while at the upgraded Tevatron a considerably smaller effect was found. The effect is observable at the LHC for a compactification scale $\mu \lesssim 7$ TeV, for a wide range of very high p_T. For example, with a minimum p_T for each of the jets of 2 TeV, the dijet cross section is about three times larger than that of the SM for $\mu = 5$ TeV. Thus, the measurements of the dijet cross sections at the LHC will either discover the indirect effects of the KK modes of the gluons or set a bound on μ of about 7 TeV, which is significantly higher than the current bound of about 2 TeV. The effect is much less discernible at the upgraded Tevatron, and will not be observed for $\mu \gtrsim 2$ TeV. For three jets in the final state, in which two of the jets are the decay products of an on-shell $g^\star$, at high p_T at the LHC, the KK enhancement over the SM cross sections is much smaller than for the dijet case. For example, with

a minimum p_T of each of the jets of 1.5 TeV, the cross section is enhanced only by about 100% for $\mu = 3$ TeV. Although the dijet effect is much greater, three-jet final state measurements can offer additional confirming information if a large effect is seen in dijet final state measurements. For four jets in the final state from double on-shell $g^\star$ production, again the cross sections are rather small unless $\mu \lesssim 2.5$ TeV.

Mass Reconstruction. In the case of single or double on-shell $g^\star$ production leading to three or four jets, respectively, in the final state, the on-shell $g^\star$'s subsequently decay primarily (the exceptions involve loop corrections) to quark and anti-quark pairs. These quark and anti-quark decay products will have very high p_T because the mass of the $g^\star$ is quite high (some multiple of the compactification scale, which is at least a TeV). If the invariant mass of the parent particle can be reconstructed using the measured high p_T of the jets, then that will be the clear signal of the first KK excitation of the gluons. In the three-jet case, such reconstruction must be done for each pair-wise configuration. Thus, for three jets in the final state, although the total cross section is not much larger than the SM background, such an invariant mass peak could potentially stand well above the SM background.

Uncertainties. Now, a discussion of some of the uncertainties in the calculations and results is presented. Firstly, in the parton distribution function $f_{a/A}(x_A, Q)$ and the strong coupling $\alpha_s(Q)$, the results are somewhat sensitive to the choice of the scale Q. The choice $Q = p_T$ was made for the SM background as well as for the KK contribution to the dijet signal, and $Q = m_n$ (*i.e.*, the mass of the $g^\star$) for single and double $g^\star$ production. The scale Q was varied from $p_T/2$ to $2p_T$ for two or three jets in the final state for the SM background, and found an enhancement of about

40% for $p_T/2$ and a reduction of about 30% for $2p_T$ compared to $Q = p_T$. Thus, if the KK effect does not exceed the SM background significantly, it may be difficult to discern in light of the uncertainty arising from the choice of Q. However, for two jets only, the same value for Q was employed in the KK and SM cases, such that this uncertainty has less relative effect on the ratio R. Therefore, R can be somewhat smaller for two jets than three or more jets and still provide indirect evidence of KK excitations of the gluons. Secondly, in the calculations of three- and four-jet cross sections, only the production of $g^\star$'s on-shell and their subsequent decays was considered. Not included were those diagrams involving virtual $g^\star$'s. Such virtual $g^\star$ contributions will naturally be small because they are higher order in the strong coupling constant $\alpha_s(Q)$. However, there are many virtual $g^\star$ diagrams (especially for four-jet diagrams) which may lead to a sizeable total contribution. Inclusion of these virtual $g^\star$ diagrams would enhance the three- and four-jet signals, thereby producing a somewhat greater effect. Finally, the running of the strong coupling constant $\alpha_s(Q)$ was evaluated with the usual logarithmic behavior of the SM. This is fine for $Q \leq \mu$, but when $Q > \mu$, the decrease is a power law behavior, in which case $\alpha_s(Q)$ would be somewhat smaller. However, since in most of these calculations, the scale Q (which is equal to p_T in the dijet case and m_{π} otherwise) is less than μ or does not exceed μ by much, the net effect would be only a relatively small reduction of these calculated cross sections (in this scenario with only one extra dimension).

Signatures Finally addressed is the issue of how to distinguish the signal due to KK excitations from other new physics that might produce a similar collider signal. For example, the colorons [30] in the top color model produce effects similar to those

of the KK excitations of the gluons. The eight colorons are like eight heavy gluons with the same mass, whereas, in the KK case, there is an infinite tower of increasing masses, $m_n = n\mu$ $(n = 1, 2, \ldots)$. One important distinguishing feature between the two cases is the difference in the details of the decay modes of the colorons and the KK excitations of the gluons. While the branching ratios of the KK $g^\star$'s to the various quark flavors are identical, the branching ratios of the coloron to various flavors of quarks ($q_i\bar{q}_i$, $i \in \{u,d,c,s,t,b\}$) depends on the mixing angle between the two SU(3)'s, $SU(3)_I$ and $SU(3)_{II}$. In the limit of zero mixing angle, the colorons couple only to $t\bar{t}$ and $b\bar{b}$. Thus, while the KK $g^\star$'s decay equally to various quark flavors, the coloron decay is flavor-dependent. In the small mixing case, the dominant decays will be to $t\bar{t}$ and $b\bar{b}$. For the $t\bar{t}$ decay, the p_T of the jets coming from the subsequent decay of the top quark will be reduced. Thus, the dijet signal at very high p_T would be much stronger in the KK case than in the coloron case.

EW Interactions

Results. Investigated here was the phenomenology of the KK excitations of the EW gauge bosons for a class of string-inspired models in which the SM gauge bosons propagate into one TeV-scale compact extra dimension, but where the SM particles are confined to the usual SM three-brane. Specifically, the effects that these KK excitations have on the cross sections for various processes at present and future high energy e^+e^- colliders were examined. Included in this study were Bhabha scattering and muon pair production, dijet production, Higgs production, and neutrino pair and single photon production. Exclusively direct-channel processes, namely, muon,

dijet, and Higgs production, produced a considerably greater effect than processes with both direct- and cross-channel Feynman diagrams, *i.e.* Bhabha scattering and neutrino and single photon production. This is due to the competing effects of the effective propagators for s-channel exchanges and t-channel exchanges: The primary effect of the KK excitations arises from the interference of the $n = 0$ (SM) mode exchanges with the $n > 0$ (KK) mode exchanges, which results in a reduction of the modulus-squared of the effective propagator and thus the corresponding amplitude-squared for direct-channel exchanges, and an opposing enlargement for cross-channel exchanges and the s-t interference.

The KK excitations of the EW gauge bosons would be particularly elusive for detection at LEP2 energies, where the largest effect for the processes that were examined is below 6% for even small compactification scales such as ~ 2 TeV and below 3% for compactification scales of ~ 3.5 TeV. Thus, quite precise measurements as well as very low compactification scales would be necessary for hints of KK excitations of the EW gauge bosons at LEP energies. However, the effects are considerably greater for prospective high energy colliders. For example, a 500 GeV collider can see about a 20% reduction in the cross section for muon pair production compared to the SM if the lowest-lying KK excitations have masses of ~ 3 TeV, and a 10% reduction for KK masses starting at ~ 4 TeV. A very high energy (TeV) collider could probe compactification scales up to 5 TeV and find a 20% effect, and up to 7 TeV with a 10% effect; meanwhile, a smaller compactification scale of 3 TeV reduces the cross section by half compared to the SM background.

It was found that the KK excitations of the EW gauge bosons could play an

important role on the discovery of the Higgs by enhancing the Higgs production cross section significantly. This is true for a Higgs boson that is confined to the SM three-brane, else the coupling of the Higgs to a single KK excitation of a gauge boson is zero.

Signatures. Addressed here are the differences between KK excitations and other new physics that might produce a similar collider signal. In particular, W' and Z' physics produce the same effects as the lowest-lying KK excitations of the W and the Z, except that the couplings of the W' and Z' to fermions can be different, and there are no restrictions on how many W''s and/or Z''s can couple to SM gauge bosons. Although the KK case involves an infinite tower of $W_n^\star$'s and $Z_n^\star$'s, the primary effect arises from the interference between the $n = 0$ (SM) and $n = 1$ (KK) modes, which is exactly the effect of the W' and Z'. In the case of multiple Z''s, for example, if the various Z''s have masses that are not integral multiples of the smallest Z' mass, then this would clearly be different from the KK tower formed by a SM Z boson that propagates into one extra dimension. Also, there has been abundant interest in Z' models with restricted couplings to fermions, such as leptophobic Z''s that couple to quarks but not to leptons, which seek to explain discrepancies between SM theoretical predictions and experimental measurements for particular processes without destroying fine agreement with processes such as charged lepton production at the Z pole. In these cases, the couplings are different from the KK model considered here, where the KK excitations couple to all fermions with a $\sqrt{2}$ relative to the SM couplings. However, it is also possible to construct models in which some fermions see extra dimensions while others do not. For example, if the leptons see an extra

dimension while the quarks are confined to the usual SM wall, then the situation will mimic the behavior of leptophobic Z' physics for e^+e^- processes.[†] Finally considered was a model in which all of the EW gauge bosons propagate into the same extra dimension. In this case, if there is a $Z_1^\star$ with a mass of 3 TeV, then there are also $\gamma_1^\star$'s and $W_1^\star$'s with masses that are approximately 3 TeV as well. However, it is also possible that the various EW gauge bosons propagate into different extra dimensions with different compactification scales, or that some do not see extra dimensions at all. All in all, there is are several differences between the KK and Z' effects that can be calculated for various processes, but the general behavior is quite similar. The chief test would come from very high energy colliders. If a Z' or $Z^\star$ is detected, then a search at twice that scale that fails to find a $Z_n^\star$ would clearly reveal that it is a Z' and not a $Z^\star$, and a search that finds a $Z_2^\star$ at the correct scale only leaves a small probability that this is coincidentally a second Z' with twice the mass of the first (in which case a search at three times the first scale could reduce this probability even further or decide in favor of the Z').

UED Model

QCD Interactions

Results. In this work, investigated in detail was the phenomenology of the UED model, which is a class a class of string-inspired models in which all of the SM fields can propagate into one TeV-scale extra dimension. Specifically, the effects that the

[†]For this KK case, the $eq \to Z_n^\star \to eq$ cross-channel process does not vanish, whereas a Z' can not couple to the leptons.

KK excitations of the quarks and gluons have on multijet final states were calculated at high energy hadronic colliders including the LHC and Tevatron Runs I and II. These calculations were performed for the case where the lowest-lying KK excitations of the light quarks and gluons are stable, as well as the case where they decay within the detector. For the decaying scenario, a scenario was examined in the context of a fat brane that may provide enough KK number violation to accommodate lifetimes that would be consistent with cosmological observations without resulting in a significant production rate for single KK final states. Presented was a detailed evaluation for the fat brane scenario, and also illustrated was the dependence of these results on the decay structure.

These results for proton-proton collisions at the Tevatron Run I place the mass bound for the first excited KK states at 350–400 GeV. For the Run II energies, the mass bound can be raised to 450–550 GeV. Proton-antiproton collisions at the LHC energy can probe much further: UED KK excitations will either be discovered or the mass limit will be raised to about 3 TeV. If the UED compactification scale is less than 1.5 TeV, then at the LHC energy it may be possible to see the first two KK excitations of the quarks and gluons, thereby uniquely establishing the extra-dimensional nature of the new physics.

Signatures. The signatures of the production of UED KK excitations will be vastly different for short-lived and long-lived states. Stable, slowly moving KK quarks produced at colliders will hadronize, resulting in tracks with high ionization. The production of heavy, charged stable particles will produce a clear signal of new physics. They will appear as a heavy replica of the light SM quarks, with both up- and down-

type quark charges, but with two KK quarks corresponding to each SM quark. The two towers, $q_n^{\bullet}$and q_n°, will be polarized with opposite chirality for all cross-channel processes due to Z_2 parity conservation. If the KK excitations of the light quarks and gluons are short-lived, then the signal will be SM dijet production with missing energy carried off by the emitted gravitons. This missing energy significantly reduces the SM background. The production of the lowest-lying KK excitations of the gluons and light quarks gives rise to only dijets plus missing energy (due to the escaping gravitons), and no multijet signals (at order α_S^2). Such final states will distinguish this new physics from supersymmetry, which will produce multijet final states in addition to dijets.

EW Interactions.

Results. The cross sections for EW processes producing KK final states at the LHC were calculated. For the case where the lowest-lying KK excitations are stable, the LHC will be able to probe up to 1500 GeV. For the case where they can decay, the fat brane scenario was adopted for the purpose of illustration, in which the LHC can probe up to 1300–1400 GeV for single or double photon events. While the LHC can probe further for QCD interactions than EW interactions, the EW processes can offer additional information if universal extra dimensions are detected, and may offer a cleaner signal relative to the SM background.

Signatures. The experimental signatures are similar for the QCD and EW processes. The production of heavy, stable, slowly moving charged particles will be a clear sign of new physics if the lowest-lying KK excitations are stable. For the de-

caying case, the formalism is quite similar, but the final states and corresponding backgrounds are different. In the EW case, events with fewer than two jets may produce a clearer signal than in the QCD case. In either case, the missing energy distribution will help to filter out the SM backgrounds.

APPENDIX A

QCD Interactions in the Fermi-Phobic Model

Effective 4D Lagrangian

5D Lagrangian. The generalization of the 4D SM Lagrangian density to the 5D Lagrangian density leads to 5D gluon field strength tensors $F^a_{MN} = \partial_M A^a_N - \partial_N A^a_M - g_5 f^{abc} A^b_M A^c_N$ described by

$$\begin{aligned}\mathcal{L}_5 &= -\frac{1}{4} F^a_{MN} F^{MNa} + i\bar{q}\gamma^\mu D_\mu q \delta(y) \\ &= -\frac{1}{4}\Big(F^a_{\mu\nu} F^{\mu\nu a} + 2F^a_{\mu 4} F^{\mu 4 a} \Big) \\ &\quad + i\bar{q}\gamma^\mu D_\mu q \delta(y)\,,\end{aligned} \tag{75}$$

where g_5 is the 5D strong coupling, A^a_M is the 5D gluon field, a,b,c are the usual gluon color indices, D_μ is the usual 4D covariant derivative, μ,ν are the usual 4D space-time indices, M,$N \in \{0,1,...,4\}$ are 5D space-time indices, and $\delta(y)$ represents that the SM fermions are localized in the D_3 brane with $y = 0$. The terms representing the kinetic energy and interactions between the g and $g^\star$ fields arise from the contraction of the $F^a_{\mu\nu}$'s:

$$\begin{aligned}F^a_{\mu\nu} F^{\mu\nu a} = {} & \partial_\mu A^a_\nu \partial^\mu A^{\nu a} - \partial_\nu A^a_\mu \partial^\mu A^{\nu a} \\ & - \partial_\mu A^a_\nu \partial^\nu A^{\mu a} + \partial_\nu A^a_\mu \partial^\nu A^{\mu a} \\ & - 2g_5 f^{abc} A^b_\mu A^c_\nu \Big(\partial^\mu A^{\nu a} - \partial^\nu A^{\mu a} \Big) \\ & - g_5^2 f^{abc} f^{ade} A^b_\mu A^c_\nu A^{\mu d} A^{\nu e}\,.\end{aligned} \tag{76}$$

Similarly, the mass terms for the $g^\star_n$'s stem from the contraction of the $F^a_{\mu 4}$'s:

$$F^a_{\mu 4} F^{\mu 4 a} = \partial_4 A^a_\mu \partial^4 A^{\mu a}\,, \tag{77}$$

where the gauge choice $A^a_4 = 0$ has been imposed. The remaining interaction of the $g^\star$'s involves the quark fields and is governed by the term in Eq. (75) involving the covariant derivative.

Compactification. Consider compactification on a S^1/Z_2 orbifold and make the identification $y \to -y$ such that $A^a_\mu(x,-y) = A^a_\mu(x,y)$. The fields $A^a_\mu(x,y)$ can then be Fourier expanded in terms of the compactified dimension $y = r\phi$ as

$$A^a_\mu(x,y) = \frac{1}{\sqrt{\pi r}}\left[A^a_{\mu 0}(x) + \sum_{n=1}^{\infty} A^a_{\mu n}(x)\cos(n\phi)\right], \tag{78}$$

where the normalization of $A^a_0(x)$ for the gluon field is one-half that of $A^a_n(x)$ for the KK excitations.

QCD Interactions

Mass Term. Integration over the compactified dimension y then gives the effective 4D theory. The terms from the integration of $-\frac{1}{4}F^a_{\mu\nu}F^{\mu\nu a}$ over y that are quadratic in the fields $A^a_\mu(x,y)$ give rise to kinetic energy terms in the effective 4D Lagrangian density of the form

$$-\frac{1}{4}\int_0^{\pi r} \partial_\mu A^a_\nu(x,y)\partial^\mu A^{\nu a}(x,y)dy = -\frac{1}{4}\Big[\partial_\mu A^a_{\nu 0}(x)\partial^\mu A^{\nu a}_0(x) + \frac{1}{2}\sum_{n=1}^{\infty}\partial_\mu A^a_{\nu n}(x)\partial^\mu A^{\nu a}_n(x)\Big]. \tag{79}$$

It is then necessary to rescale the fields as

$$A^a_{\mu 0}(x) \to A'^a_{\mu 0}(x), A^a_{\mu n}(x) \to A'^a_{\mu n}(x) \equiv \frac{A^a_{\mu n}(x)}{\sqrt{2}} \tag{80}$$

in order to canonically normalize the kinetic energy terms. Therefore, the mass and interaction terms must be expressed in terms of the rescaled fields, $A'^{a}_{\mu 0}(x)$ and $A'^{a}_{\mu n}(x)$. The masses of the KK excitations of the gluons arise from the integration of $F^{a}_{\mu 4}F^{\mu 4a}$ over y:

$$-\frac{1}{4}\int_{0}^{\pi r}\partial_4 A^{a}_{\mu}(x,y)\partial^4 A^{\mu a}(x,y)dy = -\frac{1}{2}\frac{n^2}{r^2}\sum_{n=1}^{\infty}A'^{a}_{\mu n}(x)A'^{\mu a}_{n}(x)\,. \tag{81}$$

The mass of the $g^{\star}_{n}$ is then identified as $m_n = n\mu$, where μ is the compactification scale ($\mu = 1/r$).

Feynman Rules. The Feynman rules for vertices involving $g^{\star}$'s follow from the interaction terms. The interactions of the $g^{\star}$'s with the quark fields originate from the term in the 5D Lagrangian density involving the covariant derivative. The delta function, which constrains the quark fields to the wall, takes care of the integration. Thus, the q-$\bar{q}$-$g^{\star}$ vertex receives a factor of $\sqrt{2}$, compared to the SM q-$\bar{q}$-g vertex, from the rescaling of the $A^{a}_{\mu n}$ field:

$$-i\Lambda_{q\text{-}\bar{q}\text{-}g^{\star}} = -i\sqrt{2}\Lambda_{q\text{-}\bar{q}\text{-}g}\,, \tag{82}$$

where the 4D strong coupling constant g is related to g_5 by $g \equiv g_5/\sqrt{\pi r}$. Interactions between g's and $g^{\star}$'s are somewhat more involved. The cubic interaction terms in the effective 4D Lagrangian density are

$$\begin{aligned}
&-i\frac{1}{2}g_5 f^{abc}\int_{0}^{\pi r}A^{b}_{\mu}(x,y)A^{c}_{\nu}(x,y)\Big[\partial^{\mu}A^{\nu a}(x,y)-\partial^{\nu}A^{\mu a}(x,y)\Big]dy \\
&= -\frac{1}{2}gf^{abc}\Big\{A'^{b}_{\mu 0}(x)A'^{c}_{\nu 0}(x)\Big[\partial^{\mu}A'^{\nu a}_{0}(x)-\partial^{\nu}A'^{\mu a}_{0}(x)\Big] \\
&\quad + 3A'^{b}_{\mu 0}(x)\sum_{n=1}^{\infty}A'^{c}_{\nu n}(x)\Big[\partial^{\mu}A'^{\nu a}_{n}(x)-\partial^{\nu}A'^{\mu a}_{n}(x)\Big] \\
&\quad + \frac{1}{\sqrt{2}}\sum_{n,m,\ell=1}^{\infty}A'^{b}_{\mu n}(x)A'^{c}_{\nu m}\Big[\partial^{\mu}A'^{\nu a}_{\ell}(x)-\partial^{\nu}A'^{\mu a}_{\ell}(x)\Big]\delta_{\ell,\pm m\pm n}\Big\}\,,
\end{aligned} \tag{83}$$

where the following notation is introduced: The Kronecker δ with $\pm$'s represents the summation over all of the Kronecker δ's that can be constructed by permuting the $+$ and $-$ signs (*e.g.*, $\delta_{\ell,\pm m\pm n} = \delta_{\ell,m+n} + \delta_{\ell,m-n} + \delta_{\ell,n-m} + \delta_{\ell,-m-n}$). These cubic interaction terms lead to the following Feynman rules for triple vertices involving g's and $g^\star$'s:

$$\begin{aligned} -i\Lambda_{g\text{-}g_n^\star\text{-}g_n^\star} &= -i\Lambda_{g\text{-}g\text{-}g} \\ -i\Lambda_{g_n^\star\text{-}g_n^\star\text{-}g_{2n}^\star} &= -i\frac{1}{2}\Lambda_{g\text{-}g\text{-}g} \\ -i\Lambda_{g_n^\star\text{-}g_m^\star\text{-}g_{|m\pm n|}^\star} &= -i\frac{1}{2}\Lambda_{g\text{-}g\text{-}g}\,, \end{aligned} \tag{84}$$

for $n \neq m$. Similarly, the quartic interaction terms in the effective 4D Lagrangian density are

$$\begin{aligned} &-\frac{1}{4}g_5^2 f^{abc}f^{ade}\int_0^{\pi r} A_\mu^b(x,y)A_\nu^c(x,y)A^{\mu d}(x,y)A^{\nu e}(x,y)dy \\ &= -\frac{1}{4}g^2 f^{abc}f^{ade}\Big[A'^{\,b}_{\mu 0}(x)A'^{\,c}_{\nu 0}(x)A'^{\,\mu d}_{\;0}(x)A'^{\,\nu e}_{\;0}(x) \\ &\quad + 6A'^{\,b}_{\mu 0}(x)A'^{\,c}_{\nu 0}(x)\sum_{n=1}^{\infty}A'^{\,\mu d}_{n}(x)A'^{\,\nu e}_{n}(x) \\ &\quad + \frac{2}{\sqrt{2}}A'^{\,b}_{\mu 0}(x)\sum_{n,m,\ell=1}^{\infty}A'^{\,c}_{\nu n}(x)A'^{\,\mu d}_{m}(x)A'^{\,\nu e}_{\ell}(x)\delta_{\ell,\pm m\pm n} \\ &\quad + \frac{1}{2}\sum_{n,m,\ell,k=1}^{\infty}A'^{\,b}_{\mu n}(x)A'^{\,c}_{\nu m}(x)A'^{\,\mu d}_{\ell}(x)A'^{\,\nu e}_{k}(x)\delta_{k,\pm m\pm n\pm \ell}\Big]\,. \end{aligned} \tag{85}$$

The Feynman rules for quadruple vertices involving KK excitations are then

$$
\begin{aligned}
-i\Lambda_{g\text{-}g\text{-}g_n^\star\text{-}g_n^\star} &= -i\Lambda_{g\text{-}g\text{-}g\text{-}g} \\
-i\Lambda_{g\text{-}g_n^\star\text{-}g_n^\star\text{-}g_{2n}^\star} &= -i\frac{1}{\sqrt{2}}\Lambda_{g\text{-}g\text{-}g\text{-}g} \\
-i\Lambda_{g\text{-}g_n^\star\text{-}g_n^\star\text{-}g_{|m\pm n|}^\star} &= -i\frac{1}{\sqrt{2}}\Lambda_{g\text{-}g\text{-}g\text{-}g} \\
-i\Lambda_{g_n^\star\text{-}g_n^\star\text{-}g_n^\star\text{-}g_n^\star} &= -i\frac{3}{2}\Lambda_{g\text{-}g\text{-}g\text{-}g} \\
-i\Lambda_{g_n^\star\text{-}g_n^\star\text{-}g_n^\star\text{-}g_{3n}^\star} &= -i\frac{1}{2}\Lambda_{g\text{-}g\text{-}g\text{-}g} \\
-i\Lambda_{g_n^\star\text{-}g_n^\star\text{-}g_m^\star\text{-}g_m^\star} &= -i\Lambda_{g\text{-}g\text{-}g\text{-}g} \\
-i\Lambda_{g_n^\star\text{-}g_n^\star\text{-}g_m^\star\text{-}g_{|2n\pm m|}^\star} &= -i\frac{1}{2}\Lambda_{g\text{-}g\text{-}g\text{-}g} \\
-i\Lambda_{g_n^\star\text{-}g_m^\star\text{-}g_\ell^\star\text{-}g_{|\ell\pm m\pm n|}^\star} &= -i\frac{1}{2}\Lambda_{g\text{-}g\text{-}g\text{-}g}\,,
\end{aligned}
\tag{86}
$$

for $n \neq m \neq \ell$. The relative coupling strengths are summarized in Fig. 1.

APPENDIX B

QCD Interactions in the UED Model

Effective 4D Lagrangian

Procedure. The starting point is the UED 5D Lagrangian density. The procedure for obtaining the effective 4D theory is to Fourier expand the 5D fields in terms of the extra dimension y, and then integrate over y. Here, the mass contributions to the KK excitations will be obtained from their kinetic terms as well as their interactions with the Higgs potential. The complete set of interactions between the KK excitations of the quarks and gluons will then be derived. Purely gluonic interactions were described elaborately in the context of the fermi-phobic scenario, and apply here as well.

Compactification. Each of the 5D multiplets $Q(x,y)$, $U(x,y)$, and $D(x,y)$ can be Fourier expanded in terms of the compactified dimension y, restricted in an S_1/Z_2 orbifold, as

$$Q(x,y) = \frac{1}{\sqrt{\pi R}}\left\{\begin{pmatrix} u(x) \\ d(x) \end{pmatrix}_L + \sqrt{2}\sum_{n=1}^{\infty}\left[Q_L^n(x)\cos\left(\frac{ny}{R}\right) + Q_R^n(x)\sin\left(\frac{ny}{R}\right)\right]\right\} \quad (87)$$

$$U(x,y) = \frac{1}{\sqrt{\pi R}}\left\{u_R(x) + \sqrt{2}\sum_{n=1}^{\infty}\left[U_R^n(x)\cos\left(\frac{ny}{R}\right) + U_L^n(x)\sin\left(\frac{ny}{R}\right)\right]\right\} \quad (88)$$

$$D(x,y) = \frac{1}{\sqrt{\pi R}}\left\{d_R(x) + \sqrt{2}\sum_{n=1}^{\infty}\left[D_R^n(x)\cos\left(\frac{ny}{R}\right) + D_L^n(x)\sin\left(\frac{ny}{R}\right)\right]\right\}. \quad (89)$$

where $Q^n_{L,R}(x) \equiv \frac{1}{2}(1\mp\gamma_5)q^{\bullet}_n(x)$ as in Eq. 22 and γ_5 is the usual 4D Dirac matrix. Note that the decomposition in Eq.'s ??–?? gives the correct SM zero mode chiral structure for the fermions. Similarly, the gluon field $A_M(x,y)$ can be Fourier expanded as:

$$A^a_\mu(x,y) = \frac{1}{\sqrt{\pi R}}\left[A^a_{\mu 0}(x) + \sqrt{2}\sum_{n=1}^{\infty} A^a_{\mu,n}(x)\cos\left(\frac{ny}{R}\right)\right] \tag{90}$$

$$A^a_4(x,y) = \frac{\sqrt{2}}{\sqrt{\pi R}}\sum_{n=1}^{\infty} A^a_{4,n}(x)\sin\left(\frac{ny}{R}\right). \tag{91}$$

Under the transformation $y \to -y$, the decomposed gluon fields transform as $A^a_\mu(x,-y) = A^a_\mu(x,y)$ and $A^a_4(x,-y) = -A^a_4(x,y)$. Notice that Z_2 parity and KK number are conserved in the interactions involving the gauge fields and fermions. The choice is made to work in the unitary gauge, where the gauge choice $A^a_{4,n}(x) = 0$ [18] can be applied.

QCD Interactions

Mass Matrix. The primary contribution to the KK masses stems from the kinetic term in the Lagrangian density:

$$\mathcal{L}_5 = i\bar{Q}(x,y)\left\{\Gamma^M\left[\partial_M + ig_5 T^a A^a_M(x,y)\right]\right\}Q(x,y). \tag{92}$$

There are similar terms for the other 5D multiplets. Here, g_5 is the 5D strong coupling and M is the 5D analog of the Lorentz index μ, *i.e.*, $M \in \{\mu, 4\}$. Integration of the kinetic terms in Eq. (92) over the compactified dimension y results in:

$$\begin{aligned} i\int_0^{\pi R} \bar{Q}(x,y)\,\Gamma^M\partial_M Q(x,y)dy = i\Bigg[&(\bar{u}(x)\bar{d}(x))_L\gamma^\mu\partial_\mu\begin{pmatrix} u(x) \\ d(x)\end{pmatrix}_L \\ &+ \sum_{n=1}^{\infty}\bar{Q}^n_L(x)\gamma^\mu\partial_\mu Q^n_L(x) + \bar{Q}^n_R(x)\gamma^\mu\partial_\mu Q^n_R(x) \\ &+ i\frac{n}{R}\bar{Q}^n_L(x)Q^n_R(x) + i\frac{n}{R}\bar{Q}^n_R(x)Q^n_L(x)\Bigg]. \end{aligned} \tag{93}$$

There are similar expressions for the $U(x,y)$ and $D(x,y)$ multiplets. The mass of the KK excitations are identified as $n\mu$, where μ is the compactification scale ($\mu = 1/R$).

Thus, in the absence of the Higgs mechanism, the KK excitations have masses given by $M_n = n/R = n\mu$. The corresponding mass matrix is:

$$(\bar{Q}^n(x), \bar{U}^n(x)) \begin{pmatrix} \frac{n}{R} & 0 \\ 0 & -\frac{n}{R} \end{pmatrix} \begin{pmatrix} Q^n(x) \\ U^n(x) \end{pmatrix},$$

where $Q^n(x)$ represents the upper component of the doublet, with charge 2/3. Note that there is no mixing between the different KK levels, *i*.e., between $Q^n(x)$ and $Q^m(x)$ for $n \neq m$.

Additional mass contributions arise from the Yukawa couplings of the 5D quark multiplets via the Higgs VEV's:

$$\begin{aligned} & i \int_0^{\pi R} \left[\lambda_u^5 \bar{Q}(x,y) i\sigma_2 H^*(x,y) U(x,y) + \lambda_d^5 \bar{Q}(x,y) H(x,y) D(x,y) + h.c.\right] dy = \\ & i \left\{ M_u \left[\bar{u}(x)u(x) + \sum_{n=1}^{\infty} \left[\bar{Q}_L^n(x) U_R^n(x) + \bar{Q}_R^n(x) U_L^n(x)\right] \right] \right. \\ & \left. + \lambda_u \left[\bar{u}(x)u(x)h(x) + \sum_{n=1}^{\infty} \left[\bar{Q}_L^n(x) U_R^n(x) + \bar{Q}_R^n(x) U_L^n(x)\right] h(x) \right] + \lambda_d \text{ terms} \right\}, \end{aligned} \tag{94}$$

where $\lambda_u \equiv \lambda_u^5/\sqrt{\pi R}$ and $M_u \equiv \lambda_u <H>$. The $(Q^n(x), U^n(x))$ mass matrix, including these Yukawa contributions as well as the kinetic terms, is:

$$(\bar{Q}^n(x), \bar{U}^n(x)) \begin{pmatrix} \frac{n}{R} & M_u \\ M_u & -\frac{n}{R} \end{pmatrix} \begin{pmatrix} Q^n(x) \\ U^n(x) \end{pmatrix}.$$

The eigenvalues of the this mass matrix give the net mass M_n of the KK modes in terms of the mass of the corresponding quark field M_q and the mass from the compactification n/R:

$$M_n = \sqrt{\frac{n^2}{R^2} + M_q^2}. \tag{95}$$

The $U^n(x)$ field is redefined by $U^n(x) \rightarrow \gamma_5 U^n(x)$. In the subsequent calculations, the SM quark masses are neglected except for the top mass M_t.

Feynman Rules. The interactions between the 5D $Q(x,y)$ fields and the 5D gluon fields $A_M^a(x,y)$ are given by:

$$
\begin{aligned}
&-g_5 \int_0^{\pi R} \bar{Q}(x,y)\Gamma^M T^a A_M^a(x,y) Q(x,y) dy \\
&= -g \left\{ \bar{q}_L(x)\gamma^\mu T^a q_L(x) A^a_{\mu,0}(x) + \sum_{n=1}^{\infty} \left[\bar{Q}_L^n(x)\gamma^\mu T^a Q_L^n(x) + \bar{Q}_R^n \gamma^\mu T^a Q_R^n(x) \right] A^a_{\mu,0}(x) \right. \\
&\quad + \sum_{n=1}^{\infty} \left[\bar{q}_L(x)\gamma^\mu T^a Q_L^n(x) + \bar{Q}_L^n(x)\gamma^\mu T^a q_L(x) \right] A^a_{\mu,n}(x) \\
&\quad + \frac{1}{\sqrt{2}} \sum_{n,m,\ell=1}^{\infty} \left[\bar{Q}_L^n(x)\gamma^\mu T^a Q_L^m(x) (\delta_{\ell,|m-n|} + \delta_{\ell,m+n}) \right. \\
&\quad \left. \left. + \bar{Q}_R^n(x)\gamma^\mu T^a Q_R^m(x) (\delta_{\ell,|m-n|} - \delta_{\ell,m+n}) \right] A^a_{\mu,\ell} \right\} ,
\end{aligned}
\tag{96}
$$

where $g \equiv g_5/\sqrt{\pi R}$. There are similar interactions involving the U and D fields. In terms of the $q_n^\bullet$ and q_n° fields (Eq. 22), the interactions are:

$$
\begin{aligned}
\mathcal{L}_{int} = -g \Big\{ & \bar{q}(x)\gamma^\mu T^a q(x) A^a_{\mu,0}(x) + \sum_{n=1}^{\infty} \left[\bar{q}_n^\bullet(x)\gamma^\mu T^a q_n^\bullet(x) + q_n^\circ(x)\gamma^\mu T^a \bar{q}_n^\circ(x) \right] A^a_{\mu,0}(x) \\
& + \sum_{n=1}^{\infty} \left[\bar{q}_L(x)\gamma^\mu T^a q_n^\bullet(x) + \bar{q}_n^\bullet(x)\gamma^\mu T^a q_L(x) \right] A^a_{\nu,n}(x) \\
& + \sum_{n=1}^{\infty} \left[\bar{q}_R(x)\gamma^\mu T^a q_n^\circ(x) + \bar{q}_n^\circ(x)\gamma^\mu T^a q_R(x) \right] A^a_{\nu,n}(x) \\
& + \frac{1}{\sqrt{2}} \sum_{n,m,\ell=1}^{\infty} \left[-\bar{q}_n^\bullet(x)\gamma^\mu\gamma_5 T^a q_m^\bullet(x) + \bar{q}_n^\circ(x)\gamma^\mu\gamma_5 T^a q_m^\circ(x) \right] A^a_{\mu,\ell}\, \delta_{\ell,m+n} \\
& + \frac{1}{\sqrt{2}} \sum_{n,m,\ell=1}^{\infty} \left[\bar{q}_n^\bullet(x)\gamma^\mu T^a q_m^\bullet(x) + \bar{q}_n^\circ(x)\gamma^\mu T^a q_m^\circ(x) \right] A^a_{\mu,\ell}\, \delta_{\ell,|m-n|} \Big\} .
\end{aligned}
\tag{97}
$$

The relative coupling strengths are summarized in Fig. 2.

References

[1] N. Arkani-Hamed, S. Dimopoulos and G. Dvali, Phys. Lett. **B429**, 263 (1998); Phys. Rev. **D59**, 086004 (1999); I. Antoniadis, N. Arkani-Hamed, S. Dimopoulos and G. Dvali, Phys. Lett. **B436**, 257 (1998).

[2] E. Witten, Nucl. Phys. **B471**, 135 (1996); J. Lykken, Phys. Rev. **D54**, 3693 (1996).

[3] See, for example: E.A. Mirabelli, M. Perelstein, and M.E. Peskin, Phys. Rev. Lett. **82**, 2236 (1999); G.F. Giudice, R. Rattazzi, and J.D. Wells, Nucl. Phys. **B554**, 3 (1999); J.E. Hewett, Phys. Rev. Lett. **82**, 4765 (1999); G. Shiu and S.H.H. Tye, Phys. Rev. **D58**, 106007 (1998); T. Banks, A. Nelson, and M. Dine, J. High Energy Phys. **06**, 014 (1999); P. Mathews, S. Raychaudhuri, and S. Sridhar, Phys. Lett. **B450**, 343 (1999); hep-ph/9904232; T.G. Rizzo, Phys. Rev. **D59**, 115010 (1999); C. Balazs, H.-J. He, W.W. Repko, C.-P. Yan, and D.A. Dicus, Phys. Rev. Lett. **83**, 2112 (1999); I. Antoniadis, K. Benakli, and M. Quirós, Phys. Lett. **B360**, 176 (1999); P. Nath, Y. Yamada, and M. Yamaguchi, *ibid.* **466**, 100 (1999); W.J. Marciano, Phys. Rev. **D60**, 09006 (1999); T. Han, D. Rainwater, and D. Zepenfield, Phys. Lett. **B463**, 93 (1999); K. Aghase and N.G. Deshpande, *ibid.* **456**, 60 (1999); G. Shiu, R. Shrock, and S.H.H. Tye, *ibid.* **458**, 274 (1999); K. Cheung and Y. Keung, Phys. Rev. **D60**, 112003 (1999); K.Y. Lee, S.C. Park, H.S. Song, J.H. Song and C.H. Yu, Phys. Rev. **D61**, 074005 (2000); hep-ph/0105326.

[4] T. Han, J.D. Lykken and R.-J. Zhang, Phys. Rev. **D59**, 105006 (1999).

[5] J. Lykken and S. Nandi, Phys. Lett. **B485**, 224 (2000).

[6] V. Barger, T. Han, C. Kao and R.J. Zhang, Phys. Lett. **B461**, 34 (1999); S. Cullen and M. Perelstein, Phys. Rev. Lett. **83**, 268, 1999; L.J. Hall and D. Smith, Phys. Rev. **D60**, 085008 (1999); S.C. Kappadath et. al., BAAS **30** 926 (1998); Ph.D. Thesis, available at http://wwwgro.sr.unh.edu/users/ckappada/ckappada.html; D.A. Dicus, W.W. Repko and V.L. Teplitz, Phys. Rev. D62, 076007 (2000). M. Biesiada, astro-ph/0109545; K.A. Milton, R. Kantowski, C. Kao and Y. Wang, hep-ph/0105250; S. Hannestad, G. Raffelt, hep-ph/0103201; M. Fairbairn, hep-ph/0111435.

[7] I. Antoniadis, Phys. Lett. **B246** 377 (1990).

[8] E. Accomando, I. Antoniadis, and K. Benakli, Nucl. Phys. **B579**, 3 (2000); A. Datta, P.J. O'Donnell, Z.H. Lin, X. Zhang, and T. Huang, Phys. Lett. **B483**, 203 (2000).

[9] T.G. Rizzo and J.D. Wells, hep-ph/9906234; C.D. Carone, Phys. Rev. D61 015008,2000.

[10] M. Masip and A. Pomarol, Phys. Rev. **D60**, 096005 (1999); P. Nath, Y. Yamada and M. Yamaguchi, Phys. Lett. **B466**, 100 (1999); T. G. Rizzo and J. D. Wells, Phys. Rev. **D61**, 016007 (2000).

[11] C.D. McMullen and S. Nandi, hep-ph/0110275.

[12] D.A. Dicus, C.D. McMullen and S. Nandi, hep-ph/0012259 (to appear in Phys. Rev. **D**, in Press).

[13] T. Appelquist, H.-C. Cheng and B.A. Dobrescu, Phys. Rev. **D64**, 035002 (2001).

[14] A. DeRujula, A. Donini, M.B. Gavela and S. Rigolin, Phys. Lett. **B482**, 195 (2000).

[15] T.G. Rizzo, Phys. Rev. **D64**, 095010 (2001).

[16] T. Appelquist and B.A. Dobrescu, Phys. Lett. **B516**, 85 (2001); K. Agashe, N.G. Deshpande and G.H. Wu, Phys. Lett. **B514**, 309 (2001).

[17] A. Delgado, A. Pomarol and M. Quirós, hep-ph/9812489; hep-ph/9911252; A. Pomarol and M. Quirós, hep-ph/9806263; E. Dudas, hep-ph/0006190; M. Masip and A. Pomarol, hep-ph/9902467.

[18] K.R. Dienes, E. Dudas, and T. Ghergetta, Nucl. Phys. **B537**, 47 (1999); J. Papavassiliou and A. Santamaria Phys. Rev. **D63**, 125014 (2001).

[19] G.K. Leontaris and N.D. Tracas, hep-ph/9902368 and hep-ph/9908462; M. Bando *et al.*, hep-ph/9906549; I. Antoniadis, K. Benakli, and M. Quirós, Phys. Lett. **B460**, 176 (1999); T.G. Rizzo, hep-ph/9909232; see also Ref. [21].

[20] J.A.M. Vermaseren, math-ph/0010025.

[21] K.P. Dienes, E. Dudas and T. Gherghetta, Phys. Lett. **B436**, 55 (1998); Nucl. Phys. **B537**, 47 (1999); T. Taylor and G Veneziano, Phys. Lett. **B212** 147 (1988); D. Ghilencia and G.G. Ross, Phys. Lett. **B442** 165 (1998); hep-ph/9908369;

C. Carone, Phys. Lett. **B454** 70 (1999); P. H. Frampton and A. Rasin, Phys. Lett. **B460**, 313 (1999); A. Delgado and M. Quirós, Nucl. Phys. **B559**, 235 (1999); A. Perez-Lorenzana and R. N. Mohapatra, Nucl. Phys. **B559**, 255 (1999); Z. Kakushadze and T. R. Taylor, Nucl. Phys. **B562**, 78 (1999); D. Dumitru and S. Nandi, hep-ph/9906514; K. Huitu and T. Kobayashi, Phys. Lett. **B470**, 90 (1999); H. Cheng, B. A. Dobrescu and C. T. Hill, Nucl. Phys. **B573**, 597 (2000).

[22] M. Masip, hep-ph/0007048.

[23] J.M. Cornwall, D.N. Levin and G. Tiktopoulos, Phys. Rev. Lett. 30, 1268 (1973); Phys. Rev. D10, 1145 (1974); D.A. Dicus and V.S. Mathur, Phys. Rev. D7, 3111 (1973); B.W.Lee, C. Quigg and H.B.Thacker, Phys. Rev. Lett. 38, 883 (1977); Phys. Rev. D16, 1519 (1977); M. J. G. Veltman, Acta Phys. Polon. B8, 475 (1977); C.H. Llewellyn Smith, Phys. Lett. B46, 233 (1973).

[24] R.S. Chivukula, D.A. Dicus and H.-J. He, Phys. Lett. **B525**, 175 (2002).

[25] H.L. Lai *et al.*, Phys. Rev. **D51**, 4763 (2000).

[26] F.A. Berends *et al.*, Phys. Rep. **100**, 201 (1983).

[27] S. Godfrey, P. Kalyniak, B. Kamal and A. Leike, Phys. Rev. **D61**, 113009 (2000).

[28] A. Connolly [CDF collaboration], "Search for long-lived charged massive particles at CDF," Talk at the American Physical Society (APS) Meeting of the Division of Particles and Fields (DPF 99), Los Angeles, CA, Jan 5-9, 1999, hep-ex/9904010.

[29] S.I. Bityukov, N.V. Krasnikov, Phys. Lett. **B469** 149 (1999).

[30] C.T. Hill, Phys. Lett. **B266**, 419 (1991); C.T. Hill and S.J. Parke, Phys. Rev. **D49**, 4454 (1994); D.A. Dicus, B. Dutta, and S. Nandi, Phys. Rev. **D51**, 6085 (1995).

VITA 2

Chris McMullen

Candidate for the Degree of

Doctor of Philosophy

Thesis: COLLIDER PHYSICS OF EXTRA COMPACT DIMENSIONS

Major Field: Physics

Biographical:

Education: Graduated from Downtown Business Magnet High School, Downtown Los Angeles, California in May 1990; received Bachelor of Science degree in Physics from California State University, Northridge, California in May 1994; received Master of Science degree in Physics from California State University, Northridge, California in August 1998. Completed the requirements for the Doctor of Philosophy degree with a major in Physics at Oklahoma State University in August 2002.

Experience: Taught undergraduate physics laboratories at California State University, Northridge, Department of Physics and Astronomy, 1995 to 1998; and Oklahoma State University, Department of Physics, 1998 to present.